Site-Specific Isotopes in Small Organic Molecules

Thesis by

Alison Piasecki

In partial fulfillment of the requirements for the degree of
Doctor of Philosophy in Geology

2015

California Institute of Technology
Pasadena, CA
Defended May 7, 2015

Abstract

Stable isotope geochemistry is a valuable toolkit for addressing a broad range of problems in the geosciences. Recent technical advances provide information that was previously unattainable or provide unprecedented precision and accuracy. Two such techniques are site-specific stable isotope mass spectrometry and clumped isotope thermometry. In this thesis, I use site-specific isotope and clumped isotope data to explore natural gas development and carbonate reaction kinetics. In the first chapter, I develop an equilibrium thermodynamics model to calculate equilibrium constants for isotope exchange reactions in small organic molecules. This equilibrium data provides a framework for interpreting the more complex data in the later chapters. In the second chapter, I demonstrate a method for measuring site-specific carbon isotopes in propane using high-resolution gas source mass spectrometry. This method relies on the characteristic fragments created during electron ionization, in which I measure the relative isotopic enrichment of separate parts of the molecule. My technique will be applied to a range of organic compounds in the future. For the third chapter, I use this technique to explore diffusion, mixing, and other natural processes in natural gas basins. As time progresses and the mixture matures, different components like kerogen and oil contribute to the propane in a natural gas sample. Each component imparts a distinct fingerprint on the site-specific isotope distribution within propane that I can observe to understand the source composition and maturation of the basin. Finally, in Chapter Four, I study the reaction kinetics of clumped isotopes in aragonite. Despite its frequent use as a clumped isotope thermometer, the aragonite blocking temperature is not known. Using laboratory heating experiments, I determine that the aragonite clumped isotope thermometer has a blocking temperature of 50-100°C. I compare this result to natural samples from the San Juan Islands that exhibit a maximum clumped isotope temperature that matches this blocking temperature. This thesis presents a framework for measuring site-specific carbon isotopes in organic molecules and new constraints on aragonite reaction kinetics. This study represents the foundation of a future generation of geochemical tools for the study of complex geologic systems.

Acknowledgements

First, I have to thank John Eiler. I came to Caltech with vague ideas about things that he was able to help form into scientific questions that I am addressing here today. Without his patience and guidance, I'd probably still be only seeking the obvious answers without really trying to tie everything back to important larger questions.

The ability to interact with a wide range of professors was one of the main reasons I chose to attend Caltech in the first place, and it didn't disappoint. I am incredibly grateful for the patience and open doors of the entire faculty, especially my committee members Alex Sessions, Ken Farley, and Paul Asimow. Also, there are many others from whom I have sought help over the past six years including, George Rossman, Jess Adkins, Joann Stock, Jason Saleeby, and Mitchio Okumura.

The Eiler lab group has been great. It's been excellent to have all of you around to help me figure out all of the silly things I've tried to do, including Nami Kitchen, Daniel Stolper, Max Lloyd, Kristin Bergmann, Matthieu Clog, Peter Douglas, Brooke Dallas, Itay Halevy, and many others.

Also ! My friends and family. The pit was great, Jeff M., Joel, Megan, Paul, and Erika. Stephen answers most of my sillier questions, both scientific and otherwise, with the appropriate amount of judgement. Katie, Jena, Elizabeth, and Sarah remind me that Caltech isn't just a boys club. Hayden and Max make me go outside. Jeff, who has been my support, best friend, and adventure sidekick. And Mom and Dad, who pretty much crafted me into a mini scientist from day one, and have supported me completely.

Contents

List of Figures

List of Tables

Chapter 1

Equilibrium fractionations of small alkanes using density functional theory

Abstract

Many previous studies have examined abundances of deuterium and ^{13}C within small organic molecules. Recent advances in analytical instrumentation add the abilities to measure site-specific and multiply substituted isotopologues of natural compounds. Here we perform first-principles calculations of the equilibrium distributions of ^{13}C and D in the volatile n-alkanes, as a guide to the interpretation of current measurements and as a basis for anticipating isotope effects that might be examined with future analytical techniques. We suggest that the most promising isotopic thermometers not yet attempted involve site-specific distribution of deuterium, which exhibits strong (100‰), highly temperature-dependent fractionation between methyl groups and central carbon positions in propane (and likely other larger n-alkanes).

1.1 Introduction

Stable isotopes are widely used in geochemistry as a means for constraining many kinetic and equilibrium processes. Several new measurement technologies and methods enable the observation of the distribution of naturally-occurring isotopes at molecular scales, including proportions of multiply substituted isotopologues (so-called clumped isotope species) and non-random distributions of isotopes among non-equivalent atomic sites (so-called site specific fractionations or effects). Interpretation of these new types of data will require fundamental understanding of the patterns of isotopic fractionation that result from various processes, such as thermodynamic equilibrium, diffusion, mixing, or kinetically-controlled chemical reactions. For example, an early study using methods of selective chemical degradation to make site-specific isotopic analyses demonstrated that reaction of acetaldehyde with Acetyl CoA generates a large difference in carbon isotope ratio between the methyl and carboxyl ends of the residual acetyl group (DeNiro and Epstein, 1977). This experiment illuminates our understanding of the even/odd ordering of carbon isotope ratios in some biosynthetically-formed fatty acids (Monson and Hayes, 1980), or the alkanes that form by thermal degradation of such biomolecules (Gilbert, Yamada, and Yoshida, 2013). In a second example, innovations in high-resolution multi collector gas source mass spectrometry enable the precise measurement of clumping of deuterium and ^{13}C into doubly-substituted methane (Stolper et al., 2014a). This effect can be interpreted as a thermometer through comparison with first-principles theories of the homogeneous isotope exchange equilibria among isotopologues of methane (Stolper et al., 2014b).

In this paper, we focus on the theoretical prediction of equilibrium thermodynamic fractionations involving intramolecular isotopic variations (clumping and site-specific effects) of the small n-alkanes (methane, ethane and propane). We use well-established tools for predicting molecular structures and dynamics and relatively straightforward models that use those predicted molecular properties to predict the effects of isotopic substitution on molecular vibrational and ro-vibrational energies. Briefly, we follow the model of previous studies that have calculated reduced partition functions using spectroscopic data for the frequencies of molecular vibrations, and combined those partition functions for relevant isotopologues to predict equilibrium fractionations between different co-existing compounds (Bigeleisen and Mayer, 1947; Urey, 1947). However, this approach becomes more complex when applied to larger molecules, where a large number of diverse clumped and site-specific isotopic substitutions should be considered, and measured constraints on molecular vibrations based on spectroscopic data may be incomplete. For this reason, we combine the Urey-Bigeleisn-Mayer theory of isotope effects with first-principles models that predict the lowest energy structures of compounds of interest and calculate frequencies of fundamental vibrational modes, which then serve as the foundation for predicted equilibrium fractionations.

Our intention is that by predicting the equilibrium distributions of isotopes among the isotopologues of the n-alkanes, we will provide a reference frame for the interpretation of measured isotopic signatures that include clumped- and site-specific data. These applications could include interpretation of temperatures of formation or storage for compounds that seem to exhibit equilibrium isotopic structures, or recognition of samples that deviate from expected patterns of equilibrium isotopic distribution and thus must have

undergone some non-equilibrium fractionation, such as a kinetically-controlled chemical or biochemical reaction. Finally, the models of small n-alkanes that we present here may serve as a basis for future models of larger organic molecules that are either analyzable using current SNIF-NMR techniques and/or future developments of mass spectrometric instruments and methods (e.g., Eiler et al. (2014)).

1.2 Methods

In order to calculate equilibrium fractionation factors between different isotopologues of alkanes, first-principles calculations were conducted to determine the lowest energy conformation of the compounds of interest (methane, ethane and propane). The structure and vibration frequencies of fundamental modes were calculated using density functional theory (DFT), molecular perturbation (MP2) (Scott and Radom, 1996; Becke, 1993), and coupled cluster (CCSD) (Kendall, Dunning, and Harrison, 1992) models, with various basis sets (Figure 1.1a). In all cases, we adopted the harmonic approximation. The results suggest that a DFT model using the B3LYP exchange correlation functional generally reproduces the spectroscopically-measured fundamental modes of methane, ethane, and propane. Although in some cases higher level methods were a slightly better match for the spectroscopic data, the B3LYP method with the basis set 6311G** will be the most easily applicable method for any future studies of larger molecules with multiple isotopic substitutions, because these calculations are less computationally intensive than other methods.

Although our approach involves approximations that could be improved upon with

more sophisticated treatments (e.g., anharmonic corrections), a simple and easily generalized method strikes us as the most productive approach for a study such as this, which aims to survey a wide variety of isotopologues of several compounds using an easily-generalized level of theory. Webb and Miller (2014) explore the limits of this approach by comparing its results to other methods, including path integral techniques, for select isotopologues of methane, N_2O and propane. That study demonstrates that a more refined treatment of anharmonicity and other complications results in second-order improvements in calculated equilibrium constants for isotope exchange reactions of interest to this work, but that the approach we adopt here is accurate to within current precision in isotopic measurements for several representative examples. This relative success may be due to the nature of calculating partition function ratios for different isotopologues of a molecular structure; many of the errors arising from an inadequate potential energy surface cancel out when the ratio of partition functions are used to determine an equilibrium fractionation factor (Rustad, 2009; Webb and Miller, 2014; Wang et al., 2009a). In any event, our approach is not only a convenient foundation for future studies, but also seems to be sufficiently accurate for the interpretation of experimental data.

For each isotopologue of each molecule considered in this study, we optimized the structure and calculated the frequencies of all fundamental vibrational modes based on the second derivative of the potential energy surface. We then used the reduced partition function ratio in the harmonic approximation (Urey, 1947; Bigeleisen and Mayer, 1947) to calculate equilibrium constants for homogeneous isotope exchange reactions involving isotopologues of interest:

$$\frac{Q^*}{Q} = \left(\frac{m^*}{m}\right)^{\frac{3r}{2}} \frac{\sigma}{\sigma^*} \prod_i \frac{\nu_i^*}{\nu_i} \frac{e^{-U_i^*/2}}{e^{-U_i/2}} \frac{1 - e^{-U_i}}{1 - e^{-U_i^*}} \tag{1.1}$$

$$U = h\nu_i / k_b T \tag{1.2}$$

where * indicates the isotopically-substituted species, m is mass, sigma is symmetry factor, ν is vibrational frequency, T is temperature, k_b is the Boltzmann constant, and h is Planck's constant. The product operator in equation 1 combines contributions from all of the different fundamental vibrational modes (i.e. 9 for methane). And, we may calculate the equilibrium constants for homogeneous isotope exchange reactions by combining two or more expressions of the form of 1.1. For example, consider the reaction:

$$^{13}\mathrm{CH_4} + ^{12}\mathrm{CH_3D} = ^{13}\mathrm{CH_3D} + ^{12}\mathrm{CH_4} \tag{1.3}$$

The equilibrium constant for this reaction (K) may be calculated as a function of the partition functions for each reactant and product species (Q_i), resulting in an expression that is simply the ratio of two equations of the form of 1.1:

$$K = \frac{Q_{^{13}\mathrm{CH_3D}}}{Q_{^{13}\mathrm{CH_4}}} \frac{Q_{^{12}\mathrm{CH_4}}}{Q_{^{12}\mathrm{CH_3D}}} = \frac{(Q^*/Q)_{^{13}\mathrm{CH_4}}}{(Q^*/Q)_{^{12}\mathrm{CH_4}}} \tag{1.4}$$

where the * in this case describes D substitution.

An equation such as 1.4 may be evaluated at any of a range of temperatures, yielding an estimate of the temperature dependence of the equilibrium constant for each reaction such as Equation 3. Finally, we combined these calculated equilibrium constants with assumed bulk isotopic contents (i.e., summing across all isotopologues) and principles of

mass balance to solve for the expected relative abundances of various isotopolgues as a function of temperature (i.e., following principles laid out in Wang, Schauble, and Eiler (2004) and Chacko, Cole, and Horita (2001)).

1.3 Results

Methane

Figure 1.1a illustrates that several of the computational methods that we explored result in predicted fundamental mode vibrational frequencies for methane that closely match those measured by spectroscopy (Stein, 2015)(Figure 1.1), including several of its isotopologues (Table 1.1). Agreement is generally best below 3200 cm^{-1}, and worst for previous studies (Ma, Wu, and Tang, 2008). The closest fits between calculated and measured frequencies are seen for the most computationally-intensive methods, including the coupled cluster model and DFT B3LYP 6-311G** models. Frequencies calculated with these models, including previous studies and the less computationally heavy models, yield predicted equilibrium constants for isotope exchange equilibria of interest that are closely similar to those calculated using measured frequencies (though note that all such calculations assume the harmonic approximation, so their agreement does not assure accuracy). Because we see no evidence that small systematic errors in predicted vibration frequencies lead to significant effects on calculated fractionation factors, we use the modeled frequencies as-is rather than modifying them with a scaling factor. There may be reasons for such empirical corrections to our models, but we conclude that they are

T (K)	Methane		Ethane				Propane			
	$^{13}CH_3D$	$^{12}CH_2D_2$	$^{13}CH_3$-$^{13}CH_3$	$^{13}CH_2D$-$^{12}CH_3$	$^{12}CHD_2$-$^{12}CH_3$	$^{12}CH_2D$-$^{12}CH_2D$	$^{12}CH_3$-$^{13}CH_2$-$^{12}CH_3$	$^{12}CH_3$-^{12}CHD-$^{12}CH_3$	$^{12}CH_3$-^{13}CHD-$^{12}CH_3$	$^{12}CH_3$-^{13}CHD-$^{12}CH_3$
250	7.56	28.45	0.33	7.09	25.01	1.54	18.56	130.81	159.15	6.39
300	5.66	19.08	0.21	5.31	17.32	1.06	13.44	93.20	113.18	4.85
350	4.36	13.12	0.14	4.10	12.20	0.74	9.83	68.69	83.28	3.79
400	3.42	9.22	0.09	3.23	8.73	0.53	7.35	52.04	62.96	3.01
450	2.73	6.62	0.07	2.58	6.35	0.38	5.56	40.34	48.67	2.43
500	2.20	4.84	0.05	2.09	4.69	0.28	4.26	31.89	38.33	1.97

Table 1.1: K_{eq} for different isotopologues as a function of T

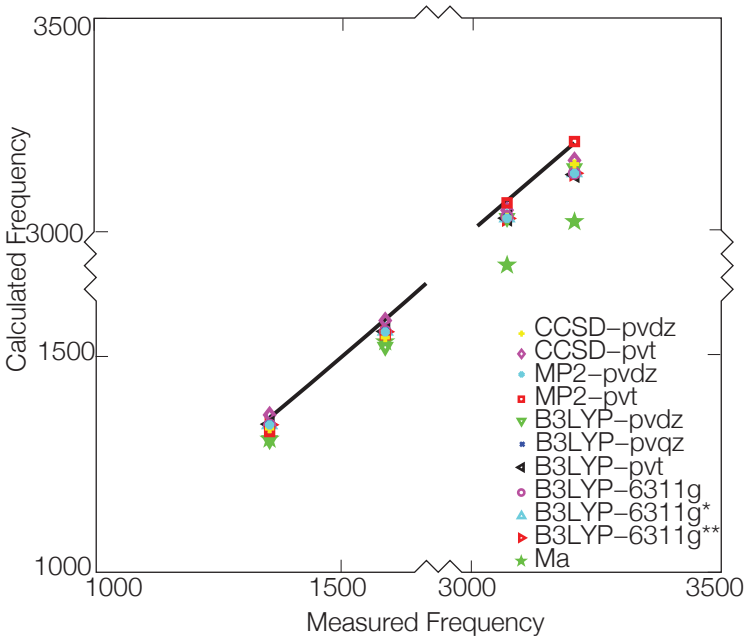

(a) Methane

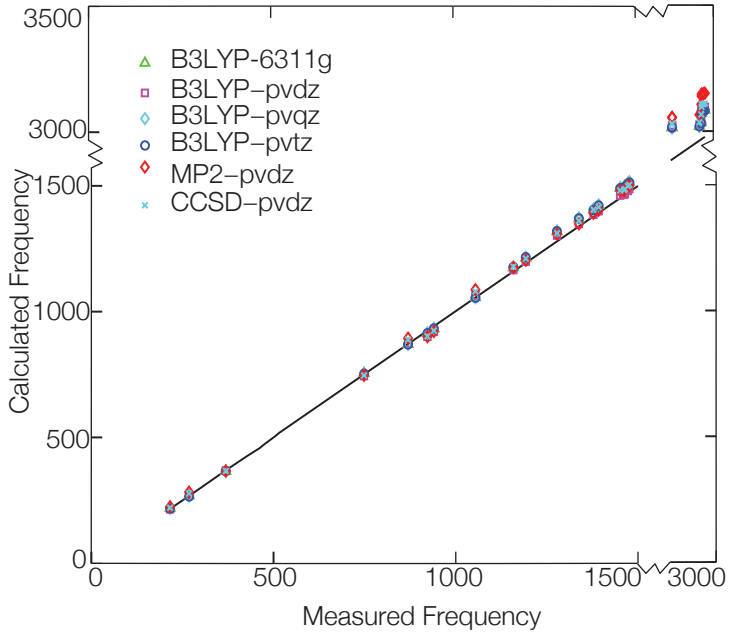

(b) Propane

Figure 1.1: A comparison of fundamental mode frequencies for methane and propane, either measured or calculated using different methods and basis sets; all values are for the non-isotopically substituted molecule. The 1:1 line is shown in black.

unnecessary and would add an additional layer of complexity that potentially obfuscates comparison of our results with related future modeling efforts.

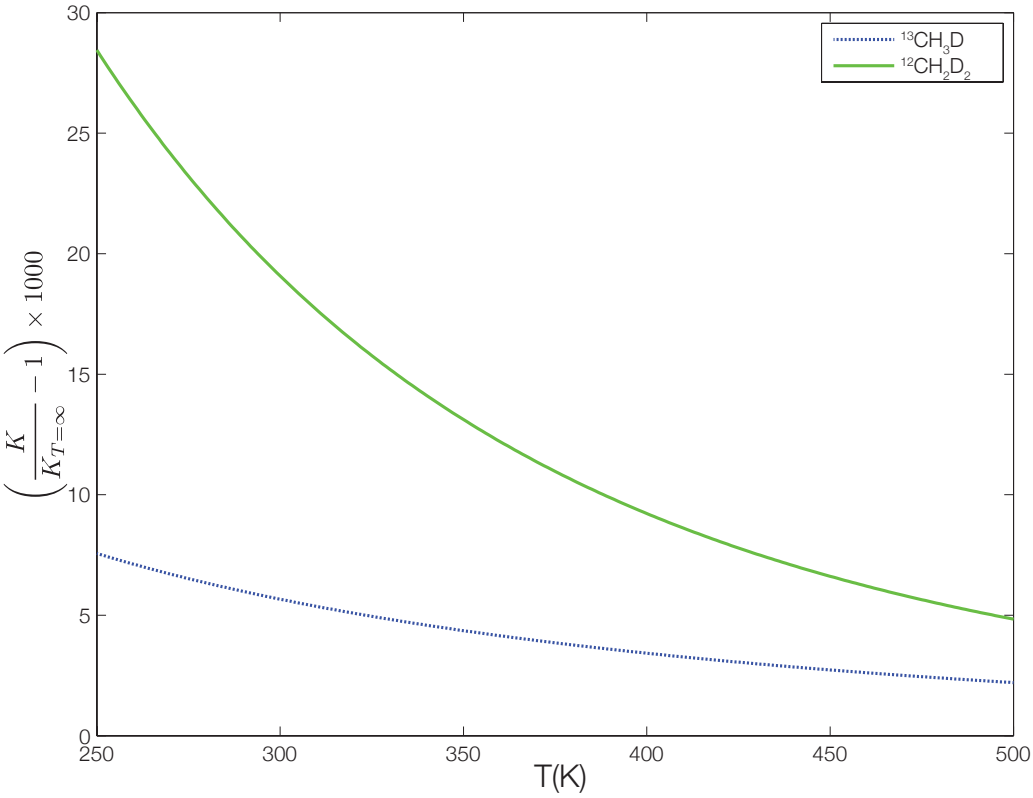

Figure 1.2: Difference from the high temperature (stochastic) limit for equilibrium constants associated with forming for two different clumped isotope species of methane.

Figure 1.2 represents predicted equilibrium fractionation as a function of temperature for two representative methane clumping reactions. This result predicts an enrichment in the abundance of the doubly-substituted (^{13}C and D) species (above the amount expected for a random distribution of isotopes among all isotopologues) of approximately 6‰ at 300K. This result agrees within plausible experimental errors (est ±0.1‰) with predictions based on spectroscopic data, the model calculations of Ma, Wu, and Tang (2008) and Webb and Miller (2014); and, we obtain essentially indistinguishable results for models using different basis sets. This is an instance in which many of the differences

between predicted and measured vibration frequency (Figure 1.1) cancel out when one calculates equilibrium constants for homogeneous exchange reactions, leading to negligible differences in K_{eq}. Another way of describing this finding is that small variations in the frequencies of the fundamental modes matter less than the differences between the isotopologues for each frequency (Ma, Wu, and Tang, 2008; Webb and Miller, 2014). Given that our results are the same as other DFT models, as well as those confirmed by more rigorous path integral methods, we are confident in this result.

The calculated proportions of methane isotopologues presented in Figures 1.2 may be compared with experimental data generated using the new analytical techniques of high-resolution gas source isotope ratio mass spectrometry (Stolper et al., 2014a) and IR absorption spectroscopy (Ono et al., 2014). The modeled isotope exchange equilibria presented here may also be compared with measured clumped isotope compositions of natural samples, as one means of evaluating whether natural methane achieves internal isotopic equilibrium and, if so, at what conditions and through what mechanisms (Stolper et al., 2014a). Methane driven to a time-invariant equilibrium by heating in the presence of catalysts takes on a range of clumped isotope compositions that vary with temperature as predicted in Figure 1.2 (Stolper et al., 2014a; Ono et al., 2014). Similarly, natural samples having well known formation temperatures, and methane produced by experimental 'cracking' of kerogens or propane, all exhibit clumped isotope compositions consistent with this model. Thus, it appears that this theoretical model supports the interpretation of these data as reflecting equilibrium at different temperatures, and provides a useful basis for interpolation and extrapolation of experimental data. Finally, studies of biogenic methane in culture and some surface environments indicates large departures from

the equilibrium stable isotope distribution (Stolper et al., 2014a; Stolper et al., 2014b; Ono et al., 2014). In these cases, a theoretical model such as that presented in Figure 1.2 can provide a reference frame that helps one identify kinetic isotope effects, mixing effects and/or other non-equilibrium isotopic fractionations.

	300K	400K	500K	600K	700K	800K	900K	1000K
$^{12}CH_3D$	1.06	1.04	1.04	1.04	1.04	1.04	1.04	1.04
$^{12}CH_2D_2$	21.23	11.33	6.93	4.81	3.71	3.11	2.76	2.54
$^{12}CHD_3$	61.10	30.92	17.65	11.28	8.00	6.19	5.13	4.49
$^{12}CD_4$	122.22	60.06	33.19	20.40	13.83	10.22	8.12	6.85
$^{13}CH_4$	0.02	0.02	0.02	0.02	0.02	0.02	0.02	0.02
$^{13}CH_3D$	6.74	4.49	3.26	2.53	2.07	1.77	1.57	1.43
$^{13}CH_2D_2$	32.77	18.23	11.36	7.78	5.77	4.56	3.81	3.32
$^{13}CHD_3$	78.99	41.41	24.33	15.74	11.07	8.36	6.70	5.64
$^{13}CD_4$	147.26	74.35	42.18	26.37	17.93	13.11	10.21	8.38

Table 1.2: Δ_i for different isotopologues of methane as a function of T

Figure 1.3 shows the deviation from stochastic of all methane isotopologues, reported as Δ_i values for each species, i, calculated following expressions such as:

$$\Delta_{^{13}CH_3D} = \left(\frac{\frac{[^{13}CH_3D]}{[^{12}CH_4]}}{\frac{[^{13}CH_3D]_{stoch}}{[^{12}CH_4]_{stoch}}} - 1 \right) \times 1000 \tag{1.5}$$

where subscript 'stoch' indicates the high-temperature stochastic isotope distribution.

In all cases, we calculated abundances of each isotopologue following the methods of (Wang, Schauble, and Eiler, 2004), which combine constraints from all independent isotope exchange equilibria and mass balance (i.e., closure) at some specified bulk isotopic content. We chose for our set of independent isotope exchange equilibria all those reactions that have one multiply substituted isotopologue plus some combination of $^{12}CH_4$, $^{13}CH_4$, and $^{12}CH_3D$ as reactants and/or products. We constructed a matrix of equations

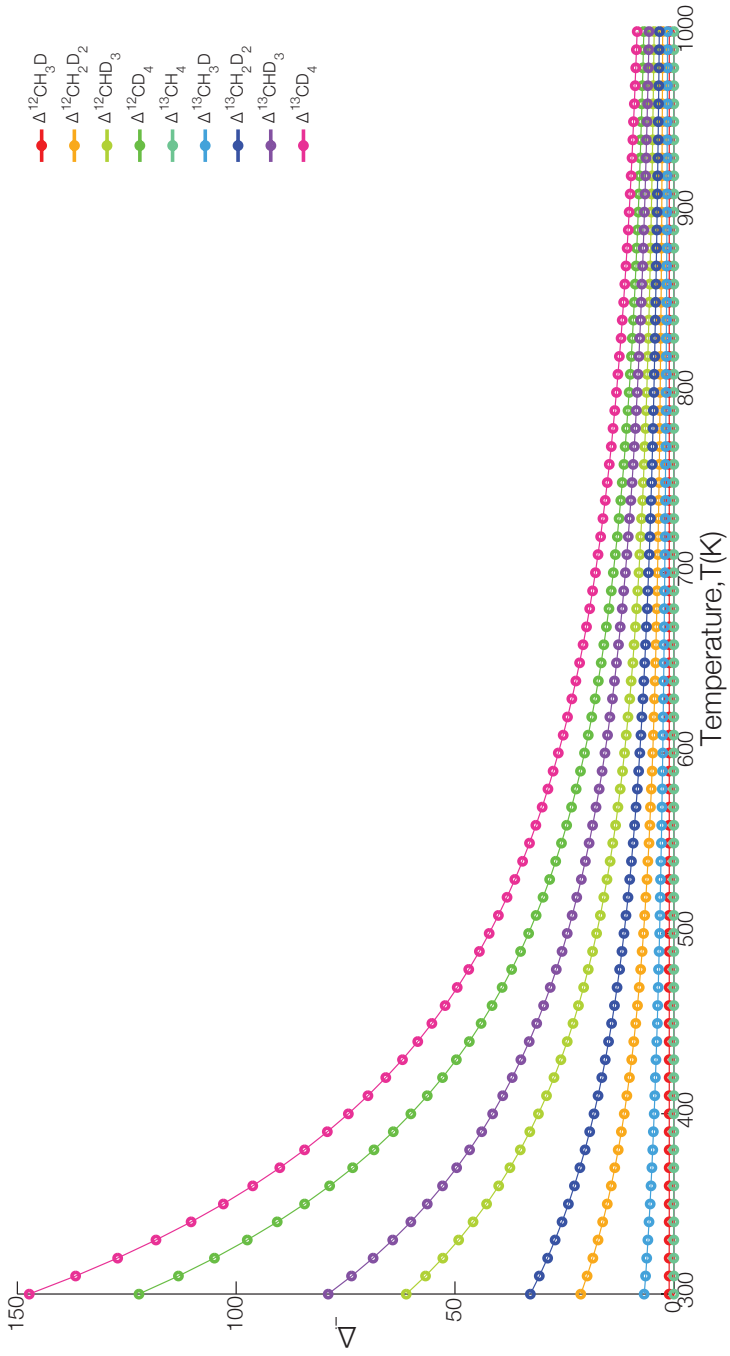

Figure 1.3: The deviation from a stochastic distribution for all of the isotopologues of methane, assuming complete homogeneous equilibrium and a gas having a D/H of VSMOW and $^{13}C/^{12}C$ of PDB. $^{12}CH_4$ is not shown because it is used as a reference for calculating proportions and anomalies of the other species (so, its anomaly is axiomatically 0, in the plotted units).

including these equilibrium constant expressions (evaluated at some specified temperature), and added expressions defining mass balance assuming a total inventory of D and ^{13}C equivalent to the VSMOW and PDB standards, respectively. The results of this calculation indicate that enrichments in multiply substituted species relative to a stochastic distribution generally increase with decreasing temperature for any one species, and that at any one temperature, such anomalies increase with the number of heavy isotope substitutions and, for a given number of substitutions, are always greater for multiple deuterations than for ^{13}C+D substitutions (e.g., Δ_i for $^{12}CHD_3$ is greater than for $^{13}CH_2D_2$). Where our model calculations reproduce the subset of species considered in previous studies, the estimates agree within a narrow range (Stolper et al., 2014a; Ono et al., 2014).

Ethane

It is challenging to compute the frequencies of fundamental modes for the coupled rotational/vibrational dynamics of ethane due to complications in the mutual rotation of two methyl groups with respect to each other–the so-called hindered rotor (Lorant et al., 2001). The results for ethane were only calculated for the basis set verified by both methane and propane, as it was deemed adequate for those molecules. A more extensive comparison was not done since there are complications due to the large effect of the hindered rotor on ethane (Speybroeck et al., 2005). Results indicated that the B3LYP with 6-311G** basis set was adequate, and all results given are for that method and basis set.

Figure 1.4 illustrates the calculated proportions of ethane isotopologues at thermo-

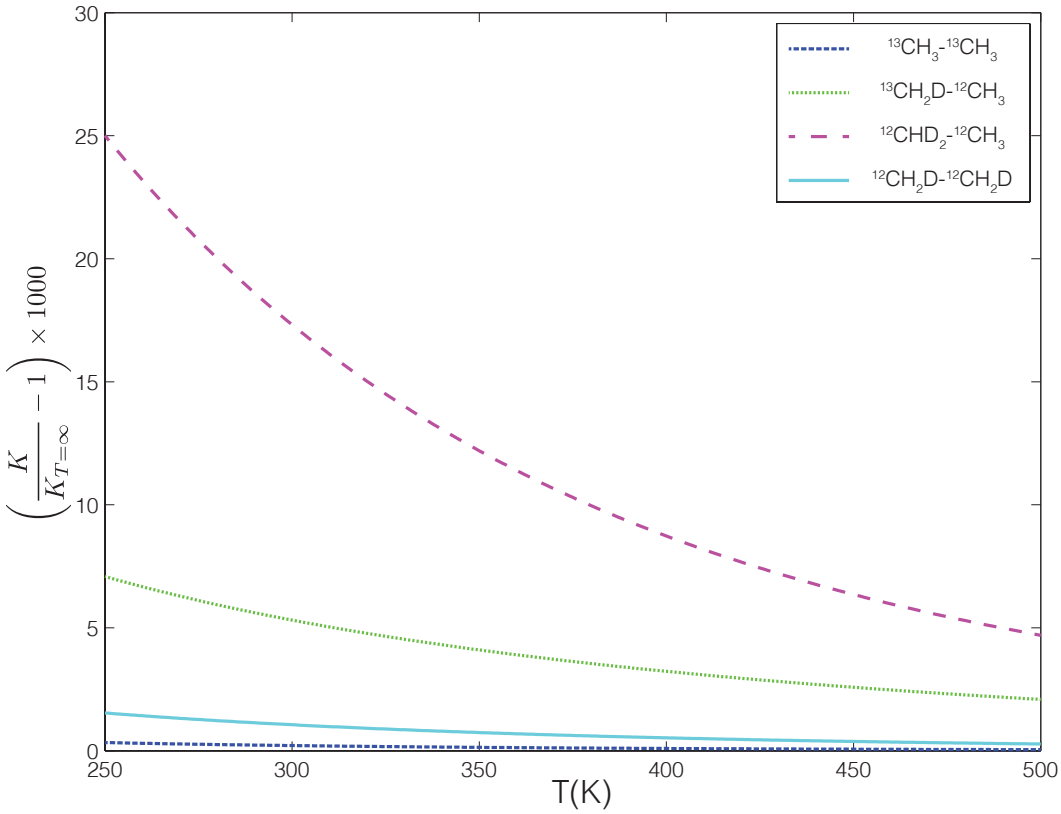

Figure 1.4: The deviation from the high temperature (i.e., stochastic) limit of the equilibrium constant for reactions that form the four listed clumped isotopologues of ethane.

dynamic equilibrium for a representative range of temperatures (250 to 500 K). All are shown as deviation from the high temperature limit of the equilibrium constant, on a per-mil scale similar to the methane Δ_i value, but without imposing mass balance constraints from all of the isotopologues because we have not presented results for all of the many possible ethane isotopologues. In any event, all of the equilibrium constants evaluated in this study favor stabilization of the clumped species (e.g., $^{13}CH_3$-$^{13}CH_3$) in amounts in excess of the stochastic abundance, and that all such excesses decrease monotonically with increasing temperature. We find that the double ^{13}C substitution exhibits only a relatively small excess (0.3‰ at 300 K). The species that contain both ^{13}C and D in the same methyl group of ethane exhibit a temperature-dependent enrichment broadly sim-

ilar in magnitude and temperature sensitivity to the equilibrium enrichment of $^{13}CH_3D$ methane. Based on the size of this effect and prior success at measuring $^{13}CH_3D$ at sub-per mil precision, we suspect a high-resolution mass spectrometric or spectroscopic technique could be used to study $^{13}CH_2D$-$^{12}CH_3$ in natural ethane. The double substitution of deuterium in the same methyl group of an ethane molecule exhibits an even larger excess of approximately a 10‰ at 300 K, again decreasing with increasing temperatures (Figure 1.4). However, both ^{13}C-D and D-D double substitutions that involve separation of the rare isotopes into separate halves of the ethane molecule lead to negligibly weak excesses relative to a stochastic distribution.

Methods of high-resolution gas source isotope ratio mass spectrometry have been used to explore the equilibrium constant for the reaction:

$$2 \times^{13} C^{12}CH_6 =^{13} C_2H_6 +^{12} C_2H_6 \tag{1.6}$$

in various experimental and natural gases. These data are so-far presented only in conference proceedings, so we simply review their general findings. The most striking finding is the large range in $\Delta^{13}C_2H_6$ of natural ethanes relative to that expected by equilibrium fractionations. Enrichments of $^{13}C_2H_6$ relative to a stochastic distribution vary by 5‰, or more than 10x the full range of equilibrium temperature dependence. Clog et al. have suggested that this large range reflects a range of factors: kinetic isotope effects during ethane generation from precursors, the sampling statistics associated with cleaving a C-2 group from an organic precursor that has site-specific differences in $\delta^{13}C$, and perhaps kinetic isotope effects associated with destruction of ethane through some

form of secondary cracking. While there is as yet no definitive interpretation for the cause of these variations (and it is possible that natural variability reflects a variety of processes), Clog et al. find evidence that values of $\Delta^{13}C_2H_6$ generally decrease with decreasing ethane abundance and increasing $^{13}C/^{12}C$ ratio, and that similar trends can be observed in experiments in which ethane is disproportionated at high temperatures and low pressures. This suggests that the $\Delta^{13}C_2H_6$ value of natural ethane is controlled by kinetic isotope effects associated with its production and, especially, destruction, and clearly violate expectations of thermodynamic equilibrium. It seems likely to us that this measurement will not provide a method of quantitative thermometry analogous to the methane clumped isotope thermometer, but may be useful as a proxy for destruction of ethane through secondary 'cracking.'

There is experimental evidence to suggest that other homogeneous isotope exchange reactions among isotopologues of ethane may have simpler behaviors and more straightforward interpretations in natural materials. Reeves et al. demonstrate that ethane undergoes hydrogen isotope exchange with water in the presence of catalysts in both natural gas and experimental systems (Reeves, Seewald, and Sylva, 2012). While this work does not precisely define the rate constants for such reactions, it seems clear that isotopic exchange of the C-H bonds in ethane occurs over time scales of months in the laboratory at 300°C and over geological time scales at the temperatures of common petroleum generating systems. This suggests that homogeneous isotope exchange equilibria involving exchange of D for H (i.e., $\Delta^{13}CH_2D$-$^{13}CH_3$) may reach thermodynamic equilibrium in natural systems. If so, 'clumping' of ^{13}C with D in ethane may potentially serve as a geothermometer in natural systems, in a fashion analogous to clumped isotope

thermometry of methane.

Propane

Propane yields some of the most interesting and potentially useful results of the small alkanes examined in this study, both because of the relatively large number and diversity of isotopologues (including site-specific fractionations) and because some of the intramolecular isotopic variations have quite large magnitudes (up to 100‰). The reactions we considered look at the equilibrium isotope effect of moving a heavy carbon atom from the terminal position to the central position of the propane molecule, the same movement for a deuterium, and the site-specific clumping of ^{13}C and/or deuterium in the center, terminal or both sites.

We present results of calculations for four reactions that were explored in detail for this study. Two of these are relatively straightforward; they examine cases where the reactant has rare heavy isotope (i.e. D or ^{13}C) in one of the two terminal CH_3 groups, and the product has that same rare isotope in the center CH_2 group. These reactions examine the strength of position specific fractionation, in isolation from other (clumping) effects. The third reaction that we examine is also relatively straightforward: it considers a $^{12}CH_3$-^{12}CHD-$^{12}CH_3$ reacting with $^{12}CH_3$-$^{13}CH_2$-$^{12}CH_3$ to make $^{12}CH_3$-^{13}CHD-$^{12}CH_3$ and $^{12}CH_3$-$^{12}CH_2$-$^{12}CH_3$ (i.e., clumping in the center position, separate from any site-specific preferences). Finally, we show the temperature-dependent equilibrium constant for one of many possible homogeneous exchange reactions that involve combination of rare heavy isotopes from one site (terminal ^{13}C and D, in separate molecules) to make

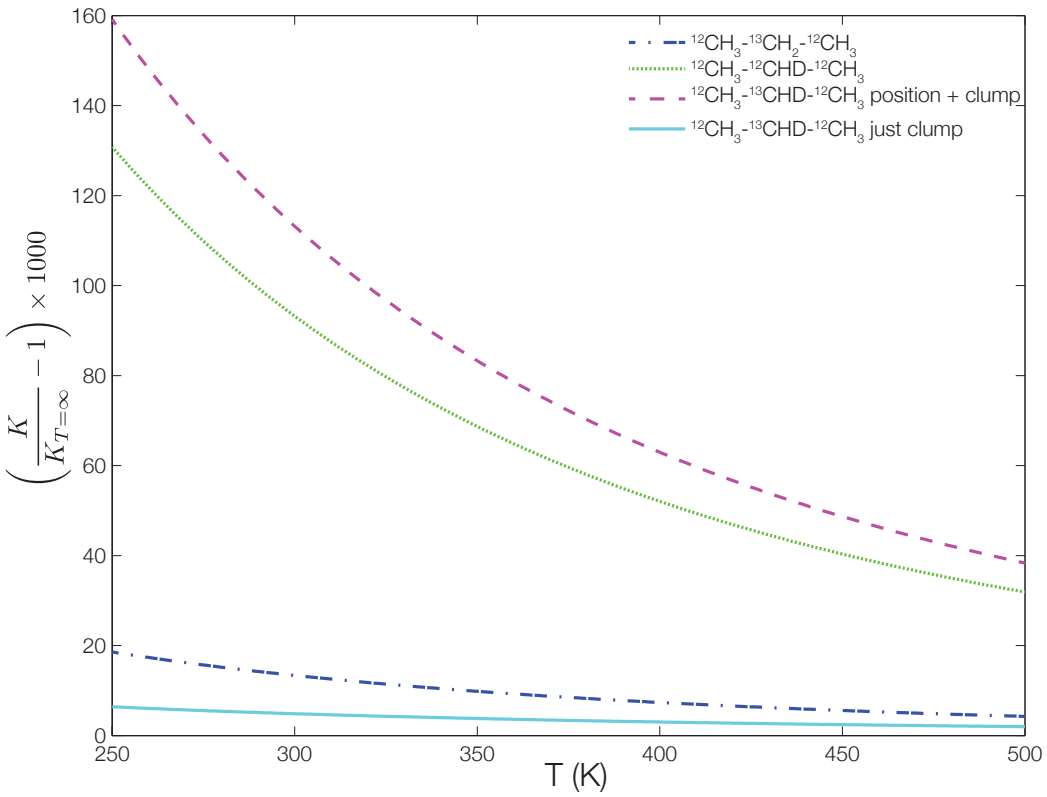

Figure 1.5: The deviation from the high temperature limit of the equilibrium constant for reactions that either concentrate heavy isotopes into the center CH_2 group of propane, or clump ^{13}C and D together relative to single substitutions in the same site, or combine all three effects to form the species with a ^{13}CHD central group, at the expense of propanes with single ^{13}C or D substitutions in terminal groups.

a clumped isotope species having heavy rare isotopes in a different position (a ^{13}CHD group in the center). This reaction effectively combines the site-specific ^{13}C and D effects with the preference for 'clumping'; perhaps unsurprisingly, it exhibits the strongest enrichments relative to a stochastic distribution of any reaction presented here. Figure 1.5 shows the temperature dependence of the equilibrium constants of these four reactions, expressed as deviations in per mil from the mass action constants for those reactions at 1000K (effectively random). We find that deuterium exhibits a strong preference to be concentrated in the center CH_2 group (approximately 90‰ at 300K). Similarly, ^{13}C exhibits a roughly 10x lower preference for the center position (10‰ at 300 K). ^{13}C-D

clumping in the center CH2 group, considered alone (i.e., compared to abundances of species with the single substitutions in the center CH_2 group) is relatively weak $\sim 5‰$ at 300 K. This effect is similar in magnitude to ^{13}C-D clumping in methane, and in the same CH_3 group in ethane. Finally, the abundance of the propane with a ^{13}CHD center group has a very strong enrichment relative to its given reactants (115‰ at 300 K), effectively combining the three effects described above.

Ongoing studies are currently looking at the site-specific carbon isotopes of propane (see other chapters of this thesis). Prior studies of the bulk carbon isotope geochemistry of natural propane lead to the expectation that the carbon isotope distribution within propane is likely controlled by kinetic effects associated with 'cracking' reactions, rather than thermodynamic equilibrium. Nevertheless, the equilibrium calculations we present are valuable as a reference point for recognizing and modeling kinetic effects (just as the equilibrium ^{13}C-D clumping in methane serves as a reference frame for discussing vital effects associated with biological methanogenesis). It is less clear what we should expect regarding the distribution of deuterium in propane. Previous experience with the clumped isotope thermometer in methane (Stolper et al., 2014b), and experiments examining the rates of hydrogen isotope exchange between propane and other compounds (Reeves, Seewald, and Sylva, 2012), could be taken as suggestive evidence that the site-specific distribution of D in propane could record its temperatures of synthesis, or perhaps temperatures of storage in petroleum reserves. For these reasons, the site-specific D distribution in propane is an attractive target for possible studies of basin thermal histories and petroleum storage temperatures. Prior work suggesting larger alkanes undergo relatively rapid H/D exchange with environmental water (Reeves, Seewald, and Sylva, 2012)

lead us to expect such a tool would be particularly useful as a storage temperature proxy. Another strength of this possible tool is that even relatively low precision measurements (say, 1-2‰) might still yield precise temperature estimates because of the nearly 90‰ range in $\Delta_{^{12}CH_3-^{13}CHD-^{12}CH_3}$ over geologically-relevant temperatures.

A potential caveat to the equilibrium constants for propane, as well as the other gases, is that they are conducted within the gas phase. In geologic systems at elevated pressures and temperatures, propane is not frequently in the gas phase. There could be serious vapor pressure effects that are being ignored by this study, since all calculations are gas phase. In the future it would be beneficial to look at propane with solvation shells of differing properties that would explore the range found in nature representing environments from methane, to oil producing, to shale gas settings still rich with larger organic molecules. These potential complications are not explored in this study but are worth noting, however since results have been experimentally confirmed for methane there is hope that the order of magnitude and sign will still be geologically relevant.

1.4 Discussion

Comparison to prior theoretical models

Wang, Schauble, and Eiler (2004) present the first study published in the modern era (i.e., subsequent to the basic papers on principles of the chemical physics of isotope exchange equilibria) to examine clumped isotope exchange equilibria and discuss their relevance for studies of natural materials. That work focused on di-atomic and tri-atomic

molecules of C, N and O (principally because these are the only sorts of species suitable for clumped isotope measurements using the low-resolution gas source isotope ratio mass spectrometers available at that time). This study emphasized the combination of spectroscopically measured, rather than calculated, fundamental mode vibration frequencies. Schauble, Ghosh, and Eiler (2006) and Eagle, Schauble, and Tripati (2010) built on this start by presenting models of isotopic clumping in carbonate ion groups in carbonate bearing minerals and aqueous solutions; these studies more closely resemble our work in that they used ab initio models to predict the frequencies of vibration of the species of interest before turning to Urey-Bigeleisen-Meyer treatments of the partition function ratio. In any event, these studies do not consider the n-alkanes, so they are similar to this work in methodology and conceptual goals but provide no direct points of comparison.

Ma, Wu, and Tang (2008) present the first model of clumped isotope equilibria in methane. Their results closely resemble those we present here, at least for the homogenous isotope exchange reactions presented in both work (Ma, Wu, and Tang, 2008). Ma, Wu, and Tang (2008) focused on $^{13}CH_3D$ clumping in methane, and did not present models of other larger alkanes or other methane isotopologues. Although their calculated fundamental mode frequencies are further from the measured spectroscopic values than those presented here (especially at the higher frequency fundamental modes; Figure 1.1), the overall calculated enrichment in $^{13}CH_3D$ relative to a stochastic distribution at a given temperature is essentially the same as presented in this study.

Webb and Miller (2014) present a set of first principles models for equilibrium constants of select homogeneous isotope exchange equilibria involving several molecules, including methane and propane. That paper presents models based on DFT calculations

of frequencies of molecular fundamental modes, and then calculates equilibrium constants for reactions of interest using one of several methods: Urey-Bigeleisen-Meyer theory in the harmonic approximation; a similar level of theory using anharmonic corrections; and the path integral (PI) method (Webb and Miller, 2014). The path integral method has the advantage of explicitly addressing anharmonic portions of the wave function without simplifying assumptions; thus, it provides a relatively accurate means of exploring systematic errors that may result from approximations made in lower level theoretical treatments (such as the approach used here). The results presented by Webb and Miller generally agree with those that we present for the molecules and isotopologues considered by both studies. The studies can be compared only for three species: $^{13}CH_3D$ methane and the site-specific ^{13}C and D preferences in propane. Our results agree with those of Webb and Miller to within 5%, relative, site-specific deuterium and carbon substitution (they did not compute the combined effect). Webb and Miller suggest that path integral methods agreed with lower levels of theory due to the relatively modest importance of anharmonic terms in the partition functions of these compounds; so, it is perhaps not surprising that ours study agrees with their path integral models as well.

Two previous studies provide some indication of the potential for extending the approaches adopted in this study to consider the complex set of homogeneous isotope exchange reactions that can occur among singly and multiply substituted isotopologues of larger organic molecules. One challenge of such work is that it is generally not possible to test the accuracy of a model of molecular structure, potentials and fundamental mode frequencies through direct comparison with spectroscopy. Wang et al. (2009a) and Wang et al. (2009b) addressed this problem by comparing the predictions of models broadly sim-

ilar in structure to those presented here against the measured equilibrium constants for heterogeneous isotope exchange reactions between organic compounds and water. This comparison could be made only for exchangeable hydrogen sites in ketones, but they argued that this anchor of experimental validation could serve as a basis for extrapolating the model predictions to the unconstrained, unexchangeable sites. The rapid advances being made in methods for measuring intramolecular isotopic variations may soon enable direct study of many or all of the sites in such compounds, possibly testing, refining and extending Wang et al.'s analysis, including clumped and position-specific equilibria analogous to those we explore for propane, above. In addition, the order of magnitude of the isotopic effect that they measured between water and alkanes is the same as for many site-specific D substitutions within our study. Similarly, Rustad (2009) presents a DFT-based model of the site-specific carbon isotope fractionations among non-equivalent sites in several amino acids, and compare those predictions to experimental observations of some features of the carbon isotope structures of biosynthetic amino acids (Abelson and Hoering, 1961; Macko et al., 1987). It is not clear whether any of the experimental observations constrain equilibrium isotope distributions, so this body of work does not yet constitute an example of experimentally-tested ab initio models of these phenomena. Nevertheless, it is easy to imagine extending this foundation to consider diverse clumped and position specific equilibria that may be measurable using emerging mass spectrometric and NMR techniques.

Application to future work

The results from this work could be used to predict many of the homogeneous isotope exchange equilibria recorded by the small n-alkanes; the limited instances in which these phenomena have been observed in nature and experiment suggest that they could be used to constrain conditions of natural formation processes (e.g., methane clumped isotope thermometry), perhaps storage temperature, and the mechanisms of kinetically-controlled reactions that may produce or consume these compounds (e.g., as is suspected for some biogenic methane and most or all thermogenic ethane and propane). Regardless of the controls of any given isotopic species or equilibrium constant of interest, it is useful to have the equilibrium distribution as a reference frame with which we compare our natural and experimental results. And, even when one property of a molecule is controlled by chemical-kinetic or other non-equilibrium processes (e.g., carbon isotopes in ethane and propane), other isotopic properties of those same molecules (e.g., ^{13}C-D clumping or site-specific D/H fractionations) might be controlled by exchange equilibria (Reeves, Seewald, and Sylva, 2012). One of the potential strengths of the study of intramolecular isotopic distributions is the great diversity of isotopic species of any one compound - some of which might record one process, and others another.

1.5 Conclusions

Using well-established DFT techniques and Urey-Bigeleisen-Meyer theories of vibrational isotope effects, we predict the isotopic distributions within populations of methane, ethane or propane, including clumped and position-specific effects, over a range of tem-

peratures relevant to geological and planetary problems. These calculations allow us to create an equilibrium framework for interpretation of data produced by emerging techniques for the measurement of multiply substituted and position-specific isotopologues, and to explore topics such as thermometry, isotopic structures inherited from substrates (and thus formation pathways), and kinetic degradation of molecules. Some of the simplest and most useful of these tools are thermometers based on temperature-dependent homogeneous isotope exchange equilibria, some of which exhibit large amplitudes compared to demonstrated analytical precisions (e.g., site-specific D distribution in propane). These geochemical tools are already demonstrably impacting the study of natural sources of methane, ethane and propane (Stolper et al., 2014b; Clog et al., 2013; Piasecki and Eiler, 2012). Extension of these methods to additional isotopologues of these small alkanes, and to other organic compounds generally, promises to advance our understanding of a variety of applied problems related to energy resources, associated pollution, biological sources and sinks of these compounds, and atmospheric chemistry of hydrocarbons, among other subjects.

1.6 Data Appendix

12CH4	12CH3D	12CH2D2	12CHD3	12CD4	13CH4	13CH3D	13CH2D2	13CHD3	13CD4
1339.5148	1182.22061	1047.3421	1021.0211	1012.7644	1331.1883	1174.1780	1040.7320	1010.874	1003.873
1339.5188	1182.29	1111.3252	1049.5553	1012.769	1331.1921	1174.2463	1101.4668	1043.7572	1003.8774
1339.6627	1334.1025	1260.1413	1049.6233	1012.8744	1331.3353	1326.9005	1252.8905	1043.8244	1003.9824
1557.5513	1496.6053	1348.9516	1312.2239	1101.7782	1557.5513	1495.5779	1348.9516	1309.9586	1101.7782
1557.5975	1496.6557	1460.6532	1312.2481	1101.81099	1557.5975	1495.6279	1458.5736	1309.9834	1101.8109
3026.7426	2270.6433	2225.5055	2182.4821	2141.0527	3026.7426	2259.4184	2218.3551	2179.0331	2141.0527
3131.9902	3057.1478	2318.6154	2318.5783	2318.4838	3120.8564	3053.5704	2302.6785	2302.6109	2302.4859
3132.0571	3131.7249	3084.1759	2318.5821	2318.5436	3120.9213	3120.5562	3077.6487	2302.6138	2302.5443
3132.06109	3131.7892	3131.4659	3108.5636	2318.5484	3120.9259	3120.6190	3120.2615	3099.51069	2302.5477

Table 1.3: Methane frequencies B3LP-6311G**

12CH4	12CH3D	12CH2D2	12CHD3	12CD4	13CH4	13CH3D	13CH2D2	13CHD3	13CD4
1342.0705	1184.2398	1048.571	1022.7424	1014.309	1333.7773	1176.2333	1012.6172	1012.6172	1005.4527
1342.0705	1184.2398	1113.4295	1050.6822	1014.309	1333.7773	1176.2333	1044.9328	1044.9328	1005.4527
1342.0705	1336.1727	1262.0986	1050.6822	1014.309	1333.7773	1329.03400	1044.9329	1044.9329	1005.4527
1557.5527	1496.9849	1349.0523	1312.9561	1101.7792	1557.5527	1495.9484	1310.6903	1310.6903	1101.7792
1557.5527	1496.9851	1461.3200	1312.95620	1101.7792	1557.5527	1495.9485	1310.6903	1310.6903	1101.7792
3054.0769	2304.7332	2253.8146	2205.9645	2160.3883	3054.0769	2293.3824	2202.5389	2202.5389	2160.3883
3186.7374	3093.0698	2359.9535	2359.9371	2359.9204	3175.2905	3089.2204	2343.5614	2343.5614	2343.5219
3186.7374	3186.51879	3127.2808	2359.9371	2359.9204	3175.2905	3175.0414	2343.5614	2343.5614	2343.5219
3186.7374	3186.5187	3186.2979	3157.9493	2359.9204	3175.2905	3175.0414	3148.5454	3148.5454	2343.5219

Table 1.4: Methane frequencies coupled cluster

12CH3-12CH3	12CH3-12CH2D	12CH3-12CHD2	12CH3-12CD3	12CH2D-12CH2D	12CH2D-12CHD2	12CH2D-12CD3	12CHD2-12CHD2	12CHD2-12CD3
309.2128	290.1702	277.2133	268.0086	269.1059	255.5076	245.6648	240.5124	230.0754
827.1915	719.2883	688.5515	682.4818	662.6675	638.1793	625.412	609.5765	603.5857
827.1920	811.4636	742.1944	682.4818	797.7368	726.317	673.7458	695.6577	637.5682
995.8152	980.8065	948.961	907.0679	909.4009	903.188	886.6204	874.3352	866.5072
1217.4675	1136.188	1100.6659	1082.9299	1070.5758	1030.4283	1004.4029	978.0775	977.7952
1217.4689	1181.048	1129.6337	1082.9313	1150.613	1093.8759	1082.777	1059.377	1023.1049
1407.5719	1324.5110	1140.7487	1130.1297	1298.4133	1121.2355	1083.1017	1086.7841	1075.3997
1422.9456	1334.5744	1329.1297	1130.1311	1310.8095	1294.9185	1096.5826	1130.6947	1083.0219
1503.3298	1415.6469	1329.9185	1134.8680	1339.0664	1320.5192	1134.6628	1283.3966	1087.8063
1503.3302	1481.2810	1415.7284	1415.4785	1350.5462	1331.3154	1321.0895	1323.1867	1147.1021
1505.5228	1504.2302	1503.4034	1503.1808	1478.8393	1350.2642	1323.2518	1337.2166	1317.9568
1505.5244	1504.3882	1504.0406	1503.1819	1484.2849	1481.4156	1481.1574	1351.4925	1330.3801
3022.8919	2244.4229	2207.6532	2172.0682	2240.7723	2207.6388	2172.0241	2207.5517	2171.8926
3023.0016	3022.9445	2282.6541	2282.6129	2247.9852	2243.6875	2243.489	2207.7037	2207.5506
3068.4951	3042.3479	3022.9425	2282.6140	3039.1954	2283.2943	2282.6025	2274.8818	2274.85
3068.4951	3068.2993	3057.9657	3022.9405	3048.5758	3043.2937	2283.4683	2290.3004	2282.7882
3093.5241	3082.6048	3081.1597	3081.1581	3068.105	3059.5118	3043.9067	3053.9355	2290.2892
3093.5259	3093.3813	3085.8402	3081.159	3093.2352	3084.601	3080.8216	3071.6311	3062.8631
12CD3-12CD3	13CH3-12CH3	13CH3-12CH2D	13CH3-12CHD2	13CH3-12CD3	13CH2D-12CH3	13CH2D-12CH2D	13CH2D-12CHD2	13CH2D-12CD3
218.7305	309.2128	290.1702	277.2133	268.0086	290.0992	269.0314	255.4311	245.5891
597.8401	826.3310	718.7998	688.5515	682.4818	717.4456	661.7018	637.8286	625.0947
597.8405	826.3315	810.7616	741.3902	682.4818	809.8863	796.4162	725.2951	673.6920
845.1802	980.5642	966.1151	935.8286	894.2747	968.9284	901.7433	894.9845	877.2273
977.4650	1209.2773	1127.5029	1099.1692	1082.8453	1128.3687	1057.2651	1019.8878	995.1291
977.4673	1209.2784	1174.57	1120.1504	1082.8467	1171.0995	1141.9881	1089.0698	1082.7562
1074.9070	1401.3712	1323.607	1133.3632	1120.7207	1314.3443	1293.4954	1113.9349	1083.0994
1074.9081	1418.9930	1332.44	1326.9640	1120.722	1334.5385	1309.3136	1291.3008	1084.8786
1075.7483	1502.62910	1405.4538	1329.9010	1131.8706	1415.5455	1333.5726	1314.2177	1131.5383
1091.4156	1502.6297	1481.2402	1405.5056	1405.2619	1478.1849	1350.2035	1330.3241	1310.3338
1091.4176	1504.319	1502.3892	1501.5273	1501.2985	1503.9024	1476.9267	1348.7594	1322.8495
1165.9169	1504.3204	1502.7463	1502.3440	1501.2995	1504.1660	1482.8371	1478.1098	1477.8119
2169.0171	3019.6311	2244.4054	2207.6297	2172.0374	2232.1578	2230.9778	2207.6093	2171.9980
2175.0862	3022.9497	3019.6325	2282.6412	2282.6001	3022.9430	2245.5259	2231.576	2231.4065
2274.818	3061.855	3041.8013	3019.6304	2282.6012	3036.3121	3035.12089	2283.1678	2282.5889
2274.8180	3061.8551	3061.7301	3055.2939	3019.6280	3061.5607	3046.3811	3037.1779	2283.3074
2290.2764	3089.1111	3072.1028	3070.1145	3070.1129	3082.3710	3061.4371	3056.8606	3037.6399
2290.2788	3089.1127	3088.8973	3077.4609	3070.1138	3089.0225	3088.806	3076.0079	3069.7323

Table 1.5: Ethane frequencies part 1

13CHD2-12CH3	13CHD2-12CH2D	13CHD2-12CHD2	13CHD2-12CD3	13CD3-12CH3	13CD3-12CH2D	13CD3-12CHD2	13CD3-12CD3	13CH3-13CH3
277.1757	255.4659	240.4668	230.0338	268.0086	245.6644	230.0752	218.7305	309.2128
686.3415	637.0625	609.0062	603.0231	679.6694	624.0519	602.7079	596.9805	825.5081
739.5969	724.0044	693.8981	637.0906	679.6694	671.1164	635.7795	596.9809	825.5086
942.3434	896.8387	868.2268	859.6440	904.2273	882.4126	861.8392	840.3161	965.0267
1091.0698	1024.3333	971.7776	971.4797	1079.7411	999.2214	970.8968	970.5164	1201.0844
1125.5092	1086.0615	1051.1189	1010.9271	1079.7425	1078.3097	1018.2242	970.51869	1201.0856
1128.4751	1108.1583	1083.1249	1072.0617	1113.0248	1079.7918	1072.1014	1069.0093	1398.0811
1323.625	1291.8876	1119.9449	1083.0219	1125.51489	1093.6814999	1079.6965	1073.2025	1412.1556
1326.5844	1320.2320	1280.1011	1086.1274	1125.5163	1113.3789	1084.3796	1073.2034	1502.2657
1415.6195	1327.6198	1321.28009	1140.5256	1415.4227	1320.5951	1130.1777	1089.8243	1502.2673
1503.2488	1346.9749	1335.78240	1311.2683	1503.06	1322.5118	1316.9984	1089.8262	1502.7136
1503.8571	1481.3340	1347.9422	1327.04289	1503.0610	1481.1025	1330.3792	1152.2648	1502.7139
2198.8258	2198.8137	2198.7867	2171.8645	2166.4449	2166.4133	2166.3285	2165.3877	3019.4695
2266.5405	2243.1500	2207.6314	2198.7444	2266.4594	2242.7743	2207.3960	2173.0673	3019.7997
3022.9414	2267.7285	2263.2516	2263.2361	2266.4605	2266.44950	2263.1718	2263.1559	3057.5758
3050.3472	3042.7379	2285.8516	2282.7766	3022.9395	2268.0315	2266.7255	2263.1563	3057.576
3081.1547	3052.2716	3048.4992	2285.8240	3081.1529	3043.9043	2285.8481	2285.8191	3082.337
3084.5979	3083.5340	3068.2069	3054.0068	3081.1538	3080.8164	3062.8593	2285.8211	3082.3386
13CH3-13CH2D	13CH-13CHD2	13CH3-13CD3	13CH2D-13CH2D	13CH2D-13CHD2	13CH2D-13CD3	13CHD2-13CHD2	13CHD2-13CD3	13CD3-13CD3
290.0991	290.0991	268.0086	268.9583	256.0930	245.5887	240.4224	230.0336	218.7305
716.9819	716.9819	679.6684	660.803	659.7242	623.7625	608.46	602.1749	596.1579
809.2327	809.2327	679.6684	795.1616	677.3024	671.07619	692.2566	635.3425	596.1583
953.8214	953.8214	890.8649	893.6195	927.7505	872.7025	861.7383	854.6780	835.1553
1119.8107	1119.8107	1079.7411	1044.1676	1009.6255	989.7622	965.4103	964.5252	963.5093
1164.5993	1164.5993	1079.7424	1133.3861	1080.9873	1076.1411	1042.4341	1006.0648	963.5113
1313.4057	1313.4057	1110.3282	1289.5017	1090.8436	1079.7745	1080.1220	1069.3861	1064.1548
1332.3714	1332.3714	1116.0006	1307.6990	1295.1262	1084.10449	1109.3013	1079.6858	1072.0055
1405.3960	1405.3960	1116.0019	1327.0736	1315.8697	1110.3892	1276.4546	1082.9236	1072.0063
1478.1302	1478.1302	1405.2447	1349.86	1328.134	1309.9404	1319.8106	1122.6967	1087.7085
1502.0464	1502.04649	1501.1637	1476.0008	1332.74669	1322.0808	1333.9141	1310.3589	1087.7104
1502.5008	1502.5008	1501.1647	1480.3934	1477.9953	1477.7515	1344.41439	1327.0399	1136.8212
2232.1442	2232.1442	2166.4207	2227.9013	2198.2303	2166.3932	2197.9861	2166.3116	2164.1320
3019.6313	3019.6313	2266.4495	2236.355	2232.6691	2230.996	2199.6039	2198.6026	2168.6871
3035.9304	3035.9304	2266.4506	3032.9657	2266.5194	2266.4389	2258.3769	2258.3200	2258.2631
3057.3564	3057.3564	3019.6273	3042.2674	3035.4856	2267.5711	2274.6502	2266.7033	2258.2631
3071.7039	3071.7039	3070.1068	3057.1392	3056.0758	3037.6374	3045.1831	2274.6239	2274.5958
3082.17349	3082.17349	3070.1077	3082.0064	3069.7273	3069.7262	3062.6622	3054.0025	2274.5981

Table 1.6: Ethane frequencies part 2

12C3H8	12D-12-12	12-12D-12	12D-12-12D	12D-12D-12	12D-12D-12D	13-12-12
219.3189	201.6949	219.3109	193.0109	203.684	192.9547	219.2095
269.3751	259.6141	265.563	238.0138	251.0344	233.9672	269.2007
366.3376	355.1954	364.2611	345.7721	354.1229	344.1714	363.4938
755.0908	707.1277	670.0738	701.7004	666.3457	632.5083	754.9941
870.5537	843.4579	807.7772	757.5706	745.8056	743.8138	862.0243
914.6184	869.2711	866.2395	838.9774	814.3914	779.6125	912.906
933.0299	915.3735	929.0753	889.1911	898.5716	860.8621	930.0292
1057.1314	1051.0626	1003.4322	1030.2639	997.4969	993.9076	1051.0451
1175.4568	1131.1886	1148.3138	1098.5922	1100.4731	1053.9955	1169.8268
1213.4906	1175.5615	1168.3591	1152.6273	1154.0877	1100.0131	1208.6722
1319.0383	1292.2171	1184.3088	1266.8491	1162.34	1148.3676	1316.259
1369.3555	1313.4902	1348.3862	1295.2029	1299.5495	1290.1581	1368.0138
1406.3648	1337.9457	1350.1473	1314.6127	1314.4061	1312.0082	1399.6396
1422.791	1379.8585	1405.0679	1331.9951	1349.5027	1315.4208	1418.9911
1491.5498	1415.2113	1422.7455	1344.4797	1359.4848	1316.9894	1490.632
1494.1528	1475.4962	1491.1184	1381.1325	1412.1838	1351.637	1493.8946
1499.4081	1495.5279	1498.2997	1475.493	1479.6059	1366.6836	1498.5524
1509.0365	1502.0424	1508.0278	1478.3994	1498.4392	1475.8498	1508.3569
1515.3801	1510.8227	1508.3642	1502.5856	1501.4584	1480.2208	1514.8226
3013.9862	2237.7277	2225.9348	2236.0338	2223.7342	2222.9757	3012.2467
3014.6985	3014.0343	3014.695	2245.3294	2245.8973	2236.6842	3013.9135
3018.5641	3016.7095	3018.2585	3012.247	3014.4507	2245.9889	3017.5694
3034.3976	3031.3726	3025.1715	3029.1419	3022.642	3021.9612	3033.1451
3071.6452	3045.7754	3071.6369	3034.0794	3034.0185	3034.0147	3064.6628
3081.2045	3076.8782	3077.7729	3043.6455	3069.2456	3040.3227	3071.6119
3083.4092	3081.6486	3081.2034	3074.4354	3075.4304	3072.6852	3080.6538
3084.0759	3083.7942	3083.992	3080.2381	3080.3257	3077.4898	3082.851
12-13-12	13-12-13	13-13-12	13-13-13	13-12D-12	13D-12-12	12-13D-12
219.3189	219.1008	219.2094	218.5816	219.2025	201.6623	219.3109
268.3813	269.0256	268.1976	267.5184	265.4017	259.3918	264.8599
363.7852	360.568	360.9754	357.9102	361.445	352.9509	361.8401
753.0813	754.8986	752.9997	752.1743	669.9405	705.9717	666.5485
863.8396	854.0201	855.1462	846.1821	807.0128	841.4774	807.7416
914.6184	911.2196	912.9046	910.241	857.8053	860.366	859.9761
932.118	927.106	929.0314	925.1193	926.506	911.588	928.5099
1042.0737	1044.5597	1035.9461	1028.4603	997.4179	1046.4976	996.9997
1164.9599	1164.064	1159.317	1152.2844	1143.039	1127.5047	1142.7803
1202.4964	1204.0638	1197.6753	1191.2832	1164.4581	1168.4107	1154.3559
1319.0383	1313.2406	1316.247	1311.3625	1179.4127	1288.7412	1171.968
1355.8808	1366.6336	1354.5515	1351.2956	1347.5618	1309.6448	1340.4777
1405.2656	1395.9336	1398.6777	1392.9297	1348.7431	1332.6095	1342.9281
1422.7475	1412.1612	1418.8839	1410.2325	1398.3229	1379.242	1404.5945
1491.5498	1489.7901	1490.6289	1488.0458	1418.8944	1415.1062	1422.6989
1492.3006	1493.6976	1492.1519	1490.143	1490.1062	1472.449	1491.1171
1498.6528	1497.6683	1497.7264	1494.601	1497.276	1495.5043	1497.7874
1508.5096	1507.6032	1507.8063	1505.1976	1507.2875	1501.9152	1507.5198
1512.5563	1514.2235	1511.8951	1508.9415	1507.6587	1510.7061	1507.9606
3008.138	3011.3824	3007.9497	3005.9833	2225.917	2225.5588	2212.7658
3014.6962	3013.1503	3012.4314	3009.5295	3012.373	3013.8854	3014.6927
3018.4311	3015.6804	3017.4011	3013.1987	3017.2382	3016.6615	3016.7574
3025.0928	3032.0682	3024.2814	3021.4817	3024.5897	3027.8812	3018.6243
3071.6452	3060.5911	3064.1776	3058.4082	3063.2954	3042.8194	3071.6369
3081.2043	3070.1687	3071.5048	3067.8628	3071.0439	3069.6204	3077.3685
3081.5937	3073.4739	3078.882	3069.7114	3076.1674	3079.1902	3081.2031
3083.8725	3074.8123	3082.7185	3070.7233	3082.701	3082.8042	3083.6187

Table 1.7: Propane frequencies part 1

12D-13-12	12D-13-12D	13-12-12D	13-12D-13	12D2-12-12	12-12D2-12	13D3-13D2-13D3
201.6315	188.0313	201.4916	219.0948	187.8286	218.7829	156.0461
258.6903	245.7407	259.4594	265.2398	251.3272	262.1763	196.9009
352.9079	341.1947	352.345	358.5488	345.7498	362.1111	299.0081
706.0755	681.5008	707.1059	669.8025	700.907	627.0952	546.8846
840.8582	786.6781	842.245	806.4014	758.6611	780.7974	665.2821
863.4092	862.9254	860.7745	849.7416	842.9454	844.1091	693.2522
914.6642	864.0757	913.1286	923.9879	892.7139	852.6407	727.1805
1037.133	1028.266	1045.4102	991.2039	1030.3589	970.064	853.0676
1121.2015	1093.0521	1124.7669	1138.2872	1092.6706	1080.655	955.1666
1165.8111	1123.6387	1171.97	1160.14	1132.5999	1104.6408	967.7143
1290.8826	1261.2461	1288.3287	1174.1282	1159.7085	1159.0237	989.1879
1310.5912	1289.7802	1312.5244	1346.5315	1287.6045	1181.9228	1056.0132
1337.1117	1319.5455	1337.2115	1347.4652	1321.2398	1218.0137	1071.9525
1367.3329	1330.4999	1378.8761	1394.4977	1334.0978	1402.3718	1073.7402
1414.5943	1348.1413	1404.9175	1412.1374	1372.8574	1420.7259	1075.1867
1475.4336	1373.6287	1475.2466	1489.1719	1412.3976	1489.0059	1080.8892
1493.5476	1475.1608	1494.8481	1496.3806	1493.5238	1495.0317	1092.243
1501.6876	1479.2152	1500.587	1506.4107	1498.791	1505.2929	1131.7304
1507.878	1498.9816	1509.8937	1506.8727	1507.9587	1505.5063	1175.7728
2237.7138	2236.8998	2237.7275	2225.8993	2203.3338	2193.6937	2158.8926
3008.2465	2238.528	3012.5781	3011.3782	2279.6104	2255.7953	2161.8891
3016.5039	3008.4189	3014.6604	3014.8915	3012.8624	3012.8317	2182.8105
3024.3363	3023.3567	3030.7029	3024.0443	3014.7455	3016.4352	2232.8085
3043.0818	3040.1588	3044.4113	3060.5862	3032.3994	3069.4305	2258.1025
3076.2116	3046.9358	3068.8317	3067.3476	3055.4204	3072.3428	2264.3852
3081.1517	3081.0027	3071.6938	3070.1682	3076.6489	3078.8827	2265.4528
3083.3785	3081.2732	3082.0079	3073.6712	3080.2811	3079.798	2266.1487

Table 1.8: Propane frequencies part 2

References

Abelson, P H and T C Hoering (1961). "Carbon Isotope Fractionation in the Formation of Amino Acids by Photosynthetic Organisms." English. In: *Proceedings of the National Academy of Sciences of the United States of America* 47.5, p. 623. URL: http://www.ncbi.nlm.nih.gov/pmc/articles/PMC221413/.

Becke, Axel D (1993). "Density-functional thermochemistry. III. The role of exact exchange." English. In: *The Journal of Chemical Physics* 98.7, p. 5648. DOI: 10.1063/1.464913. URL: http://scitation.aip.org/content/aip/journal/jcp/98/7/10.1063/1.464913.

Bigeleisen, Jacob and Maria Goeppert Mayer (1947). "Calculation of Equilibrium Constants for Isotopic Exchange Reactions." English. In: *The Journal of Chemical Physics* 15.5, p. 261. DOI: 10.1063/1.1746492. URL: http://scitation.aip.org/content/aip/journal/jcp/15/5/10.1063/1.1746492.

Chacko, Thomas, David R Cole, and Juske Horita (2001). "Equilibrium Oxygen, Hydrogen and Carbon Isotope Fractionation Factors Applicable to Geologic Systems." English. In: *Reviews in Mineralogy and Geochemistry* 43.1, pp. 1–81. DOI: 10.2138/gsrmg.43.1.1. URL: http://rimg.geoscienceworld.org/content/43/1/1.full.

Clog, M et al. (2013). "Doubly 13C-substituted ethane." English. In: *Mineralogical Magazine* 77.5, pp. 805–933. URL: http://openurl.ingenta.com/content/xref?genre=article&issn=0026-461X&volume=77&issue=5&spage=805.

DeNiro, M J and S Epstein (1977). "Mechanism of carbon isotope fractionation associated with lipid synthesis." English. In: *Science* 197.4300, pp. 261–263. DOI: 10.1126/science.327543. URL: http://www.sciencemag.org/cgi/doi/10.1126/science.327543.

Eagle, R A, Edwin A Schauble, and A K Tripati (2010). "Body temperatures of modern and extinct vertebrates from 13C-18O bond abundances in bioapatite." In: *Proceedings of the National Academy of Sciences*. DOI: 10.1073/pnas.0911115107/-/DCSupplemental. URL: http://www.pnas.org/content/107/23/10377.short.

Eiler, J et al. (2014). "Isotopic Anatomies of Organic Compounds." In: *Goldschmidt Conference*.

Gilbert, Alexis, Keita Yamada, and Naohiro Yoshida (2013). "Exploration of intramolecular ^{13}C isotope distribution in long chain n-alkanes (C_{11}-C_{31}) using isotopic ^{13}C NMR." In: *Organic Geochemistry* 62.C, pp. 56–61. DOI: 10.1016/j.orggeochem.2013.07.004. URL: http://dx.doi.org/10.1016/j.orggeochem.2013.07.004.

Kendall, Rick A, Thom H Dunning, and Robert J Harrison (1992). "Electron affinities of the first-row atoms revisited. Systematic basis sets and wave functions." English. In:

The Journal of Chemical Physics 96.9, p. 6796. DOI: 10.1063/1.462569. URL: http://scitation.aip.org/content/aip/journal/jcp/96/9/10.1063/1.462569.

Lorant, François et al. (2001). "Ab Initio Investigation of Ethane Dissociation Using Generalized Transition State Theory." English. In: *The Journal of Physical Chemistry A* 105.33, pp. 7896–7904. DOI: 10.1021/jp004094a. URL: http://pubs.acs.org/doi/abs/10.1021/jp004094a.

Ma, Qisheng, Sheng Wu, and Yongchun Tang (2008). "Formation and abundance of doubly-substituted methane isotopologues (." In: *Geochimica et Cosmochimica Acta* 72.22, pp. 5446–5456. DOI: 10.1016/j.gca.2008.08.014. URL: http://dx.doi.org/10.1016/j.gca.2008.08.014.

Macko, S A et al. (1987). "Isotopic fractionation of nitrogen and carbon in the synthesis of amino acids by microorganisms." English. In: *Chemical Geology: Isotope Geoscience Section* 65.1, pp. 79–92. DOI: 10.1016/0168-9622(87)90064-9. URL: http://linkinghub.elsevier.com/retrieve/pii/0168962287900649.

Monson, K D and J M Hayes (1980). "Biosynthetic control of the natural abundance of carbon 13 at specific positions within fatty acids in Escherichia coli. Evidence regarding the coupling of fatty acid and phospholipid synthesis." English. In: *Journal of Biological Chemistry* 255.23, pp. 11435–11441. URL: http://www.jbc.org/content/255/23/11435.abstract.

Ono, Shuhei et al. (2014). "Measurement of a Doubly Substituted Methane Isotopologue, 13CH 3D, by Tunable Infrared Laser Direct Absorption Spectroscopy." English. In: *Analytical Chemistry* 86.13, pp. 6487–6494. DOI: 10.1021/ac5010579. URL: http://pubs.acs.org/doi/abs/10.1021/ac5010579.

Piasecki, A and J Eiler (2012). "Direct Mass Spectrometric Analysis of Position Specific δ^{13}C in Organics." In:

Reeves, Eoghan P, Jeffrey S Seewald, and Sean P Sylva (2012). "Hydrogen isotope exchange between n-alkanes and water under hydrothermal conditions." English. In: *Geochimica et Cosmochimica Acta* 77, pp. 582–599. DOI: 10.1016/j.gca.2011.10.008. URL: http://linkinghub.elsevier.com/retrieve/pii/S0016703711005953.

Rustad, James R (2009). "Ab initio calculation of the carbon isotope signatures of amino acids." English. In: *Organic Geochemistry* 40.6, pp. 720–723. DOI: 10.1016/j.orggeochem.2009.03.003. URL: http://linkinghub.elsevier.com/retrieve/pii/S0146638009000643.

Schauble, Edwin A, Prosenjit Ghosh, and J Eiler (2006). "Preferential formation of 13C–18O bonds in carbonate minerals, estimated using first-principles lattice dynamics." English. In: *Geochimica et Cosmochimica Acta* 70.10, pp. 2510–2529. DOI: 10.1016/j.gca.2006.02.011. URL: http://linkinghub.elsevier.com/retrieve/pii/S0016703706000913.

Scott, A P and L Radom (1996). "Harmonic vibrational frequencies: an evaluation of Hartree-Fock, Møller-Plesset, quadratic configuration interaction, density functional theory, and semiempirical scale factors." English. In: *The Journal of Physical Chemistry* 100.41, pp. 16502–16513. DOI: 10.1021/jp960976r. URL: http://pubs.acs.org/doi/abs/10.1021/jp960976r.

Speybroeck, V Van et al. (2005). "Why does the uncoupled hindered rotor model work well for the thermodynamics of n-alkanes?" English. In: *Chemical Physics Letters*

402.4-6, pp. 479–484. DOI: 10.1016/j.cplett.2004.12.104. URL: http://linkinghub.elsevier.com/retrieve/pii/S000926140402010X.

Stein, S.E. (2015). *NIST Chemistry WebBook, NIST Standard Reference Database Number 69*. Ed. by W.G. Mallard P.J. Linstrom. National Institute of Standards and Technology.

Stolper, D A et al. (2014a). "Combined 13C-D and D-D clumping in methane: Methods and preliminary results." English. In: *Geochimica et Cosmochimica Acta* 126, pp. 169–191. DOI: 10.1016/j.gca.2013.10.045. URL: http://adsabs.harvard.edu/cgi-bin/nph-data_query?bibcode=2014GeCoA.126..169S&link_type=EJOURNAL.

Stolper, D A et al. (2014b). "Formation temperatures of thermogenic and biogenic methane." English. In: *Science* 344.6191, pp. 1500–1503. DOI: 10.1126/science.1254509. URL: http://www.sciencemag.org/cgi/doi/10.1126/science.1254509.

Urey, Harold C (1947). "The thermodynamic properties of isotopic substances." English. In: *Journal of the Chemical Society (Resumed)* 0, pp. 562–581. DOI: 10.1039/jr9470000562. URL: http://xlink.rsc.org/?DOI=jr9470000562.

Wang, Ying et al. (2009a). "Equilibrium 2H/ 1H fractionations in organic molecules: I. Experimental calibration of ab initio calculations." English. In: *Geochimica et Cosmochimica Acta* 73.2, pp. 7060–7075. DOI: 10.1016/j.gca.2009.08.019.

— (2009b). "Equilibrium 2H/ 1H fractionations in organic molecules. II: Linear alkanes, alkenes, ketones, carboxylic acids, esters, alcohols and ethers." English. In: *Geochimica et Cosmochimica Acta* 73.2, pp. 7076–7086. DOI: 10.1016/j.gca.2009.08.018.

Wang, Zhengrong, Edwin A Schauble, and J Eiler (2004). "Equilibrium thermodynamics of multiply substituted isotopologues of molecular gases." English. In: *Geochimica et Cosmochimica Acta* 68.23, pp. 4779–4797. DOI: 10.1016/j.gca.2004.05.039. URL: http://linkinghub.elsevier.com/retrieve/pii/S001670370400451X.

Webb, Michael A and Thomas F Miller (2014). "Position-Specific and Clumped Stable Isotope Studies: Comparison of the Urey and Path-Integral Approaches for Carbon Dioxide, Nitrous Oxide, Methane, and Propane." English. In: *The Journal of Physical Chemistry A* 118.2, pp. 467–474. DOI: 10.1021/jp411134v. URL: http://pubs.acs.org/doi/abs/10.1021/jp411134v.

Chapter 2

Analysis of the site-specific carbon isotope composition of propane by gas source isotope ratio mass spectrometry

Abstract

Site-specific isotope measurements potentially provide valuable information about the formation and degradation of complex molecules–information that is lost in conventional bulk isotopic measurements. Here we present a technique for studying the site-specific carbon isotope composition of propane, based on mass spectrometric analysis of fragment ions. We demonstrate the feasibility of this approach through measurements of mixtures of natural propane and propane synthesized with a site-specific ^{13}C enrichment, and we document the limits of precision of our technique. We further demonstrate the accuracy of the technique by measuring the site-specific carbon isotope fractionation associated with gas phase diffusion of propane, confirming that our measurements conform to the predictions of the kinetic theory of gases. Finally, we show that mass balance calculations of the bulk δ^{13}C of propane based on our site-specific measurements is generally consistent

with independent constraints on bulk $\delta^{13}C$. This method can be applied to propane samples of moderate size (tens of micromoles) isolated from natural gases. Thus, it provides a means of studying the site-specific stable isotope systematics of the natural geochemistry of propane. This method may also serve as a model for future techniques that apply high-resolution gas source mass spectrometry to study the site-specific isotopic distributions in larger organic molecules, with potential applications to biosynthesis, forensics and other geochemical subjects.

2.1 Introduction

The naturally-occurring stable isotopes are widely used to constrain problems in the natural and applied sciences; e.g., paleothermometry, geochemical budgets, and forensic identification (Snell et al., 2014; Eiler et al., 2000; Lamprecht and Pichlmayer, 1994). Such work focuses on the stable isotopes of light elements (D, ^{13}C, ^{15}N, ^{18}O, etc.) in simple volatile compounds (H_2, N_2, CO_2), measured using gas source isotope ratio mass spectrometry. These techniques require that most analytes must be chemically converted to such simple volatile molecules; a common example is carbon isotope analysis of organics, which is often accomplished by oxidation to yield CO_2 that is then analyzed by mass spectrometry for its $^{13}CO_2/^{12}CO_2$ ratio.

Such measurements constrain the compound-specific isotopic content for that analyte, averaged over all positions within its molecular structure. This approach necessarily obscures intramolecular variations in isotopic content. For example, there is evidence that adjacent carbon positions within fatty and amino acids can differ from one

another in $^{13}C/^{12}C$ ratio by up to 30‰ (Abelson and Hoering, 1961; DeNiro and Epstein, 1977; Monson and Hayes, 1980). Such differences reflect isotope effects associated with biosynthetic pathways, and potentially serve as forensic identifiers and/or records of metabolic strategy, environmental conditions, stress, and perhaps other information. Large, structurally complex molecules potentially record a number of equilibrium and kinetic processes in their isotopic anatomies, perhaps 'fingerprinting' the organism from which they are derived, processes and pathways involved in their creation, as well as local environmental variables like temperature, or potentially even more obscure environmental variables like humidity and oxidation state. Whatever these intramolecular variations might record, analytical techniques that yield bulk isotopic content obviously result in the loss of information. Larger organic molecules suffer the most from these techniques. Similarly, conventional methods based on chemical conversion of analytes to H_2 or CO_2 also destroy any information that might be recorded by the abundances of multiply substituted (or 'clumped') isotopologues.

A variety of methods have been developed to observe intramolecular isotopic distributions, including position-specific and multiple substitutions. 'Clumping' or multiple substitution, has been studied in several molecules, including (but not limited to) CO_2, ethane, N_2O, O_2 and methane (Schauble, Ghosh, and Eiler, 2006; Stolper et al., 2014a; Yeung, Ash, and Young, 2014; Magyar et al., 2012; Clog et al., 2013; Stolper et al., 2014b).These measurements have been enabled by innovations in gas source isotope ratio mass spectrometry, including detector arrays configured with high-sensitivity detectors for quantification of the low-intensity multiply-substituted ion beams, and a prototype instrument with a high-resolution, double-focusing analyzer capable of mass resolving iso-

baric interferences such as $^{13}CH_4$ vs. $^{12}CH_3D$ or $^{15}N^{14}N^{16}O$ vs. $^{14}N_2^{17}O$. (Note that some measurements of this kind may also be possible using IR absorption spectroscopy (Ono et al., 2014)). Measurements of site-specific isotopic substitutions have been attempted using several approaches; the earliest work of this kind used chemical techniques to isolate carbon from specific moieties from organic compounds. For example, Abelson and Hoering (1961) decarboxylated amino acids to measure the $\delta^{13}C$ of their CO_2H groups (Abelson and Hoering, 1961; Macko et al., 1987), and Monson and Hayes degraded fatty acids with a combination of ozonolysis and decarboxylation to analyze the site-specific ordering of ^{13}C (Monson and Hayes, 1980; Monson and Hayes, 1982). Advancements in the sensitivity and stability of NMR have led to 'SNIF-NMR' techniques that determine natural abundances of stable isotopes in organic structures (Singleton and Szymanski, 1999). These techniques are so-far capable of observing only singly-substituted isotopologues and require large sample sizes (100's of mgs), but have proven effective at recognizing even subtle (per mil level) differences among sugars, alkanes and other compounds (Gilbert, Yamada, and Yoshida, 2013). Gas source isotope ratio mass spectrometry has been used to measure site-specific ^{15}N distribution in N_2O, based on comparison of the ^{15}N content of the N_2O^+ molecular ion and the NO^+ fragment ion (Toyoda and Yoshida, 1999; Westley, Popp, and Rust, 2007). Finally, IR absorption spectroscopy techniques have proven capable of precisely measuring site-specific ^{15}N distribution in N_2O (Uehara et al., 2003).

Here we extend the concepts behind the mass spectrometric analysis of site-specific isotopic compositions of N_2O to the problem of ^{13}C distributions in organics, using a high-resolution IRMS instrument, the Thermo 253 Ultra, to mass resolve isobaric interferences

that commonly occur in the mass spectra of hydrocarbons (Eiler et al., 2012). We focus on propane, which is among the smallest and simplest organic molecules that could record site-specific carbon isotope variations. And, there are reasons to believe such differences could give rise to useful geochemical tools: most natural propane is derived from thermal degradation ('cracking') of components of kerogen, which itself derives from catagenesis of biosynthetic compounds, like fatty acids, that are known to possess site-specific carbon isotope variations (DeNiro and Epstein, 1977; Monson and Hayes, 1982; Monson and Hayes, 1980). Thus, propane could inherit an isotopic structure from its precursors, and/or record the mechanisms and conditions of cracking reactions. In addition, propane is destroyed in natural environments through thermal degradation, biological consumption, and atmospheric photo-oxidation, (Berner et al., 1995; Clayton, 1991; Hinrichs et al., 2006; Takenaka et al., 1995) all of which could impart a distinctive signature on the site-specific carbon isotope content of residual propane.

This paper describes the methods, including limits of precision and accuracy, of a new mass spectrometric technique for site-specific carbon isotope analysis of propane. We include measurements of natural propanes and products of experiments, but focus here on simple tests of the measurement technique. A companion paper (chapter 3 of the thesis) presents fuller interpretations of these and other data for natural and synthetic gases, as well as a broader discussion of the expected systematics of site-specific carbon isotope composition of propane.

2.2 Sample preparation

Sample purification

The mass spectrometric method that we present calls for a typical sample size of 50 μmol of purified propane (less is possible, but this quantity assures adequate source pressure over the course of several measurements each of several molecular fragment ion beams). Sample preparation typically calls for separation from other gases, particularly in the case of natural gases, where propane is typically a minor component ($\leq\sim$5%). We achieve this purification through cryogenic distillation. Although alternate methods, such as preparatory gas chromatography, may be equally or more effective, this approach was chosen because it is easily used for a wide range of sample size and purity, and can be combined with methods for separation of related analytes (methane, ethane, etc.).

An aliquot containing a sufficient amount of propane of each bulk gas sample (i.e., a mixture of hydrocarbons and/or other gases containing at least 50 μmols of propane) is introduced into a glass vacuum line that contains, in addition to various traps and calibrated volumes, a liquid-helium-cooled cryostat. The aliquot of bulk sample gas is first exposed to the cryostat at 20K, which condenses propane along with ethane, methane and contaminant species such as CO_2 and N_2. The remaining vapor, consisting of highly non-condensable species like He and H_2, is pumped away.

Next, methane is removed from the sample gas mixture first following Stolper et al. (2014a): We cycle repeatedly through a series of operations that begins by fluctuating the temperature of the crystoat between 80K and 45K in order to release N_2 while retaining CH_4 (Stolper et al., 2014a). Once this step is completed, the cryostat is raised to 72K,

and methane is released from the cryostat and trapped on a molecular sieve held at liquid nitrogen temperature and removed from the vacuum line for isotopic analysis (Stolper et al., 2014a).

Next, a similar process is used to separate ethane from propane and propane from higher-order hydrocarbons: The temperature is raised to 135K for 5 minutes, and then lowered to 115K with the valve to the cryostat closed. It is then opened and exposed to a trap immersed in liquid nitrogen, into which ethane condenses. The cryostat is re-closed, and the temperature is raised to 150K for 5 minutes and then lowered to 135K. The propane is then exposed to and condenses in a trap immersed in liquid nitrogen, separating it from higher-order hydrocarbons like butane. The cryostat is then closed again, the temperature raised to 150K, and then the cryostat is re-opened and the residual gas is pumped away. The cryostat is then lowered to 60K, the ethane is frozen into it, and the processes are repeated, each time adding the propane fraction to the previously separated propane. This process is repeated 5 times, or until the pressure on the ethane and propane fractions does not change between cycles.

A further complication arises when CO_2 is present in a sample, because CO_2 is similar in vapor pressure to propane. We separate CO_2 from otherwise purified propane by passing the gas released between 135K and 150K (above) over ascarite multiple times, until its pressure does not significantly change with further ascarite exposure.

In order to verify purification techniques a series of tests were completed. Propane and ethane were mixed together and run through the purification technique in approximately equal aliquots on the glass line. The recovery of propane and ethane was nearly complete (97%, starting pressure of 157.7 torr, ending pressure of 152.5 torr). Although this was

not total, the sample was run as versus the standard and it was within error of 0‰. To verify the CO_2 removal step, a similar experiment was also completed. In this case, not all of the CO_2. The starting pressure of propane was 24.2 torr, 8.8 torr of CO_2 was added, and 24.4 torr of propane was recovered from the mixture. This was sufficient to yield within error 0‰ measured relative to the standard. Due to these results we are confident in the reproducibility and non-fractionating nature of the purification procedure.

Contaminant characterization

The cryogenic purification procedure outlined above does not always perfectly isolate propane from propene, butane and pentane, which have small but significant vapor pressures at 150K. We search for evidence of these contaminants by conducting a full mass scan on each purified propane sample, looking for diagnostic departures from the mass spectrum of pure propane. We also measure ratios of intensities of several characteristic masses and compare them to those ratios for pure propane from our reference tank, again to recognize evidence of contaminants and calculate their contributions to masses of interest. For example, the intensity ratio of masses 57 and 58 constrains the abundance and speciation of butane contamination: If there is negligible 57 or 58, then we conclude that there is no butane contamination; if masses 57 and 58 are present and $58/57 < 1$ then butane is present and dominated by n-butane contaminant; if they are present and the ratio is greater than 1, then the contaminant is dominated by iso-butane. Similar indices can be used to recognize and approximately quantify contamination by CO_2, ethane, and propene: CO_2 and ethane are recognized by a combination of the 29/28

mass ratio (propane = 1.7, CO_2 = 0.01, ethane = 0.2), while propene is noticed by the 44/43 mass ratio (propane = 1.18, propene = 0.043). By doing linear additions of the suspected contaminants, the species present in the gas can be calculated, and further cryogenic separations are preformed until the contaminants are less than 1% of the highest intensity propane beam at mass 29. In practice, this has not worked to identify an enigmatic contaminant that produces an excess of methyl ions in the sample. Currently, the ratios are used as a guideline, and if the sample is not within 20% of the standard value measured at the same time, the sample is rejected. The numbers listed above for propane are taken from the National Institute of Standards, but do not always match the measured value, so the ratio for propane is calculated from the standard on that given day (the NIST value is generally within 1% of the measured reference value for each of the listed ratios).

While we have evidence to suggest that our procedure can yield gases of sufficient purity for accurate analysis, trace contaminants are often still present; we can generally detect propane in the ethane fraction and ethane in the propane separate. (Though the ethane in the propane is harder to detect because there is no mass range where there are ethane peaks and not propane peaks; i.e., it can only be recognized by changes in proportions of fragment ions). We have found no evidence for propene within any of the samples yet measured. CO_2 is common in most of the samples that have been analyzed so far, both traditional natural gas samples as well as shale gas samples. Even after multiple ascarite cleanups, trace CO_2 remains.

There is a very narrowly defined mass range that the potential contaminant present in many shale gas samples could have. IT has the mass range of 30-36 Da, generates

CH_3 ions in abundance that are depleted relative to those generated by propane, and has a similar vapor pressure to propane. Due to the abundance and density of peaks that propane generates it is difficult to directly fingerprint this species. In the future, we hope to use column chemistry to completely separate propane from all other species, as well as preserving CO_2 so analysis can be completed on it.

2.3 Mass spectrometry

The goal of the analytical method that we present is to determine variations from sample to sample in the relative enrichment of ^{13}C between the terminal and central carbon position within propane. The strategy that we employ combines two previously demonstrated innovations: (1) Eiler et al. (2012) and Stolper et al. (2014a) demonstrate that the recently developed Thermo IRMS 253 Ultra, a prototype high-resolution gas source mass spectrometer, is capable of mass resolving isobaric interferences among ^{13}C- and D-bearing isotopologues and H-adducts of methane. We explore here whether this capability can be applied with useful precision to fragment ions generated by electron bombardment of propane. And, (2) Yoshida and Toyoda (2000) demonstrate that comparison of the $^{15}N/^{14}N$ ratio of N_2O^+ and NO^+ ions generated by electron bombardment of N_2O constrains the distribution of 15N between the terminal and central N position. By analogy, we explore here whether comparison of the $^{13}C/^{12}C$ ratios of fragment and molecular ions of propane can constrain the distribution of ^{13}C between its center and terminal positions.

Figure 2.1 illustrates the low-resolution mass spectrum (i.e., only cardinal masses are

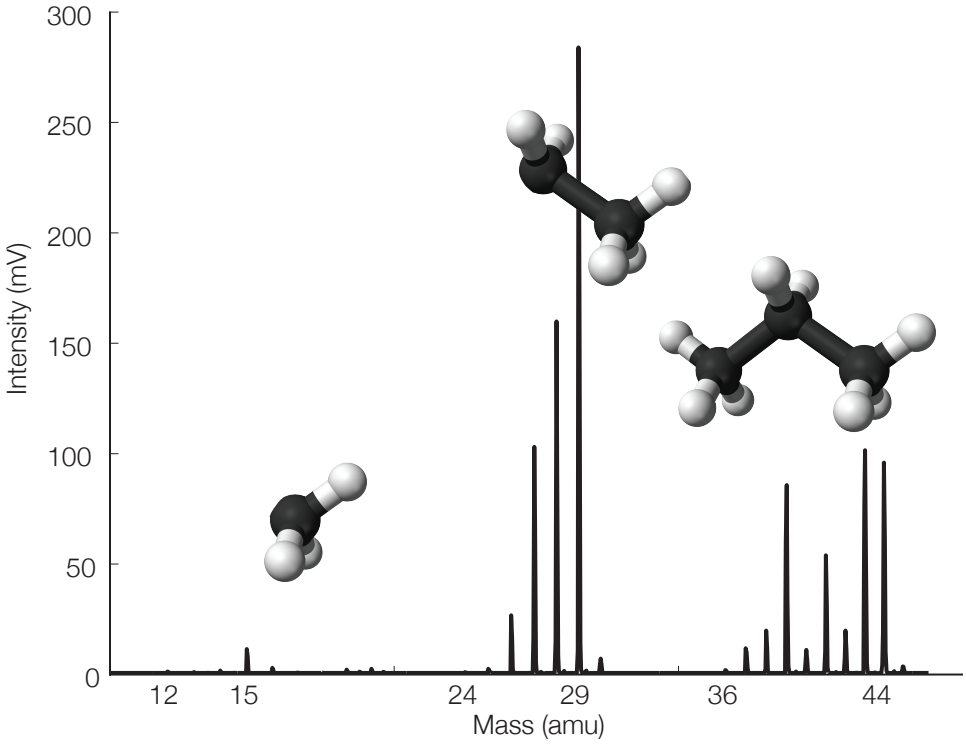

Figure 2.1: Mass spectrum of propane from the MAT 253 Ultra. Major fragments shown with ball and stick figures. Species collected on a 10^8 ohm resistor.

shown) generated by electron bombardment of propane under commonly-used gas ion source conditions (10^{-7} mbars pressure; 70 eV electron impact energies). The most abundant ion is $C_2H_5^+$, with a nominal mass of 29 Da. The adjacent peak at mass 30 consists of $^{13}C^{12}CH_5^+$ and lesser amounts of $^{12}C_2H_4D^+$ and $^{12}C_2H_6^+$, and the family of peaks of descending abundance from 28 to 24 amu each is dominated by $^{12}C_2^+$ with 4, 3, 2, 1 or no hydrogens (plus small amounts of ^{13}C and D-bearing isopologues and traces of multiply substituted species containing fewer hydrogens). This pattern is mirrored by less abundant but generally similar mass spectra for the CH_n^+ and $C_3H_n^+$ ionic species (masses 12-16 and 36-45, respectively). We use a shorthand for these families of peaks throughout the rest of this paper: the three-carbon species are referred to as the 'propyl fragments,' the two-carbon species as the 'ethyl fragments' and the one-carbon species as

the 'methyl fragments.' Similarly, we refer to the terminal carbon positions of the parent molecule as the 'terminal' positions, methyl, or the 'C1' and 'C3' positions (the two are symmetrically equivalent), and the central carbon position as the 'center', 'methylene', or 'C2' position.

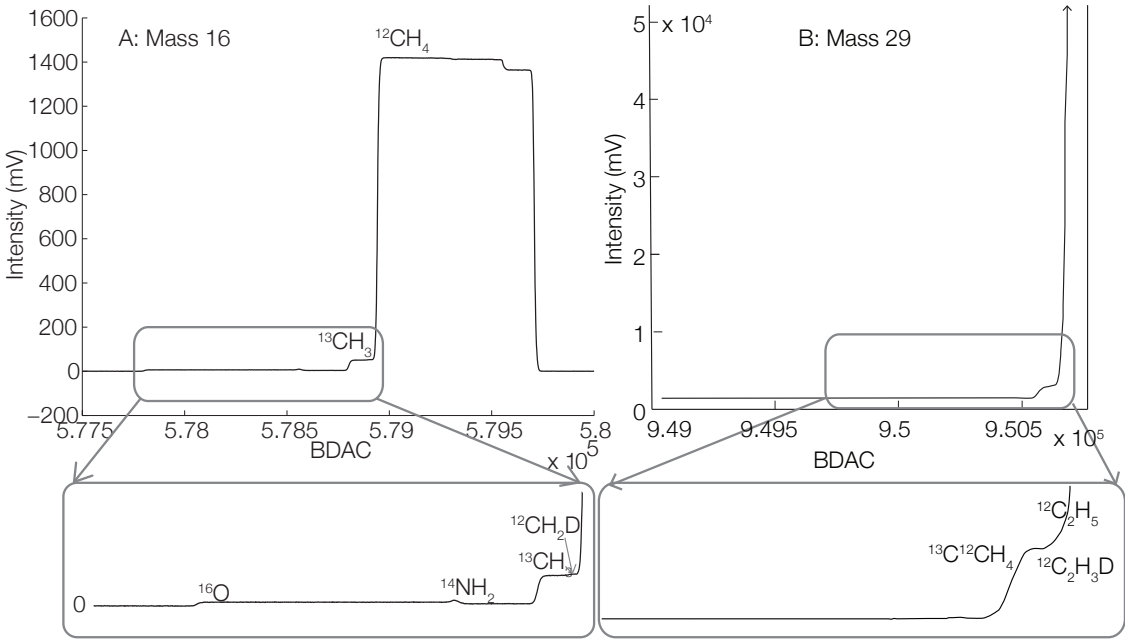

Figure 2.2: Mass spectrum showing the main peaks that are measured and their background species. The mass 16 peak is no longer measured due to the $^{14}NH_2$ fragment, which is variable through time and cannot be resolved from the $^{13}CH_3$ peak. The mass 29 peak appears to be a small shoulder, but it is easily measured at high resolution. BDAC is the magnetic step used by the mass spec and is equivalent to mass in this figure.

Our analytical strategy calls on the high resolution of the Thermo IRMS 253 Ultra to measure the intensity ratios of ^{12}C and ^{13}C-bearing isotopologues of ionic species that share the same stoichiometry, free from interferences by other species that share the same cardinal mass (Eiler et al., 2012). Following a method first developed for site-specific ^{15}N analysis of N_2O, we constrain the differences in ^{13}C content between the center and ends of propane by comparing the $^{13}C/^{12}C$ ratios of fragments that sample different proportions of these two sites. In particular, we attempt to constrain the $^{13}C/^{12}C$ ratio of the terminal

carbon position by analyzing one of the C1 fragments (under the assumption that, to first order, the methyl fragments will preferentially come from the terminal carbon positions). We add to this a separate measurement of the $^{13}C/^{12}C$ ratio of one of the ethyl ionic species, which we assume mostly consist of the center carbon plus one terminal carbon. If these assumptions are correct (we test them experimentally below), then the difference in $^{13}C/^{12}C$ ratio (R13) between the center and terminal carbon position can be calculated approximately as:

$$\left[{}^{13}R_{\text{methyl}}\right] = {}^{13}R_{\text{terminal}} \tag{2.1}$$

$$\left[{}^{13}R_{\text{ethyl}}\right] = \frac{{}^{13}R_{\text{center}} + {}^{13}R_{\text{terminal}}}{2} \tag{2.2}$$

$$\left[{}^{13}R_{\text{center}}\right] = 2 * {}^{13}R_{\text{ethyl}} - {}^{13}R_{\text{methyl}} \tag{2.3}$$

And the bulk $^{13}C/^{12}C$ ratio of the whole molecule can be calculated as :

$$\left[{}^{13}R_{\text{bulk}}\right] = \frac{1}{3}\left(2 \times {}^{13}R_{\text{ethyl}} + {}^{13}R_{\text{methyl}}\right) \tag{2.4}$$

It would be possible to obtain the same information by combination of other constraints like the analysis of both a methyl and propyl ion species; analysis of the methyl ionic species combined with a conventional measurement of compound specific $\delta^{13}C$; or even analysis of the ethyl fragment ion and the full molecular ion. And, each of the major groups of fragments (methyl, ethyl and full molecular) exists in several versions that differ in their numbers of associated hydrogens. Thus, the approach we explore here could be

performed in any of a variety of ways, and the version we present should be thought of as a representative case. Similarly, any such measurement of two fragments that differ in number of carbons can be compared with a conventional $\delta^{13}C$ value (generated by any of the commonly used methods) to independently check of the accuracy of our technique (i.e., eqn. 2.2 should be consistent with the independently known $\delta^{13}C$ value).

We face three challenges to turning this conceptual approach into a precise and accurate analytical method:

1. We must be able to analyze both the ^{12}C and ^{13}C isotopologues of the two chosen fragments, resolved from closely adjacent isobaric interferences (e.g., $^{13}CH_3^+$ vs. $^{12}CH_2D^+$) and free from (or corrected for) other possible contaminant isobars.

2. We must test our assumptions regarding the ways in which various ionic species sample the two different carbon sites, through analysis of labeled propane. And, if our assumptions are found to be flawed (e.g., if the methyl fragment is found to contain some contribution from the central carbon position), then we must establish whether or not this artifact can be corrected for.

3. We must establish a reference frame based on the assumed or (preferably) known site-specific carbon isotope composition of some standard propane. This, it turns out, was the greatest challenge of this method, and was not resolved to our complete satisfaction over the course of this study (though, in principle, it need only be solved once).

Selection of fragment ions to measure

$C_2H_4^+$ presents an obvious target for isotopic analysis because it is the second most abundant ion generated by electron bombardment of propane (at least, at the impact energies commonly employed by isotope ratio mass spectrometers). It is chosen instead of $C_2H_5^+$ due to stability of the background measurement. The choice of a second, non-ethyl fragment or molecular ion is less obvious: the methyl fragment ions are low in abundance, but potentially provide a 'pure' measurement of one molecular site (presumably the terminal carbon position). Most of the C3 (three-carbon) molecular and fragment ions are more abundant, but contain a 2:1 mixture of terminal and central position carbons. If one of these were chosen (or, equivalently, a separate, conventional molecular $\delta^{13}C$ measurement is used), then both constraints on the site-specific fractionation would be diluted, meaning the analytical errors would be further magnified when the terminal vs. central position difference is computed.

An analysis of the propagated errors associated with these various possibilities suggests they are roughly equivalent. However, two factors lead us to focus first on a methyl fragment species as the second necessary constraint: (1) we prefer making a complete analysis on the Ultra rather than combining one Ultra measurement with a conventional bulk $\delta^{13}C$ value, because it removes the potential systematic errors associated with combining data from multiple methods, standards and laboratories. (2), the methyl fragment ions are a minor but ubiquitous feature of the mass spectra of a wide variety of organics. Thus, by producing a method capable of studying propane, we may have effectively met many of the technical requirements to position-specific analysis of other compounds.

And, (3) the mass resolution needed to separate the relevant species is relatively low at lower masses, making tuning a less time consuming and constraining process. We present data for both the CH_3 fragment ion (the most abundant methyl species and therefore the obvious choice) and the CH_2 fragment ion (a less obvious choice, but, as it happens, preferable due to common interferences by NH_n species). Finally, we present measurements of the C3 full molecular ion for a subset of samples examined here, both as a test of analytical accuracy and as an alternative method that may be desirable in cases where the methyl fragment measurement is unusually difficult (e.g., due to the presence of an isobaric interference, or a contaminant that anomalously changes the fractionation behavior of the methyl fragment ion).

Instrument configuration

All of the measurements presented here were made in dual-inlet mode, meaning approximately equal pressures of sample and standard gases are introduced into the bellows of a dual inlet system, and the capillary bleeds and changeover valve block of the Ultra are used to alternately introduce one and the other into the ion source. Typical bellows pressures are 10 mbars and typical source pressures are $6x10^{-8}$ mbars (both values are background corrected). While it is imaginable that measurements similar to those we present could be made at higher or lower gas pressures, we that find these values provide a successful compromise between the desire for high signal intensity (so acceptable errors can be reached in a reasonable time) and the need to avoid space-charge effects and uncontrolled, time-varying reactions in the ion source (which are problematic at high

source pressures).

Cup configurations

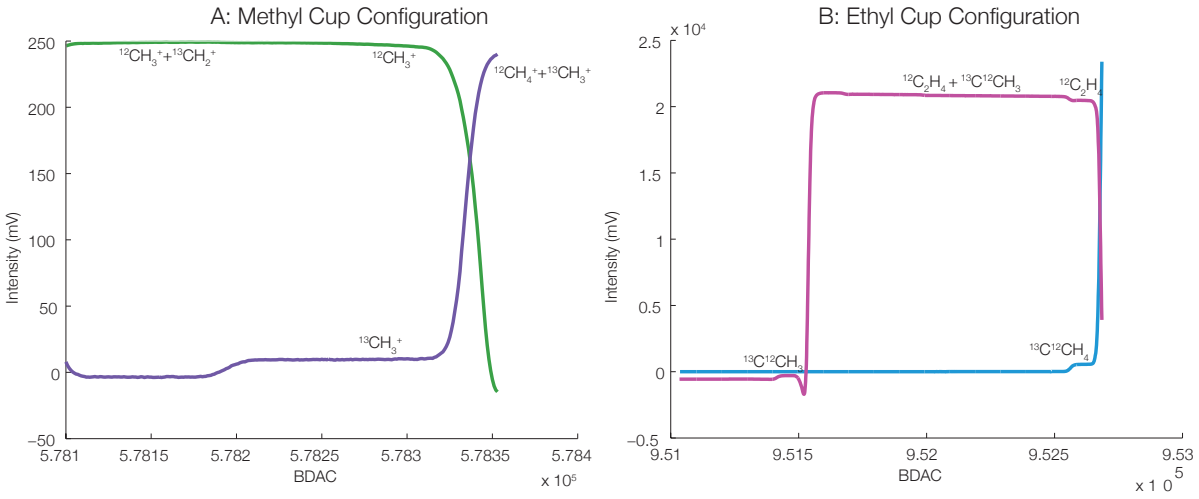

Figure 2.3: In both of the figures the different colored lines represent beams measured on different collectors. Figure A shows the overlapping peaks that are measured for the methyl measurement. The shoulder is wide enough that the deuterium can be mass resolved from the carbon enrichment. Figure B shows the cup configuration for the two-carbon measurement. The shoulder is narrower for this measurement, but there are significantly more counts so, the error is lower. The three-carbon measurement is not shown because the two peaks are completely overlapping because the relevant species cannot be separated on the Ultra, and another measurement is necessary to ion correct contributions of D to the combined signal for ^{13}C and D substituted species.

The ion beams of interest for our analysis include: $^{12}C_2H_4^+$ and $^{13}C^{12}CH_4^+$ (for analysis of the ethyl fragment ions), for the methyl fragment ions, either $^{12}CH_3^+$ and $^{13}CH_3^+$ (our first target when this method was first developed) or $^{12}CH_2^+$ and $^{13}CH_2^+$ (our current preferred target), and, for the full molecular ion, $^{12}C_3H_8^+$ and $^{12}C_2^{13}CH_8^+$. This family of ion beams is measured in three separate acquisitions having different cup configurations. These configurations are summarized in Table 2.1, and briefly described as follows:

The MAT 253 Ultra has 7 collector positions, 6 of which are movable, three on either

side of the fixed central collector. All collector positions can detect ions using either a faraday cup, which can be read through an feedback electrometer that varies in resistance between 10^7 to 10^{12} ohms, or an electron multiplier. The electron multipliers on the movable collectors positions are of the relatively small compact discrete dynode (CDD) design, while that in the central collector position is a larger, conventional secondary electron multiplier (SEM), positioned behind a 'retardation lens' (or RPQ) for improved abundance sensitivity. Because of the large number of movable collector positions and range of detector sensitivities at each position, it is possible to make three separate measurements of the methyl and ethyl fragment and full molecular ion species simply by changing the magnet current and a quick movement of the movable collectors.

When $^{12}CH_3^+$ and $^{13}CH_3^+$ are measured as the constraint on the isotopic composition of a methyl fragment, mass 15 is measured on a faraday cup read through a 10^{12} Ohm amplifier, on the 'L2' collector trolley (Figure 2.3). This collector is positioned so that the high-mass side of the family of mass 15 peaks (i.e., where $^{12}CH_3$ sits) enters the collector, and lower-mass species (mostly $^{13}CH_2$ and a trace of ^{12}CHD) are excluded. $^{13}CH_3$ is simultaneously measured with the SEM detector in the central collector position, with the magnetic field set such that the low-mass side of the family of mass-16 peaks (i.e., where ^{13}CH3 sits) enters the collector and higher-mass, nearly isobaric species (e.g., $^{12}CH_2D$ and $^{12}CH_4$) are excluded.

The alternate method in which CH_2 is the analyzed methyl fragment ion species uses a similar cup configuration: $^{12}CH_2$ is measured on the high-mass side of the mass 14 peak using the 'L3' faraday cup registered through a 10^{12} ohm amplifier, and $^{13}CH_2$ is measured on the low-mass side of the mass 15 peak, using the center collector SEM.

Mass	Cup	Cup Location	Detector	mV or cps	fA
14	2	55.7	1.E+12	550	550
15	5	–	SEM	34000	5.4468
15(old)	3	49.33	1.E+12	1050	1050
16	5	–	SEM	75500	12.0951
28	4	25.33	1.E+11	1900	19000
29	5	–	1.E+12	430	430
44	4	17.623	1.E+11	1100	11000
45	5	–	1.E+12	360	360

Table 2.1: Instrument setup and counts

When analyzing the ethyl fragment ion, $^{12}C_2H_4^+$ is measured on the high-mass side of the mass 28 peak, collected in a faraday read through a 10^{12} Ohm amplifier on the 'L1' collector trolley (Figure 2.1), and $^{13}C^{12}CH_4^+$ is measured on the low-mass side of the mass 29 peak, using a faraday cup registered through a 10^{12} Ohm amplifier on the central (fixed) collector position.

The measurement of the three-carbon ions involves repositioning one of the movable collectors (L1, or cup 4) after making the two-carbon measurement. The cup location is reproducible, so it is not difficult or time-consuming. A $10^{12}\Omega$ resistor is used on cup 5 to measure mass 45, and a $10^{11}\Omega$ resistor is used on cup L1 to measure mass 44. We generally do not fully resolve $^{13}C^{12}CH_8$ from $^{12}C_3H_7D$ at mass 45 (this calls for a mass resolution close to the formal limit achieved for the Ultra; thus, a minor component (a few percent) of each beam will contaminate the other. Our solution to this is to simply combine the signals from these species on the Ultra, and then separately measure the $D/^{13}C$ ratio of the sample on a very high-resolution single collector mass spectrometer, a modified version of the Thermo DFS. The DFS is a high-resolution gas source mass spectrometer, having a reverse geometry and a single collector detector. Eiler et al. (2014)

have shown that this instrument can be outfitted with a dual inlet system and used to measure ratios of nearly isobaric isotopologues by untangling the shape of the resulting adjacent peaks. This measurement, combined with some second constraint (like the sum of ^{13}C+D) typically yields an error of 0.5-2 ‰ in δD, and no significant increase in error in δ^{13}C beyond that created by that second constraint. For our purposes, we only use this measurement to ion correct the contribution of D to the ^{13}C+D signal in the Ultra measurement.

Analyzer tuning and resolution

At the beginning of each analytical session, it takes approximately half a day to tune the mass spectrometer to achieve adequate resolution of 20,000 MRP with a high-resolution slit. The resolution tuning is done on the high-mass side of the mass 15 peak (i.e., on the high-mass side of the $^{12}CH_3$ ion beam) to have an intense ion beam in the mass range of interest that does not have significant interferences from closely adjacent nearly isobaric species. The machine is first auto-tuned for intensity, and then the focus and rotation quadrupole lenses are manually adjusted in order to achieve the necessary resolution (see Eiler et al. (2012) for relevant instrument details). The instrument typically retains a stable high-mass resolution for time scales on the order of 1-2 weeks, with minor adjustments to source and analyzer lens potentials done at the beginning of each day.

Signal intensities and counting statistics limits

Given typical source pressures, ion source tuning parameters set to maximize sensitivity, and use of the high-resolution entrance slit, the ion intensities of the $^{12}CH_2^+$ fragment ion are typically on the order of 550 fA, whereas that for the ^{13}C substituted species, $^{13}CH_2^+$, is typically on the order of 5 fA. When the CH_3^+ fragment ions are instead used to analyze the methyl fragment ion species, intensities are typically 1050 fA for $^{12}CH_3^+$ and 12 fA for $^{13}CH_3^+$. Similarly, typical intensities for the ion beams used to measure the ethyl fragment are 19,000 fA for $^{12}C_2H_4^+$ and 430 fA for $^{13}C^{12}CH_4^+$. $^{12}C_3H_8$ has a typical intensity of 11000 fA, and $^{13}C^{12}C_2H_8$ has a typical intensity of 360 fA for the three-carbon measurement (Table 2.1).

Background corrections

Given the mass resolutions typically achieved for the instrument and method that we present, all plausibly significant interferences with the target analyte ion beams are formally resolved (i.e., the $M/\Delta M$ values for all interferences of interest are substantially less than the formal 5/95 % resolution measured when the analyzer is tuned). However, over the course of this study, the Ultra used relatively wide exit slits (i.e., detector apertures) to achieve a 'flat-topped peak' condition that facilitates high-precision measurements. Therefore, in any case where a target analyte is 'sandwiched' between closely adjacent higher- and lower-mass interfering peaks, the analyte ion beam must always be collected along with at least one of those interferences. For this reason, it is essential to our method that the intensities of these co-collected neighboring peaks be measured and

used to correct the measured intensity of the analyte plus interference(s). Similarly, corrections must be applied for background contributions from scattered ions and for signal associated with detector dark-noise (generally, all significant corrections of this kind can be made using a single measurement adjacent to the analyte peak). For example, Figure 2.2 shows a scan of the 16 amu peaks, revealing that the $^{13}CH_3^+$ peak can be delivered to the detector without significant contributions from adjacent $^{12}CH_4^+$, but in this case must include contributions from the other closely adjacent background species, $^{14}NH_2^+$.

There are two separate background corrections done on each measurement. The first is done for the species on the central collector. The magnet is set to a current typically 200-300 BDAC units (or, 0.01 amu) lower than that for the targeted peak, and signal at this position is recorded for two minutes. For the first 60 seconds of this period, gas from the sample reservoir is allowed to flow into the ion source; then, the changeover block is switched so that the standard gas flows into the ion source. After the two minute period is complete, we cull the data to exclude the 15 seconds of unstable gas pressures associated with switching the changeover valve block, and average over a 30-second period in the middle of each 1 minute of signal from each gas. After the isotope ratio acquisition is completed, a second background measurement is made for the lower-mass species being detected on either on cup L1 or L3 (depending on which fragment ion is being measured). If the SEM is in use it is first turned off, and then the magnet is set to a current 200-300 BDAC units (0.01 AMU) greater than the magnet setting for the measurement; once more, signal is observed for one minute on each bellows, and averaged for the middle 30 seconds of that time.

We find that background intensities are generally a positive function of the pressure

within the ion source. When the pressure within the source is within the range that we specify for our default method, background intensities are approximately stable through time (at least, over the course of several acquisitions). However, if source pressure is significantly higher (i.e., $> 8\text{x}10^{-8}$ mbars) both of the intensities of monitored ion beams and background intensities measured as described above fluctuate too much for precise (sub-per mil) isotope ratio analysis over seconds to minutes.

2.4 Results

Experimental constraints on fragmentation/recombination reactions

The method described above assumes that the methyl and ethyl fragment ions consistently sample fixed proportions of the terminal and central carbons from their parent propane molecules, preferably with strong separation in the relative contributions of each site to each molecular ion species. This assumption, as articulated above, is clearly an idealized scenario that is unlikely to be strictly true. For example, it is possible that some of the methyl fragment ions come from center-position carbons, or that some of the ethyl fragment ions form by recombination of two terminal carbons.

We studied this issue by analysis of propane that was a physical mixture of natural propane and propane that had been artificially labeled in ^{13}C in one of its terminal carbon positions (i.e., ^{13}CH3^{12}CH2^{12}CH3). A set of experiments was conducted in which we added this labeled propane to the reference gas in varying amounts. If no exchange

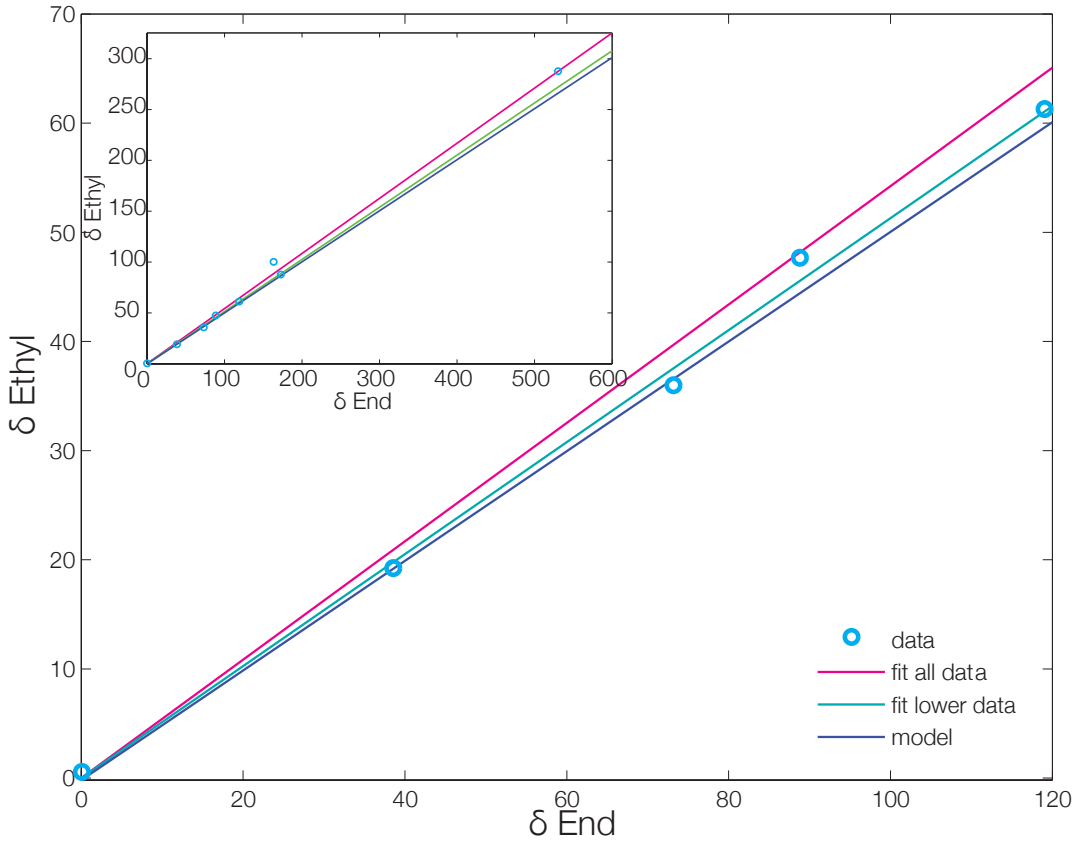

Figure 2.4: Plot showing the enrichment as a result of mixing terminally-labeled propane with the standard. Slight recombination is observed, but within the limit of other methods. The fit of all of the data that is within a reasonable amount of the standard (120‰) has a very similar slope to the ideal model. When all of the data, shown in the inset, is included, there is slightly more recombination.

of carbon within or between propane molecules occurred during mixing and gas handling (something we consider implausible), and if the production of methyl and ethyl fragment ions follows the simplified assumptions on which our method is based, then a slope in a plot of the ^{13}C enrichment in the methyl fragment versus that for the ethyl fragment should be 0.502, for any modest mixing ratio of labeled propane in natural propane. We observe a slope in which a plot of 0.54 when all points are included (including a mixture with 500‰ enrichment in the methyl ion fragment). However, this result may be influenced by inaccuracies and non-linearities in our measurements of highly enriched

gases. A slope of 0.51 is found when we consider only those mixtures that had $\delta^{13}C$ values for the methyl fragment ion within 120‰ of the reference gas (Figure 2.4). We conclude that there is minor (∼2-8 %; most likely in the lower end of this range) mixing of center position carbon into the methyl fragment ion and/or excess terminal position carbon into the ethyl fragment ion during ionization. This is broadly similar to the extent of fragmentation/recombination involved in mass spectrometric analysis of the site-specific ^{15}N content of N_2O (Yoshida and Toyoda, 2000; Westley, Popp, and Rust, 2007; Toyoda and Yoshida, 1999) or the clumped isotope analysis of CO_2 (Huntington et al., 2009; Dennis et al., 2011). We conclude that our method can potentially recover at least relative differences (i.e., as compared to a reference standard (CIT-P1)) in the site-specific ^{13}C content of propane with only modest compression, or mixing of methyl and methylene positions, of the scale of variability. Currently, we do not correct any of the data for this scale-compression effect. The majority of the data is relatively similar to the standard (within 10‰ in both methyl and ethyl fragment composition), so corrections would be on the order of 0.2‰, which is similar to or smaller than our typical analytical error. In the future, if we study samples that differ markedly in site-specific carbon isotope composition from our standard, or if analytical precision improves significantly, say, to 0.1‰ or better, it may become important to correct the data for scale compression artifacts. At this time, we believe it is more straightforward to present the data in the uncorrected form.

Sample measurement method

Measurements of unknown samples are standardized by comparison with a reference gas (described below). Each acquisition consists of 8 cycles of sample/standard comparison, with integration times of 16 seconds per cycle on each gas. One analysis of each fragment molecular ion species (i.e., one of the methyl fragments, or ethyl or C_3H_8) is typically the average of four or five acquisitions, i.e., a total of 8-10 acquisitions are needed to calculate the difference in site-specific ^{13}C enrichment between the sample and reference gas based on analysis of two of the three possible species (i.e., two of C1, C2 or C3), and an additional 4-5 are needed to also gather redundant information on the third species.

Standardization

One challenge to developing a new measurement of a previously un-studied isotopic property is establishing a reference frame that can be used to track long-term precision, report differences in composition between samples, and (in the event that this method is adopted elsewhere) compare data across labs. In order to do this, we obtained a tank of propane from Air-Liquide and designated it as our official intralaboratory reference tank. Its bulk carbon isotope ratio (averaged across all sites) was measured by GC-online combustion IRMS in the laboratories of the PEER institute, yielding a $\delta^{13}C$ PDB = -33.23 $\pm$0.55‰.

In principle, it should be possible for us to constrain the absolute site-specific ^{13}C content of our reference gas based on the results of our mixing experiments; i.e., these mixtures provide a kind of 'standard additions' experiment that constrains the abun-

dance of the terminally-substituted propane isotopologue in the standard into which labeled propane was mixed. However, when one propagates the error in independently known mixing ratios of the natural and labeled end members (i.e., from manometry), this constraint offers no meaningful (per mil level) determination of the difference in δ^{13}C between the central and terminal carbons in the reference gas.

Therefore, we currently report all data for unknown samples in a reference frame in which our intralaboratory standard (CIT-P1) is defined to be the '0' point on the δ^{13}C scale for both the central and terminal position δ^{13}C scales. This implies the following nomenclature:

$$\delta^{13}C^{\text{center}}_{\text{CIT-P1}} = \left({}^{13}R^{\text{center}}_{\text{sample}}/{}^{13}R^{\text{center}}_{\text{CIT-P1}} - 1\right) \times 1000 \tag{2.5}$$

$$\delta^{13}C^{\text{terminal}}_{\text{CIT-P1}} = \left({}^{13}R^{\text{terminal}}_{\text{sample}}/{}^{13}R^{\text{terminal}}_{\text{CIT-P1}} - 1\right) \times 1000 \tag{2.6}$$

Where equations 2.1 and 2.2 and the sample/reference gas comparisons of the methyl, ethyl and/or full molecular ions made during each analysis are combined to calculate $\text{R13}_i^{sample}/\text{R13}_i^{standard}$.

This approach does not differ in any fundamental way from the commonly-used reference frames for reporting stable isotope data (PDB, SMOW, etc.). However, it is unsatisfying because it prevents direct and unambiguous comparison of measured variations in site-specific isotopic differences with theoretical predictions or other methods that might differ in their analytical artifacts. Furthermore, while in the immediate future the method we present will exist in only one laboratory and so it is not important that all

data refer to an arbitrary material we have chosen as a standard, eventually other laboratories might adopt this method and not wish to establish a separate arbitrary reference frame or adopt the one based on CIT-P1. For these reasons, we are currently working on alternative methods for determining the absolute distribution of isotopes within the standard based on selective chemical degradation and/or NMR analysis of our reference gas. These attempts have not yet succeeded, but when they do we anticipate that it should be straightforward to re-calculate all previously generated data to some other reference scale (e.g., PDB).

Internal and external precision

We performed a series of measurements to document and illustrate the internal and external precision of our measurements, and their conformance to expectations for physically simple, readily predicted fractionations.

The shot noise or counting statistic limit for each measurement is calculated for the given source pressure. Typically, the limit for the single carbon acquisition of 8 cycles is 0.6‰ given the number of counts collected for the ^{13}C-bearing species on the SEM. The actual achieved limit of in-run stability for this measurement is between 0.8 -0.6‰. For the two-carbon measurement, the shot noise limit is around 0.05-0.075‰ depending on the number of counts, and the in-run stability is closer to 0.1‰. For the three-carbon measurement, the shot noise is 0.05‰, and the in-run statistics are approximately the same. The reason why the three-carbon measurement achieves its limit and the others do not is most likely due to the size of the flat peak on which signal is integrated. When

Sample	dδEnd	stdev	sterr	δEthyl	stdev	sterr	δEnd	δcenter	δFull	δ^{13}C CH_4	δ^{13}C C2H6	δ^{13}C C3H8	δ^{13}C nC4H10	δ^{13}C iC4H10
Diffusion														
Dif-1	-3.21	1.99	0.35	-3.50	0.59	0.11	-3.21	-3.80	-3.41					
Dif-3	-3.32	1.90	0.34	-3.53	0.73	0.13	-3.32	-3.74	-3.46					
Res-1	2.34	2.82	0.58	1.60	0.40	0.07	2.34	0.86	1.85					
Res-3	1.52	1.85	0.34	1.27	0.59	0.10	1.52	1.01	1.35					
Mixing														
Aa	163.35	2.28	0.30	100.16	0.28	0.04	163.35	36.96	121.22					
Ab	530.42	4.11	0.55	287.62	15.59	2.85	530.42	44.83	368.55					
B3	119.06	10.01	1.25	61.04	0.67	0.09	119.06	3.02	80.38					
B1	172.80	3.95	0.70	87.67	0.50	0.09	172.80	2.54	116.05					
C4	73.19	3.58	0.63	35.75	3.25	0.57	73.19	-1.69	48.23					
C1	88.83	3.44	0.54	47.43	0.36	0.06	88.83	6.03	61.23					
D4	38.58	3.54	0.47	19.00	0.96	0.13	38.58	-0.57	25.53					
Potiguar														
1	6.82	1.65	0.24	4.88	0.85	0.13	6.82	2.94	5.53	-40.79	-31.21	-29.29	-28.49	-27.94
01a	4.67	1.62	0.26	5.67	0.51	0.08	4.67	6.66	5.33	-40.79	-31.21	-29.29	-28.49	-27.94
02b	1.66	1.69	0.69	0.46	0.67	0.12	1.66	-0.74	0.86	-48.25	-38.01	-34.81	-33.75	-34.64
3	4.84	2.41	0.38	3.72	0.39	0.07	4.84	2.59	4.09	-47	-34.84	-32.26	-31.75	-33.52
3 b	3.19	1.76	0.31	1.41	0.84	0.12	3.19	-0.37	2.00	-47	-34.84	-32.26	-31.75	-33.52
03a	4.58	1.11	0.24	0.41	1.42	0.25	4.58	-3.77	1.80	-47	-34.84	-32.26	-31.75	-33.52
4	4.55	1.92	0.34	4.29	0.51	0.09	4.65	3.94	4.41	-45.02	-32.61	-29.84	-29.4	-31.28
4	4.56	1.50	0.22	5.53	1.17	0.19	4.56	6.51	5.21	-45.02	-32.61	-29.84	-29.4	-31.28
04a	6.28	1.89	0.33	4.73	0.63	0.11	6.24	3.23	5.23	-45.02	-32.61	-29.84	-29.4	-31.28
07a	0.76	2.96	0.52	0.05	0.38	0.29	0.76	-0.67	0.28	-47.14	-36.79	-34.27	-33.51	-34.53
7m	0.17	2.68	0.42	-0.22	0.61	0.11	0.17	-0.60	-0.09	-47.14	-36.79	-34.27	-33.51	-34.53
9	3.53	0.82	0.17	1.64	1.17	0.21	3.53	-0.24	2.27	-44.19	-32.87	-30.68	-30.87	-31.65

Table 2.2: Data table of diffusion experiments, mixing experiments, and select natural samples

the pressure decreases through time on the other measurements, this leads to subtle shift in peak position (Eiler et al., 2012), which potentially has a much greater effect on measurements of small 'shoulders' of peaks than on larger flat peak tops, since there is only a window of approximately 10 BDAC units where the magnet can sit to make the measurement.

In addition to acquisition precision, replicates of samples were also run. At the beginning of each session, after the collectors are aligned, two 'zero enrichment' measurements (i.e., comparison of the aliquot of the standard being used that day to a second aliquot of that same standard) are run for each of the ion species that are examined by the measurement. The average of the zero enrichments are within one standard deviation of zero. We also replicated some of the analyses of propane from Potiguar basin natural gases. These samples have been extracted from a mixed gas container at different times, cleaned of other gases separately, and then analyzed on the mass spec separately (generally as part of different sessions separated by weeks or months). Thus, these measurements test the experimental reproducibility of all elements of our measurement (at least for gases similar in composition to these 'wet' thermogenic natural gases). Most replicates of each fragment ion exhibit reproducibility similar to the 1-sigma standard error of one measurement, and the average of the replicates is within two-sigma error (of an acquisition) of the average of the other replicate (Table 2).

Third, we conducted an experiment in which a fractionation was created by gas-phase diffusion, and then the products were analyzed to determine whether the measured change in isotopic composition conforms to the predictions of the kinetic theory of gases. An aliquot of gas from the cylinder of CIT-P1 standard was expanded into a 5-liter bulb

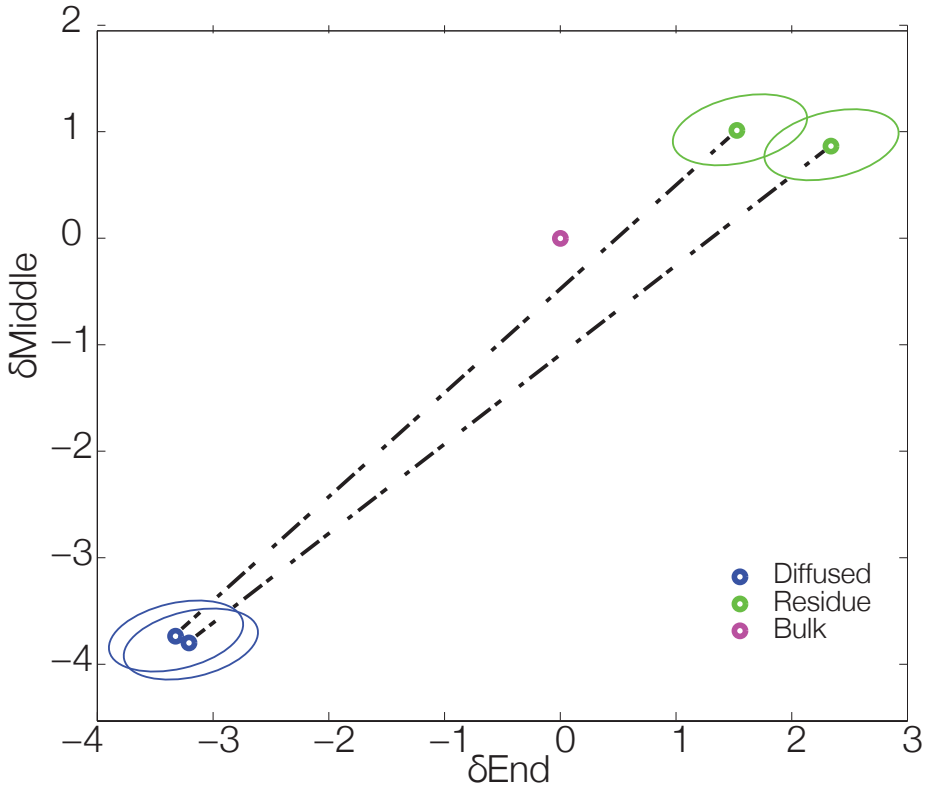

Figure 2.5: Results from the diffusion experiment. Both the end and the middle position are relative to the standard value. The bulk isotopic value is from the reference, which does not exactly match the initial value due to differences in starting composition.

attached to a vacuum line, with a pressure of 12.7 torr at 23°C. Propane was diffused through a needle valve into a break seal submerged in liquid nitrogen, which is below the freezing temperature of propane, creating an effective pressure of 0 bar on that side of the needle valve. The fraction of the gas collected in the break seal was measured as well as an aliquot that remained in the line between the bulb and the needle valve. The combination of the temperature and pressure of the experiment and the aperture of the needle valve led us to expect that the escape of gas from the 5-liter reservoir to the cold trap should follow the gas phase inter-diffusion regime. In this case, the fractionation factor ($R13_{diffused\ gas}/R13_{residue}$) should be 0.9944 (Slattery and Bird, 1958). This fractionation factor, plus the constraints of mass balance, let us predict the

changes in δ^{13}C that should be produced in both the diffused and residual gas. If we calculate the bulk δ^{13}C of these gas fractions based on measured isotopic compositions of the methyl and ethyl fragments (i.e., following equations 2.1-2.4), this experiment tests the accuracy of both of these fragment ion analyses (i.e., an error in either or both should lead to discrepancies from our prediction, unless the errors fortuitously balance). Furthermore, we expect that there should be no site-specific fractionation associated with this diffusion experiment because the site of a given isotopic substitution has no effect on the overall mass of the molecule. This is an approximation, and may be violated in cases where a molecule's diffusion rate is significantly influenced by its rotational moment of inertia, and/or nearest-neighbor interactions that involve weak bonding. Nevertheless, we consider it unlikely that a small, high-vapor-pressure compound like propane will exhibit low-pressure diffusion rates that violate the kinetic theory of gases. Thus, the methyl and ethyl fragment measurements, if accurate, are predicted to result in equal changes in the terminal and central carbon position δ^{13}C values.

The measured difference between the diffused portion and the residue was observed to be within error of 5.6‰, as predicted, for the bulk, terminal and central positions. Thus, our measurements match the kinetic theory of gases for both fragment ion measurements of both fractions of all experiments. We conclude that our method determines the size and direction of changes in central and terminal carbon isotope composition in propane, with accuracy as good as the external precision of each measurement. The only discrepancy from expectations is that the reconstructed average isotopic composition of all experimental products (i.e., the weighted average composition of diffused + residual gas) does not exactly match that of the reference. This could reflect a subtle experimen-

tal error (i.e., a fractionation associated with gas transfer and collection), or a subtle contaminant or mass spectrometric fractionation that disturbs the sample-reference difference but not sample–sample differences. Or, it may be that a difference in isotopic composition has developed between the large cylinder that is a reserve of CIT-P1 and the smaller reservoir in which our daily working standard is kept (the aliquots used to perform these experiments were sampled 1 year after the working standard reservoir was filled). In any event, this discrepancy is on the order of the external error of our measurements and does not imply a significant systematic measurement error.

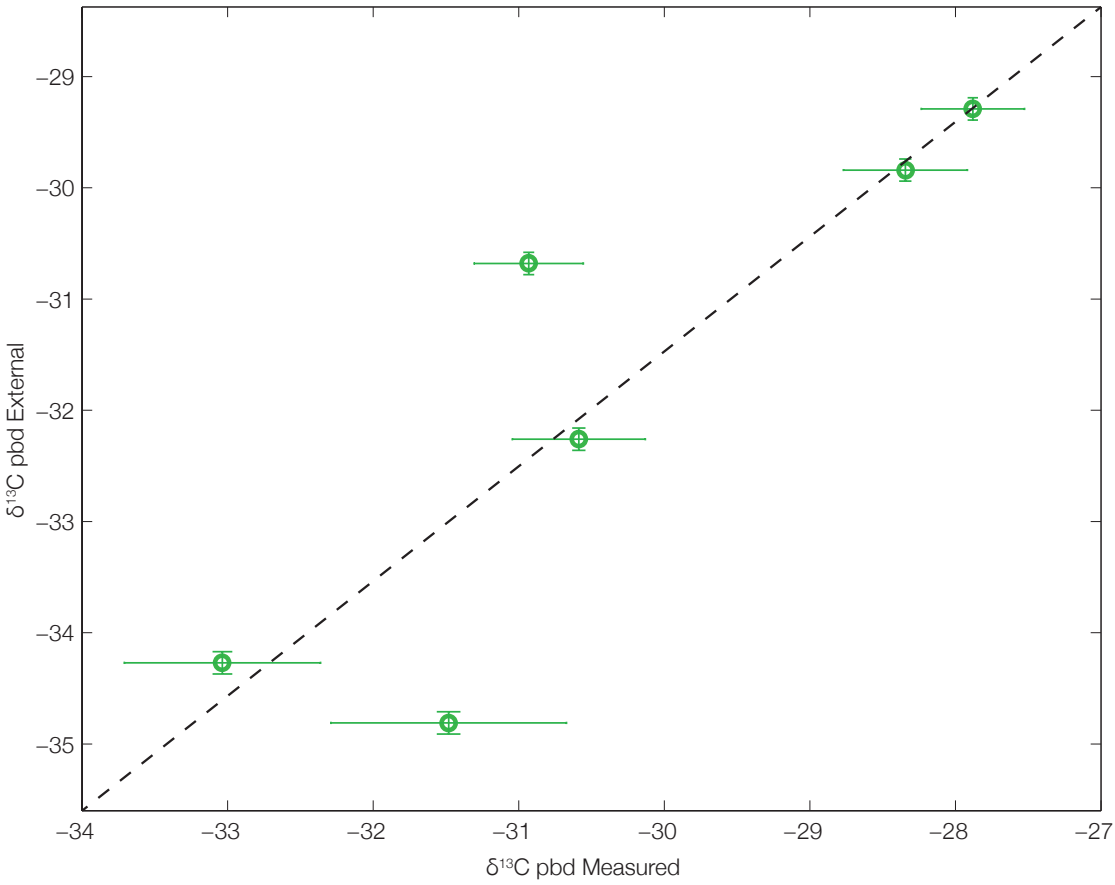

Figure 2.6: Plot of Petrobras molecular δ^{13}C composition versus calculated bulk composition, assuming a symmetrical 0.1 error bar for the Petrobras measurement because the error was not listed.

Finally, we can test the accuracy of the method by comparing differences in calculated

compound-specific $\delta^{13}C$ between two or more samples (i.e., based on measured differences in compositions of the methyl and ethyl fragment ions, in the CIT-P1 reference frame; Equation 2) to independently measured differences in $\delta^{13}C$ between aliquots of those same samples measured by conventional techniques in another laboratory. Such a comparison must contend with the fact that the interlaboratory (and even intralaboratory) precision of $\delta^{13}C$ measurements of propane is not well-established, so there is a significant probability that we would observe a difference in $\delta^{13}C_{PDB}$ between our accepted value for CIT-P1 tank and a given sample measured in some other laboratory simply because of lab-to-lab variations in the accuracy of GC-combustion-IRMS measurements of alkanes. For this reason, we apply this test by examining our ability to reproduce differences in $\delta^{13}C$ between samples from a single suite of natural gases analyzed in a single session in a single independent laboratory. We choose for this purpose a suite of natural gases recovered from production wells in the Potiguar basin, Brazil, and analyzed for the $\delta^{13}C$ of propane at the Petrobras CENPES research center, Rio de Janeiro. We fit a line between our calculated bulk $\delta^{13}C$, and the externally measured $\delta^{13}C$. The slope is 1.03 with an intercept of -0.5, indicating that our standard would be -34.80 in the CENPES research center. Based on the statistical significance of the fit of the line (r^2 = 0.849) and the slope of approximately 1 (Figure 2.6), this comparison suggests that our method accurately reproduces sample-sample differences in bulk $\delta^{13}C$, and thus that our measured variations in methyl and ethyl fragment ions accurately sample variations in central and terminal carbon positions.

2.5 Conclusions

The method we present suggests that high-resolution mass spectrometry of two or more fragment ions can be used to reliably measure differences among materials in site-specific carbon isotope fractionations. While we demonstrate this here only for propane, there is no obvious reason why the same approach could not be applied to various other volatile organic molecules. This method can be used in the future on larger organic molecules and combined with other 'clumped' isotope measurements for adjacent deuterium enrichment to explore the multi-dimensional isotopic fingerprints of the processes that form a population of molecules. The ability to measure site-specific isotope values to within 1-0.5‰ accuracy, given appropriate standards, makes this a very useful tool. Given the sample volume required for NMR, this new approach is very promising for a wide array of applications that formerly would have been impossible.

References

Abelson, P H and T C Hoering (1961). "Carbon Isotope Fractionation in the Formation of Amino Acids by Photosynthetic Organisms." English. In: *Proceedings of the National Academy of Sciences of the United States of America* 47.5, p. 623. URL: http://www.ncbi.nlm.nih.gov/pmc/articles/PMC221413/.

Berner, U et al. (1995). "Primary cracking of algal and landplant kerogens: kinetic models of isotope variations in methane, ethane and propane." English. In: *Chemical Geology* 126.3-4, pp. 233–245. DOI: 10.1016/0009-2541(95)00120-4. URL: http://linkinghub.elsevier.com/retrieve/pii/0009254195001204.

Clayton, C (1991). "Carbon isotope fractionation during natural gas generation from kerogen." English. In: *Marine and Petroleum Geology* 8.2, pp. 232–240. DOI: 10.1016/0264-8172(91)90010-X. URL: http://linkinghub.elsevier.com/retrieve/pii/026481729190010X.

Clog, M et al. (2013). "Doubly 13C-substituted ethane." English. In: *Mineralogical Magazine* 77.5, pp. 805–933. URL: http://openurl.ingenta.com/content/xref?genre=article&issn=0026-461X&volume=77&issue=5&spage=805.

DeNiro, M J and S Epstein (1977). "Mechanism of carbon isotope fractionation associated with lipid synthesis." English. In: *Science* 197.4300, pp. 261–263. DOI: 10.1126/science.327543. URL: http://www.sciencemag.org/cgi/doi/10.1126/science.327543.

Dennis, Kate J et al. (2011). "Defining an absolute reference frame for 'clumped' isotope studies of CO." In: *Geochimica et Cosmochimica Acta* 75.22, pp. 7117–7131. DOI: 10.1016/j.gca.2011.09.025. URL: http://dx.doi.org/10.1016/j.gca.2011.09.025.

Eiler, J et al. (2000). "Oxygen isotope geochemistry of oceanic-arc lavas." In: *Journal of Petrology*. DOI: 10.1093/petrology/41.2.229. URL: http://petrology.oxfordjournals.org/content/41/2/229.short.

Eiler, J et al. (2012). "A high-resolution gas-source isotope ratio mass spectrometer." In: *International Journal of Mass Spectrometry*, pp. 1–12. DOI: 10.1016/j.ijms.2012.10.014. URL: http://dx.doi.org/10.1016/j.ijms.2012.10.014.

Eiler, J et al. (2014). "Isotopic Anatomies of Organic Compounds." In: *Goldschmidt Conference*.

Gilbert, Alexis, Keita Yamada, and Naohiro Yoshida (2013). "Exploration of intramolecular ^{13}C isotope distribution in long chain n-alkanes (C_{11}-C_{31}) using isotopic ^{13}C NMR." In: *Organic Geochemistry* 62.C, pp. 56–61. DOI: 10.1016/j.orggeochem.2013.07.004. URL: http://dx.doi.org/10.1016/j.orggeochem.2013.07.004.

Hinrichs, K U et al. (2006). "Biological formation of ethane and propane in the deep marine subsurface." English. In: *Proceedings of the National Academy of Sciences* 103.40, pp. 14684–14689. DOI: 10.1073/pnas.0606535103. URL: http://www.pnas.org/content/103/40/14684.full.

Huntington, K W et al. (2009). "Methods and limitations of 'clumped' CO 2isotope (Δ 47) analysis by gas-source isotope ratio mass spectrometry." English. In: *Journal of Mass Spectrometry* 44.9, pp. 1318–1329. DOI: 10.1002/jms.1614. URL: http://doi.wiley.com/10.1002/jms.1614.

Lamprecht, G and F Pichlmayer (1994). "Determination of the authenticity of vanilla extracts by stable isotope ratio analysis and component analysis by HPLC." English. In: *Journal of Agricultural and ...* 42.8, pp. 1722–1727. DOI: 10.1021/jf00044a027. URL: http://pubs.acs.org/doi/abs/10.1021/jf00044a027.

Macko, S A et al. (1987). "Isotopic fractionation of nitrogen and carbon in the synthesis of amino acids by microorganisms." English. In: *Chemical Geology: Isotope Geoscience Section* 65.1, pp. 79–92. DOI: 10.1016/0168-9622(87)90064-9. URL: http://linkinghub.elsevier.com/retrieve/pii/0168962287900649.

Magyar, P et al. (2012). "Measurement of nitrous oxide isotopologues and isotopomers by the MAT 253 Ultra." In: *Mineralogical Magazine*. URL: http://resolver.caltech.edu/CaltechAUTHORS:20130807-132330822.

Monson, K D and J M Hayes (1980). "Biosynthetic control of the natural abundance of carbon 13 at specific positions within fatty acids in Escherichia coli. Evidence regarding the coupling of fatty acid and phospholipid synthesis." English. In: *Journal of Biological Chemistry* 255.23, pp. 11435–11441. URL: http://www.jbc.org/content/255/23/11435.abstract.

— (1982). "Carbon isotopic fractionation in the biosynthesis of bacterial fatty acids. Ozonolysis of unsaturated fatty acids as a means of determining the intramolecular distribution ..." English. In: *Geochimica et Cosmochimica Acta* 46.2, pp. 139–149. DOI: 10.1016/0016-7037(82)90241-1. URL: http://linkinghub.elsevier.com/retrieve/pii/0016703782902411.

Ono, Shuhei et al. (2014). "Measurement of a Doubly Substituted Methane Isotopologue, 13CH 3D, by Tunable Infrared Laser Direct Absorption Spectroscopy." English. In: *Analytical Chemistry* 86.13, pp. 6487–6494. DOI: 10.1021/ac5010579. URL: http://pubs.acs.org/doi/abs/10.1021/ac5010579.

Schauble, Edwin A, Prosenjit Ghosh, and J Eiler (2006). "Preferential formation of 13C–18O bonds in carbonate minerals, estimated using first-principles lattice dynamics." English. In: *Geochimica et Cosmochimica Acta* 70.10, pp. 2510–2529. DOI: 10.1016/j.gca.2006.02.011. URL: http://linkinghub.elsevier.com/retrieve/pii/S0016703706000913.

Singleton, Daniel A and Michael J Szymanski (1999). "Simultaneous Determination of Intermolecular and Intramolecular 13C and 2H Kinetic Isotope Effects at Natural Abundance." English. In: *Journal of the American Chemical Society* 121.40, pp. 9455–9456. DOI: 10.1021/ja992016z. URL: http://pubs.acs.org/doi/abs/10.1021/ja992016z.

Slattery, John C and R Byron Bird (1958). "Calculation of the diffusion coefficient of dilute gases and of the self-diffusion coefficient of dense gases." English. In: *AIChE*

Journal 4.2, pp. 137–142. DOI: 10.1002/aic.690040205. URL: http://doi.wiley.com/10.1002/aic.690040205.

Snell, Kathryn E et al. (2014). "High elevation of the 'Nevadaplano' during the Late Cretaceous." In: *Earth and Planetary Science Letters* 386.C, pp. 52–63. DOI: 10.1016/j.epsl.2013.10.046. URL: http://dx.doi.org/10.1016/j.epsl.2013.10.046.

Stolper, D A et al. (2014a). "Combined 13C-D and D-D clumping in methane: Methods and preliminary results." English. In: *Geochimica et Cosmochimica Acta* 126, pp. 169–191. DOI: 10.1016/j.gca.2013.10.045. URL: http://adsabs.harvard.edu/cgi-bin/nph-data_query?bibcode=2014GeCoA.126..169S&link_type=EJOURNAL.

Stolper, D A et al. (2014b). "Formation temperatures of thermogenic and biogenic methane." English. In: *Science* 344.6191, pp. 1500–1503. DOI: 10.1126/science.1254509. URL: http://www.sciencemag.org/cgi/doi/10.1126/science.1254509.

Takenaka, S et al. (1995). "Photooxidation of Propane over Alkali-Ion-Modified V 2 O 5/SiO 2 Catalysts." In: *Journal of ...* 155.2, pp. 196–203. DOI: 10.1006/jcat.1995.1203. URL: http://linkinghub.elsevier.com/retrieve/doi/10.1006/jcat.1995.1203.

Toyoda, Sakae and Naohiro Yoshida (1999). "Determination of Nitrogen Isotopomers of Nitrous Oxide on a Modified Isotope Ratio Mass Spectrometer." English. In: *Analytical Chemistry* 71.20, pp. 4711–4718. DOI: 10.1021/ac9904563. URL: http://pubs.acs.org/doi/abs/10.1021/ac9904563.

Uehara, K et al. (2003). "Site-selective nitrogen isotopic ratio measurement of nitrous oxide using 2 μm diode lasers." English. In: *Spectrochimica Acta Part A: Molecular and Biomolecular Spectroscopy* 59.5, pp. 957–962. DOI: 10.1016/S1386-1425(02)00260-3. URL: http://linkinghub.elsevier.com/retrieve/pii/S1386142502002603.

Westley, Marian B, Brian N Popp, and Terri M Rust (2007). "The calibration of the intramolecular nitrogen isotope distribution in nitrous oxide measured by isotope ratio mass spectrometry." English. In: *Rapid Communications in Mass Spectrometry* 21.3, pp. 391–405. DOI: 10.1002/rcm.2828. URL: http://doi.wiley.com/10.1002/rcm.2828.

Yeung, Laurence Y, Jeanine L Ash, and Edward D Young (2014). "Rapid photochemical equilibration of isotope bond ordering in O 2." English. In: *Journal of Geophysical Research: Atmospheres*, n/a–n/a. DOI: 10.1002/2014JD021909. URL: http://doi.wiley.com/10.1002/2014JD021909.

Yoshida, N and S Toyoda (2000). "Constraining the atmospheric N2O budget from intramolecular site preference in N2O isotopomers." In: *Nature* 405.6784, pp. 330–334. DOI: 10.1038/35012558. URL: http://www.nature.com/doifinder/10.1038/35012558.

Chapter 3

Site-specific ^{13}C distributions within propane from experiments and natural gas samples

Abstract

Site-specific carbon isotope measurements of organic compounds potentially record information that is lost in a conventional, 'bulk' isotopic analysis, due to the fact that isotopically fractionating processes may have different effects at different molecular sites, and because thermodynamically equilibrated populations of molecules tend to concentrate heavy isotopes in one site vs. another. Most recent study of site-specific carbon isotope compositions of organics use specialized NMR techniques or complex chemical degradations prior to mass spectrometric measurements. Here we present the first results of the application of a new mass spectrometric technique that reconstructs the site-specific carbon isotope composition of propane based on measurements of the $^{13}C/^{12}C$ ratios of two or more fragment ions that sample different proportions of the terminal and central carbon sites. We apply this method to propane from laboratory experiments and natural gas basins to explore the relationships between site-specific carbon isotope composition,

bulk carbon isotope composition, thermal maturation, and variation in organic matter precursors, with the goal of advancing our understanding of the sources and histories of small alkanes within these geologic systems. Our findings suggest that propane evolves in its site-specific carbon isotope structure in a distinctive way with increasing maturity, first increasing in terminal position δ^{13}C and then increasing in both center and terminal position δ^{13}C. This pattern is observed in both experiment and natural suites, and plausibly is explained by the combination of distillation of precursor compounds and transition from kerogen to oil and/or bitumen precursors with increasing maturity.

3.1 Introduction

Stable isotopes are useful for studying natural gas systems, as they provide a measure of different source compositions, an index of maturity, and an indicator of mixing between different reservoirs (Chung and Sackett, 1979; Schimmelmann and Sessions, 2006; Tang et al., 2005). However, many natural gases are influenced by several of these factors, leading to δ^{13}C values (either for bulk gas or specific compounds) that have non-unique interpretations. Differences in δ^{13}C between co-existing compounds (i.e., methane, ethane and propane) may help deconvolve these various factors influencing stable isotope composition (Chung, Gormly, and Squires, 1988). Nevertheless, it remains true that the stable isotope compositions of natural hydrocarbons are in many cases enigmatic (Zou et al., 2007). We present the results of a recently-developed method of site-specific carbon isotope analysis of propane, which adds additional constraints to help separate the influences of source and maturity on stable isotope compositions. A recent study re-

ports site-specific C isotope compositions of various commercially-available long-chain n-alkanes (Gilbert, Yamada, and Yoshida, 2013). But, to the best of our knowledge, this is the first systematic study of the C isotope structures of alkanes having well-constrained synthetic or natural origins, and thus may serve as an example for future studies of larger organic molecules.

Background: The carbon isotope structures of organic compounds

It has long been suggested that the biologic formation of molecules like amino acids and fatty acids should have complex site-specific isotope patterns that depend on their synthesis mechanisms (DeNiro and Epstein, 1977). For example, the cleavage of pyruvate to form acetyl groups, which are then used as substrates for diverse metabolic processes, was observed in acetaldehyde and predicted to create an even-odd ordering of carbon isotopes within fatty acids. This was eventually measured using complex preparation procedures involving multi-stage molecular decompositions (Monson and Hayes, 1980; Monson and Hayes, 1982). Broadly similar (though less well-understood) metabolic kinetic isotope effects are responsible for site-specific carbon isotope variations in amino acids (Abelson and Hoering, 1961), and contribute to differences in δ^{13}C between different amino acids (Macko et al., 1987). It has also been predicted by first-principles theory that equilibrium thermodynamic driving forces should tend to promote intra and intermolecular differences in δ^{13}C of amino acids, broadly resembling those observed in biological samples (Rustad, 2009).

Recent advances in NMR analysis of natural isotope distributions (so-called 'SNIF-NMR') have substantially expanded the range of site-specific isotope effects that have been seen, and the classes of compounds in which they can be observed. These methods have been used to quantify proportions of deuterium isotopomers of cellulose (Betson, Augusti, and Schleucher, 2006), oxygen and carbon fractionations in cellulose (Guy, Fogel, and Berry, 1993), and, most surprisingly the most economically important until this point, vanillin (Caer et al., 1991). These methods likely provide the best means currently available for observing the diversity of site-specific isotope effects in common, abundant organic compounds that can be obtained as large (100's of mg), pure samples. However, it will be challenging to apply SNIF-NMR methods to sample sizes more typical of environmental samples (μg to mg) (Gilbert et al., 2012).

Here we apply a new method that uses the characteristic fragmentation spectrum created during electron ionization to probe the isotopic enrichment of different parts of the molecule, where the fragments are analyzed for their isotopic proportions using high-resolution gas source mass spectrometry. We use this technique to explore the site-specific carbon isotope signatures associated with the competing factors that govern the bulk isotopic content of propane.

3.2 Methods

We measure the site-specific carbon isotopes of propane using a high-resolution gas source mass spectrometry technique described in Piasecki (2015a) and only summarized here.

Sample Preparation

First, we isolate propane from other constituents of a gas sample (e.g., methane, ethane, CO_2). This is done first with a series of vapor-pressure distillation steps using a cryostat. Methane, ethane, propane, and butane can all be separated from one another based on their differences in vapor pressure (though a molecular sieve is useful for recovering methane). Propane isolated cryogenically is often contaminated by CO_2 due to their similarities in vapor pressure; in this case, CO_2 is removed by exposure to ascarite (after which the sample is also exposed to drierite to remove water that is released in the ascarite reaction, followed by exposure to a trap held at dry ice ethanol slush temperatures to remove any remaining water). Our typical sample size of purified propane is approximately 50 μmol. Most of the samples described in this paper have been archived for additional future study.

Mass spectrometry

Once propane is isolated, it is introduced into the MAT-253 Ultra, a high-resolution gas source mass spectrometer (Eiler et al., 2012). Propane has a highly reproducible mass spectrum composed of 1, 2 and 3 carbon species containing variable numbers of hydrogens. Piasecki (2015a) establish that the 1-carbon species dominantly sample the terminal carbon position of analyte propane, whereas the two-carbon species are equal mixtures of central and terminal position carbons. The three-carbon piece obviously samples these carbon positions in their proportions in the full propane molecule (small–per cent level–departures from these generalizations occur due to fragmentation/recombination

reactions in the ion source and must be corrected for by analysis of isotopically labeled standards). Thus, a measurement of any two species differing in their carbon numbers (or combination of a measurement of a 1- or 2-carbon piece with a conventional bulk $\delta^{13}C$ value) can be used to solve for the difference in $\delta^{13}C$ between the terminal and central positions.

Ordinarily, we perform sample/standard comparisons of the $^{13}C/^{12}C$ ratios of a one-carbon species (CH_3^+ or CH_2^+) and a two-carbon species ($C_2H_4^+$). However, in cases where one or both of these measurements appears to be compromised (see below), we will also attempt a measurement of a three carbon species ($C_3H_8^+$; note, this species is measured in such a way that we collect ^{13}C and D species together, and then ion-correct the combined signal as described below). Note that the one-carbon fragment ion population was measured in two different ways over the course of this study: The initial method, which was used for some of the Potiguar Basin samples as well as the mixing experiments, involved measuring the ratio of $^{13}CH_3^+/^{12}CH_3^+$. However, nearby isobaric interferences from NH_2^+ required a background correction that proved to be unstable over time, degrading precision and accuracy. Therefore, we changed our method to look at species one cardinal mass lower, or the ion ratio $^{13}CH_2^+/^{12}CH_2^+$. The two methods were shown to be in agreement when background species were low for both (Piasecki, 2015a).

For each measurement, we determine intensities of background species that partially overlap the detector when it is positioned to measure analyte species of interest, and their contributions are subtracted. The precision for the two carbon and three carbon fragments are 0.1‰, and the single carbon fragment has a precision of 0.5‰. In cases where the three-carbon species has been analyzed (along with a small contribution

from nearly isobaric $^{12}C_3H_7D$), we recover the sample for separate analysis of the ratio, $^{12}C_3H_7D/^{13}C^{12}C_2H_8$ using a modified Thermo DFS gas source mass spectrometer (Eiler et al., 2014). This is done to remove the contributions of the D-bearing species to the Ultra measurement, so that the $^{13}C/^{12}C$ ratio of the three-carbon can be evaluated. This procedure may appear complex because it involves multiple stages of analysis, but proved faster and more straightforward than attempting to explicitly mass resolve the ^{13}C and isotopologues of C3H8 on the Ultra. This separation calls for a formal mass resolution of only 15,400. The maximum mass resolution of the Ultra (27,000) exceeds this value, but the large difference in relative abundance between ^{13}C and D means D is barely resolved from the tail of ^{13}C. This problem is not present in the DFS measurement, which cleanly separates the two species.

The primary analytical problem that we encounter is anomalous fractionation behavior in the ion source in the presence of minor contaminants. For example, we have established that the presence of even small amounts of butane in a sample compromises the apparent isotopic composition of the 1-carbon species (either by butane contributions to the 1-carbon ion population, or because its presence modifies the instrumental isotopic fractionation associated with ionization and fragmentation of propane). We explain below, in the section titled 'data table,' how we evaluate the accuracy of our results in the face of this problem. In some of the instances where a measurement of the 1- and 2-carbon fragments failed to pass these criteria, we attempted a second measurement examining the 2- and 3- carbon species, which together yield a less precise estimate of the difference in $\delta^{13}C$ between the terminal and central carbon positions (simply because neither is observed in isolation, as in our standard method). This approach usually resulted in a

more robust measurement that passed our criteria for accuracy.

Data table

All sample analyses, including supporting data such as independently measured bulk δ^{13}C values, are presented in Table 1. Note that not all of the four possible measurements (molecular δ^{13}C; 1-carbon δ^{13}C, 2-carbon δ^{13}C, 3-carbon δ^{13}C) were done for all of the samples. If there is a blank space in the data table, it is an indication that this measurement was not done on that sample.

Table 3.1 includes only data that pass two criteria that we applied to evaluate data accuracy: (1) we require that the bulk δ^{13}C value implied by our measurement of two or more fragment ions is consistent with an independently known value determined by some other technique (generally on line combustion GC-IRMS), with an accepted range of agreement of ±1‰ (except the Potiguar Basin suite which we identify as being self consistent but offset). In the latter half of this study, as we moved to work on gases with lower propane abundance and greater proportions of the more troublesome contaminant gases, we also developed contamination indices based on the relative heights of peaks in the propane mass spectrum. In particular, a measurement is considered valid only if its measured intensity ratios for all of: 29/28, 43/42 and 44/43 are within 20% of the value observed for a concurrently run standard, with no evidence for CO_2 or butane in the mass spectrum. Data for samples that fail one or both of these metrics are presented in the appendix, but we do not attempt to interpret them, as we suspect they one or more of their fragment ion species has an inaccurate δ^{13}C value due to an analytical

artifact related to contaminant gases. These problems do not arise from isobaric interferences (which would be noted in scans of the mass spectrum near the analyzed peaks); rather, we suspect they arise from changes in the fragmentation behavior and associated instrumental mass fractionations when gases other than propane are present in the ion source.

Reference frame and plotting conventions

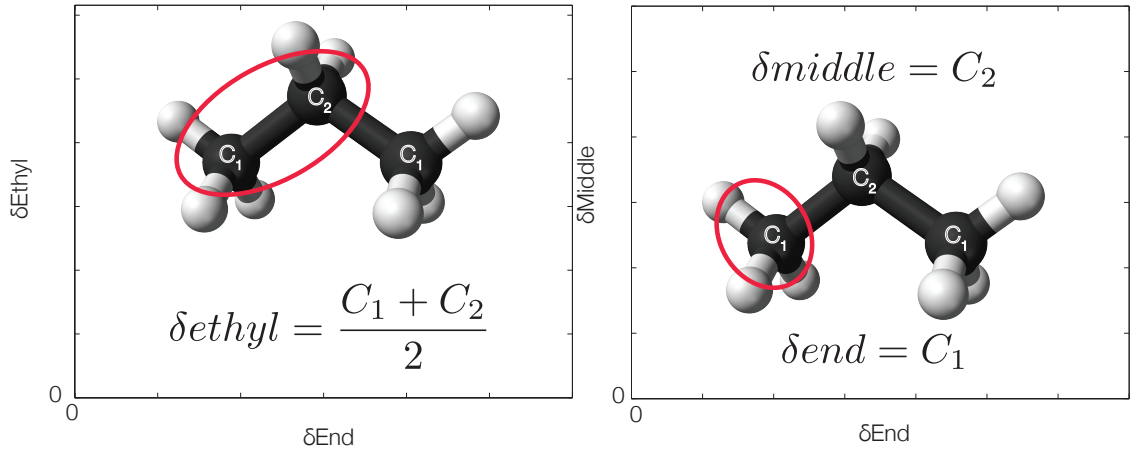

Figure 3.1: Shows a representation of the reference frame for site-specific carbon substitutions in propane. Panel A shows the average of the terminal and central position plotted versus the terminal position. Panel B shows the central position plotted versus the terminal position. Propane measurements are treated as symmetric within this study for natural samples, although modeling results can differentiate between double or single terminal substitutions.

The relative novelty of the site-specific carbon isotope fractionations that we discuss necessitate the definition of a reference frame for reporting differences in composition and, when we wish to visualize results of measurements or calculations, plotting conventions. Some (though not all) previous NMR-based studies of site-specific carbon isotopes are able to draw on the capacity of that technique to observe absolute differences in ^{13}C

content between sites, nominally with no analytical artifacts. When such data are combined with a known δ^{13}C value (for instance, through a conventional combustion-based analysis), it is possible to calculate the δ^{13}C of each site vs. some common scale (e.g., PDB) based on obvious mass balance arguments. In other cases (Gilbert, Yamada, and Yoshida, 2013), NMR observes only the site-specific C isotope compositions of a subset of sites, meaning such mass balance calculations are not fully defined, and one must report only differences in δ^{13}C between constrained sites.

We face a different problem: Gas source mass spectrometry involves an intrinsic analytical mass fractionation that must be corrected for by comparison with a known standard. Site-specific and clumped isotope standards can potentially be prepared by selective chemical degradation followed by conventional analysis of the 'pieces' (e.g., N_2O (Toyoda and Yoshida, 1999)), or by driving a standard to thermodynamic equilibrium at known temperature and assuming quantum mechanical calculations of that equilibrium state are correct (e.g., CO_2, O_2, CH_4 and N_2O (Wang, Schauble, and Eiler, 2004)). We have not succeeded at either of these strategies and so, for the time being at least, are left in the position of reporting variations in site-specific carbon isotope ratio as differences from a standard.

The standard used for these measurements, Caltech Propane 1, or 'CITP1,' was obtained from Air Liquide; we suspect they concentrated from an unknown conventional natural gas basin. The $\delta^{13}C_{PDB}$ of the standard is -33‰, and the δD_{VSMOW} of the standard is -197.7‰± 1.4. That is, when we report the δ^{13}C of the terminal or central position measured for some unknown sample, it is relative to a reference frame in which the δ^{13}C of the terminal and central position carbons of our standard, CITP1, are ax-

iomatically set to equal 0. For clarity, all such values are reported as: $\delta^{13}C_{end}^{CITP1}$ or $\delta^{13}C_{center}^{CITP1}$.

When we report the results of theoretical calculations, we face none of these standardization problems and can simply report the calculated value of each position, relative to any arbitrary reference frame such as PDB. In these cases, we will label these values: $\delta^{13}C_{\text{end PDB}}$ or $\delta^{13}C_{\text{center PDB}}$.

Most plots presented in this paper present the $\delta^{13}C$ of the terminal position ('end'; note that this always averages the compositions of the two indistinguishable terminal carbons) on the horizontal axis vs. the $\delta^{13}C$ of the center position ('center') on the vertical axis. Or, where clearly labeled, we plot the difference in $\delta^{13}C_{\text{ PDB}}$ between center and terminal position vs. some other variable (such as temperature). In all cases, the reference frame of the delta value is indicated by the subscript, as described above. Note that in the case of analytical data, the $\delta^{13}C$ of the terminal and center positions has been calculated by combination of two independent constraints. For example, the terminal position might be set equal to the measured value of a methyl fragment (based on prior demonstration that this site is sampled almost exclusively by this fragment ion (Piasecki, 2015a)), whereas the central position might be calculated based on the difference between the measured 1-carbon and 2-carbon fragment ions. In all cases, we have propagated analytical errors for the constraint in question through the relevant mass-balance calculation.

3.3 Theoretical and experimental constraints on the position-specific stable isotope effects of end-member processes

Homogeneous Isotope Exchange

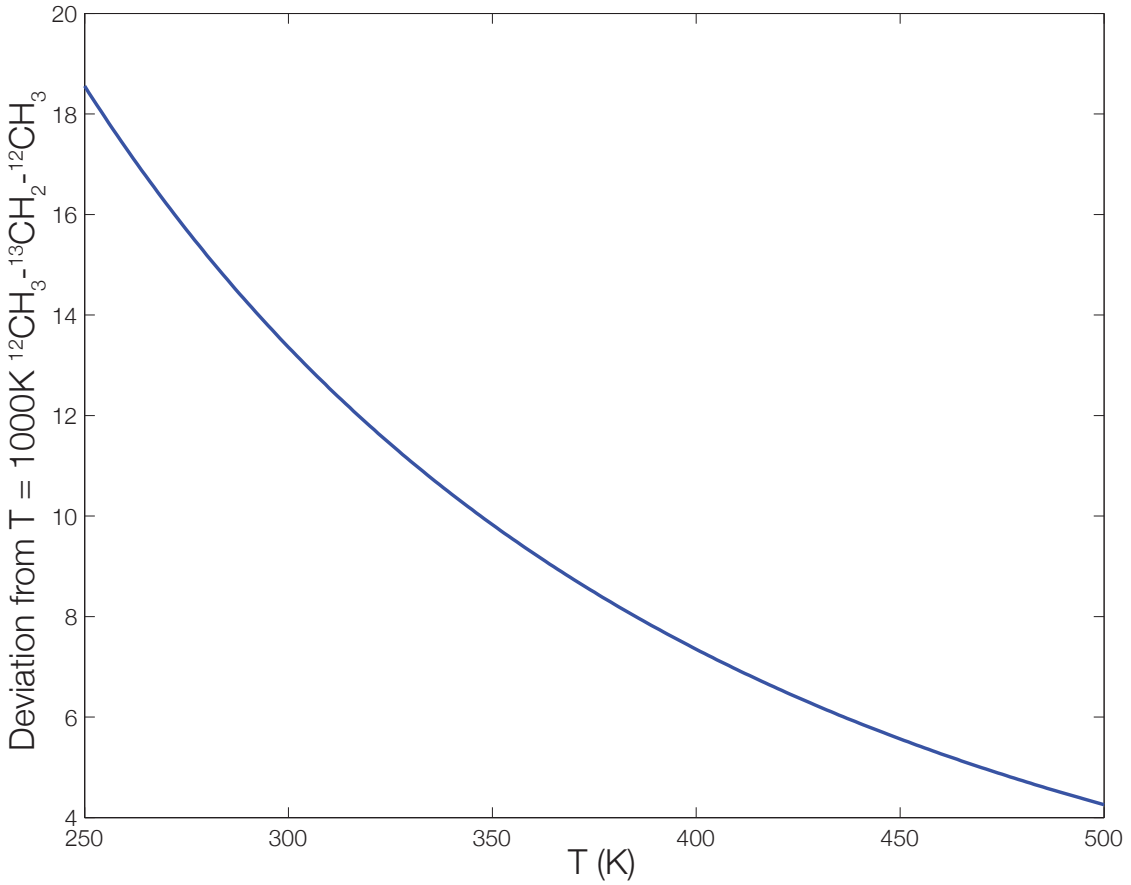

Figure 3.2: Shows the predicted equilibrium site-specific isotope fractionation favoring heavy carbon in the center position of the molecule.

It is unclear whether or not natural propane should achieve internal isotopic equilibrium with respect to the various possible site-specific and/or clumped isotope exchange reactions. And, we did not succeed in experimentally producing a bracketed equilibrium

as part of this study. Nevertheless, it is useful to estimate the direction, strength and temperature dependence of isotopic variations driven by such exchange reactions; it is possible that we may recognize patterns resembling these predictions in data sets for natural gases or experimental products, and in any case, such models can contribute to a framework for interpreting our site-specific measurements.

Here we summarize and discuss the implications of a quantum mechanical model of site-specific ^{13}C distribution in propane, first presented in (Piasecki and Eiler, 2012). Briefly, this study uses density functional theory (DFT) to estimate the frequencies of fundamental vibrational modes for gaseous propane and the frequency shifts and free energy changes associated with ^{13}C substitution in the center or terminal carbon positions. These data are used to estimate the equilibrium constant for the reaction:

$$^{13}CH_3 -^{12} CH_2 -^{12} CH_3 \longleftrightarrow ^{12} CH_3 -^{13} CH_2 -^{12} CH_3 \tag{3.1}$$

The results indicate that for propane, as with most small molecules that have been studied for geological purposes (Wang, Schauble, and Eiler, 2004; Ma, Wu, and Tang, 2008; Wang et al., 2009a), it is energetically favorable to partition the heavy isotopologues into the center of the molecule, where their substitution will lead to the greatest reduction in the total molecular vibrational energy (Bigeleisen and Mayer, 1947; Urey, 1947). Figure 3.2 shows the predicted deviation of the equilibrium constant for this reaction, in parts per thousand, from the high temperature limit of that equilibrium constant, plotted as a function of temperature. The results show that minimization of vibrational energy favors partitioning ^{13}C in the center position of the molecule. The effect is quite

large at low temperature (19‰ at 250 K), and remains significant (5-12‰) over geologically relevant temperatures. The amplitude and temperature variations of this predicted equilibrium effect should be easily resolved given the precision of our site-specific measurements (which result in an external error of 1‰ in the contrast in δ^{13}C between the terminal and central carbon positions).

There are reasons to suspect that the equilibrium effects described above are unlikely to manifest in natural propane. The majority of propane on earth is formed from the degradation of larger organic molecules during digenesis and burial, through reactions that are generally considered to be irreversible and thus should manifest kinetic isotope effects rather than equilibrium distributions (see below). It is less clear what we should expect of less common pathways for propane formation, like Fischer-Tropsch synthesis (McCollom and Seewald, 2006) or biological synthesis (Hinrichs et al., 2006). It seems imaginable to us that one or more of these propane synthesis mechanisms might equilibrate the carbon isotope structure of propane. And, perhaps even more familiar 'cracking' reactions could result in internally equilibrated propane if they occur in the presence of catalysts. If these cases exist and can be recognized, this effect could serve as a usefully precise geothermometer. It also seems likely that similar phenomena exist in larger molecules, perhaps open for future study with methods related to those used here.

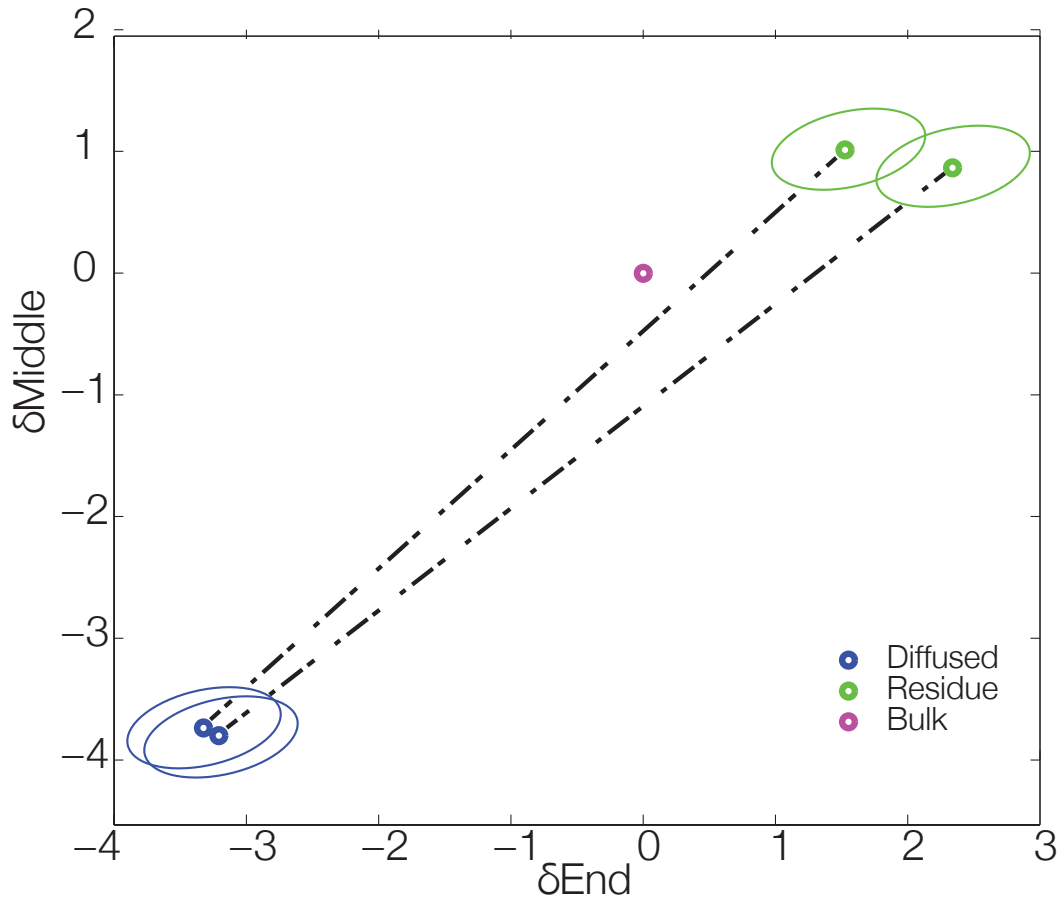

Figure 3.3: Shows the results of a diffusion experiment of propane through a needle valve. No site-specific preference was expected or measured, and the measured offset between the diffused and residue is within error of the expected value.

Diffusive fractionations

Diffusion of molecules through an aperture or some other medium can lead to isotopic fractionations. When molecules diffuse through liquids or solids, the resulting fractionations are generally low in amplitude and follow mass laws that are not easily predicted. However, gas phase diffusion (either Knudsen diffusion through a hole, or gas phase interdiffusion through a gaseous medium) is often large in amplitude (multiple per mil to tens of per mil) and can be predicted relatively confidently using the kinetic theory of gases.

Knudsen diffusion of gaseous propane (i.e., at sufficiently long mean free path that collisions with other molecules can be neglected) follows the square-root mass law ($\alpha_{\text{diffusion}} = [m/m'] \times 0.5$), leading to the expectation that δ^{13}C of diffused propane will be 11.26‰ lower than its residue (calculated as $1000 \times \ln(\alpha)$; note that this may be enhanced by Rayleigh distillation effects or diminished by retro-diffusion). If propane diffuses through a gas medium (i.e., where molecule-molecule collisions are more frequent than escape), the resulting fractionation depends on the mean molecular mass of that gas medium. For the example of propane diffusing through itself (mean molecular mass of 44.09 amu), diffused gas is 5.60‰ lower than the residue. Important for our purposes, these predictions are independent of the site of ^{13}C substitution (except in extreme cases where ^{13}C enrichment greatly exceeds that of common natural materials, in which case multiple substitutions become common and non-linearities emerge in the relationships between concentrations, ratios and delta values). Thus, we predict that diffusive fractionations of propane will be observed as equal changes in the δ^{13}C of central and terminal carbon positions. This expectation might be violated if propane does not behave as a classical point mass, for example if its collisions with surfaces or other molecules involve London?s forces or other chemical interactions.

We tested these predictions by performing a laboratory experiment. A 5L glass bulb was filled with a low pressure of propane (12.7 torr). At the exit of the glass bulb was a needle valve, beyond which was a glass finger submerged in liquid nitrogen. Propane diffused through the needle valve for half an hour and was collected beyond the valve with an effective pressure of 0 bar due to propane being completely frozen in liquid nitrogen (thus, retro-diffusion should be minimal). The change in pressure for the experiment is

0.18 torr after 50 μmol of propane was frozen into the glass sample finger. This indicates that only about 1.5% of the reservoir was depleted, so we do not believe that there were significant distillation effects.

We estimate based on the pressure and temperature in the bulb that the sample was in the gas phase inter-diffusion regime, leading to a predicted fractionation factor (δ^{13}C CITP1 of diffused gas minus the residual gas in the bulb) of -5.60‰. The diffused portion that was frozen into the glass finger was measured for its site-specific carbon isotope composition, as was an aliquot from the residual gas remaining in the glass bulb. The results for two separate experiments of this type are shown in Figure 3.3.

The results are consistent with the predicted fractionation factor for gas phase inter-diffusion. In addition, the terminal and central positions are fractionated by the same amount (within analytical error), indicating as expected that the diffusive fractionation depends only on molecular mass and not on the molecular location of the heavy-isotope substitution (at least under the conditions of these experiments).

In both diffusion experiments, we observe a small but statistically significant difference between the calculated weighted average of the diffused and residual gas vs. the inferred composition of the starting gas. We suspect that this is because the aliquots of gas used for each experiment were taken from the same large pressurized gas cylinder as the standard, but at a much later date. The gas cylinder is at high enough pressure that much of the propane is in liquid form, so removal of aliquots involves a phase transformation that may be isotopically fractionating. Thus, we suspect that the large gas cylinder has fractionated approximately 0.5‰ from its initial isotopic composition. The aliquot that we use as a daily working standard was taken from the cylinder approximately 1 year

prior to these experiments, and is stored at below atmospheric pressure to insure that it is in the gas phase and not fractionated (at least, by recognized processes).

While it is perhaps unsurprising that we observe site-specific fractionations in propane that follow the simple predictions of the kinetic theory of gases, it is worth considering whether other molecules, or propane at other conditions (e.g., very high pressure, or in the presence of a reactive medium), might exhibit fractionations that differ from the kinetic theory of gases due to chemical or physical phenomena. We think it imaginable that hindered rotations or electrostatic and chemical interactions, for example, could lead to site-specific isotope effects in diffusion. This possibility is an attractive target for future research. Finally, we note an important conclusion that one can reach about our methodologies based on the diffusion experiments described above: assuming our expectations based on the kinetic theory of gases are valid, the close agreement between these expectations and our results suggests that we are able to recover site-specific compositions of propane with accuracy similar to the formal precision of our measurements.

Mixing effects?

It is well-established that clumped isotope compositions of molecular gases can exhibit relatively large anomalies (i.e., differences from random proportions of multiply substituted species) simply due to mixing of end members that differ in bulk composition. These effects arise because the random probability of forming a doubly substituted species goes as the square of the concentration of the isotope in question; thus mixing of heavy-isotope rich and heavy-isotope poor end members should generally result in mixtures that con-

tain more doubly substituted species than expected for the new rare isotope content. This effect is well-established for CO_2, O_2, CH_4, N_2O, C_2H_6 and has been explored in theory for H_2.

At first glance, it might seem obvious that no such effects should exist for site-specific isotopic fractionations (e.g., difference in $\delta^{13}C$ between the terminal and central position of propane). However, subtle changes in site-specific fractionation should be introduced by mixing end members that differ in total ^{13}C content, both because of non-linearities in the probabilities of multiple substitutions (including multiply substituted species that our techniques would 'count' as part of a singly substituted population; i.e., because we combine signals for fragment ions that could have come from two or more different isotopologues), and because the ratios and delta values used to report fractionations do not have a perfectly linear dependence on concentrations of isotopologues. Nevertheless, our exploration of these issues through model calculations suggests they lead to changes in site-specific carbon isotope fractionation in propane that are on the order of 0.01 per mil for most cases one is likely to encounter, and thus are insignificant for our purposes. We suggest that they can be ignored, at least for propane having $\delta^{13}C$ values in the natural range.

Chemical-kinetic fractionations

Most natural propane is believed to form through catagenetic 'cracking' reactions that decompose buried organic matter to release more volatile hydrocarbons. The exact mechanisms of these reactions (specific reactant molecules; bonds being broken; sites that con-

tribute carbon to newly formed propane; transition state structures) are generally not known. However, previous studies that have considered the stable isotope systematics of propane formation through cracking assume (implicitly or explicitly) that they involve breaking a single C-C bond to abstract a 3-carbon 'unit,' without re-ordering of carbon atoms from the parent molecule. If this is correct, propane should inherit the pre-existing carbon structure of the components of kerogen from which it forms, perhaps altered by kinetic isotope effects associated with cleaving a C-C bond (Chung, Gormly, and Squires, 1988; Tang et al., 2005).

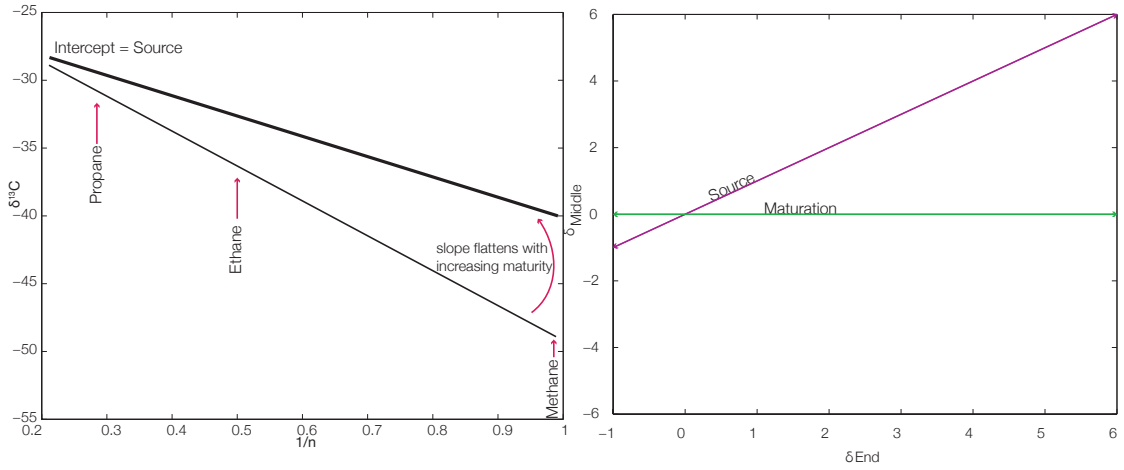

Figure 3.4: This figure shows the expected fractionation within the defined propane space during cracking. Following the theory of the Chung diagram, maturation should move you left to right, while source will affect both terminal and center positions equally.

Our understanding of the isotopic structure of kerogen and the kinetic isotope effects associated with propane formation is likely too crude to make a confident prediction of the resulting site-specific isotopic structures of natural propanes. The goal of this section is to make a prediction based on previous work on how kinetic degradation of larger organic molecules in a natural gas basin will affect the distribution of isotopes within a propane molecule. In particular, we develop a 0th-order model extrapolated from the

assumptions underlying existing models of the bulk δ^{13}C of propane, and then test and modify that model by examining propane generated by controlled cracking experiments.

We begin with a widely-used model for the interpretation of δ^{13}C values of n-alkanes in natural gases (Chung, Gormly, and Squires, 1988). This model assumes a starting reservoir of kerogen having some defined $\delta^{13}C_{kerogen}$ value, and a fractionation ϵ, equal to the δ^{13}C of kerogen minus the δ^{13}C of carbon abstracted from that kerogen by breaking a carbon-carbon bond. ϵ is generally held constant over the model calculation and is assumed to be the same for reactions that form all small alkanes (methane, ethane, propane and butane) (Chung, Gormly, and Squires, 1988). Given these assumptions, and adopting the approximation that δ^{13}C and ϵ values can be added and subtracted without error, the first methane derived from cracking the kerogen will have a δ^{13}C value equal to: $\delta^{13}C_{kerogen} - \epsilon$. The first ethane formed will have bulk initial δ^{13}C equal to $\delta^{13}C_{kerogen} - (1/2) * \epsilon$, because the fractionation only influences the carbon adjacent to the cleaved bond, not the other carbon (i.e., we are to imagine a reaction such as: [C1–C2–C3–C4...Cn] goes to Ethane + [C3–C4...Cn]). Similarly, in this model the δ^{13}C of the first propane formed will be equal to $\delta^{13}C_{kerogen} - (1/3) * \epsilon$ (again, because the kinetic isotope effect influences only the carbon adjacent to the breaking bond in the kerogen, and not the other two carbons).

A critical question from our perspective is, which of the three carbon atoms in a propane molecule records that bond-breaking event by taking on a low δ^{13}C value? The Chung et al. model is mute on this point, and we are not aware of any other constraint that provides the answer. However, we think it is most plausible to assume that propane is abstracted by breaking a bond between one of its terminal carbons and an adjacent

carbon (as would occur if a C3 group were cleaved from the end of an n-alkane). In this case, a measurement of the terminal site in product propane will be lower in δ^{13}C than the source kerogen (by a factor of $\epsilon/2$, since only one of two equivalent terminal carbons are affected), whereas the central carbon position should maintain its initial δ^{13}C value, presumably equal to $\delta^{13}C_{kerogen}$. The effect could also be altered by the presence of non-linear alkanes like isobutane. The preferential degerdation of iso-butane early (and other similar species), switching to linear n-alkanes at higher temperatures or maturities, could also alter the pattern.

It would be challenging for us to test the predictions outlined above using our method, because our analyses are reported relative to an arbitrary standard–i.e., we can examine relative changes in site-specific C isotope fractionation, but not absolute values. However, the model of Chung et al. implies a second expectation that we can test: The isotopic composition of kerogen (or, at least, the components of that kerogen that break down to produce propane) will evolve through time, as cracking reactions preferentially remove ^{12}C-bearing species, and therefore the isotopic composition of propane will evolve through time (i.e., as it tracks the evolution in its source). In the limiting case where nearly all kerogen C, besides that which is residual graphite due to C/H ratio, has been transformed to natural gas, we should expect all of the small n-alkanes should be identical in δ^{13}C to the initial kerogen. If, as we assume, the cracking reactions only influence one of the two terminal carbon sites, we should expect this phenomenon to express itself as an evolution of δ^{13}Cend, from low to high values, as gas maturity increases. Thus, our starting hypothesis is that the δ^{13}C of the terminal position in thermogenic propane will record the kinetic fractionations of cracking, and be a marker of the extent of maturity, whereas

the center carbon position in propane will be invariant in $\delta^{13}C$, equaling $\delta^{13}C_{kerogen}$ at all maturities, and that increasing thermal maturity will be associated with an increase in that terminal $\delta^{13}C$, until at maximum maturity the produced propane will have $\delta^{13}C$ values in both terminal and central positions that approach the source kerogen. This hypothesis may seem overly specific, but it is a logical (perhaps necessary) extension of the widely used Chung et al. model, provided that one adopts the assumption that propane-forming reactions 'crack' a C-C bond between the substrate and what will become the terminal carbon of the product propane.

Cracking experiments

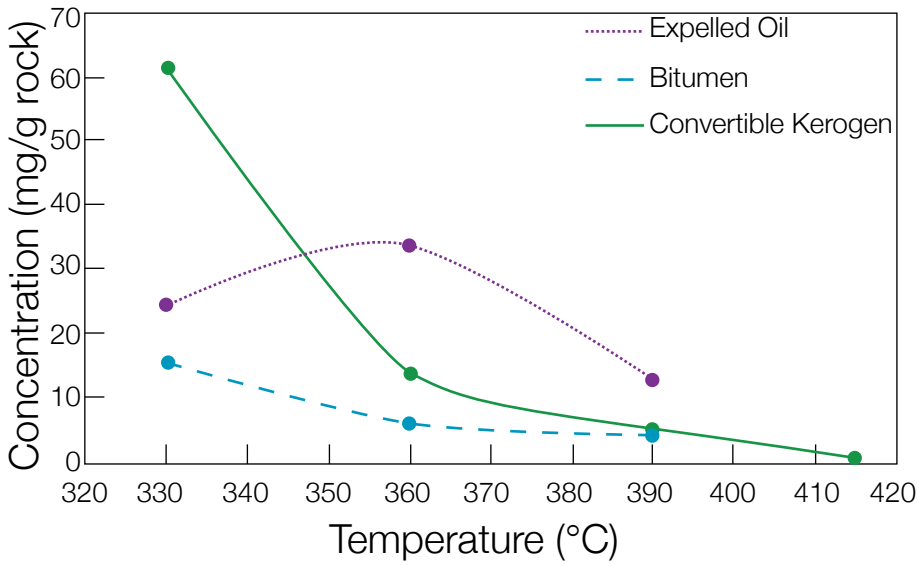

Figure 3.5: Shows the different components as a function of temperature within the USGS Cracking experiments.

We test the model outlined above by measurement of propane produced by cracking experiments. More generally, these experiments provide at least a first look at the experimental basis for using site-specific carbon isotope composition of propane as proxy

for thermal maturity in natural gas basins.

The experiments were completed by the USGS at Denver. The substrate was Woodford Shale, and all experiments were conducted with water present ('hydropyrolysis'). The starting material was heated in a closed system for 72 hours at four different temperatures. The 330° experiment has the majority of the gas being derived from kerogen cracking as shown in figure 3.5. As temperature increases, the amount of remaining kerogen and evolved bitumen decreases significantly, but the oil that is released increases. This indicates that there is a greater proportion of oil available as a possible source substrate for forming propane. The bitumen at both of these temperatures remains a minor constituent. By 390° the oil amount has also decreased, and the majority of the sample at this point is natural gas. The highest temperature experiment conducted at 415°C leaked and fractionated; therefore, there is no data for that experiment.

Before discussing our findings for these experimental gases, we consider the accuracy of the data for this group of samples by comparing our constraints on bulk molecular δ^{13}C with independent constraints from conventional bulk measurements (we also consider evidence of the peak intensity ratios that we use to judge sample purity). For experiments run at 330°C and 360°C, the bulk δ^{13}C of propane calculated based on measurements of the one- and two-carbon fragment ions matched the independently-known bulk δ^{13}C value within error. However, the 390°C experiment resulted in an implausibly low apparent δ^{13}C for the methyl fragment ion, a common feature of samples that are contaminated with something that promotes extra production of single carbon fragment ions within the source of the mass spectrometer. It is unknown why only the single sample appeared to be contaminated, despite the similarity among all samples in method of production gas

Sample	δEnd	st dev	st err	δEthyl	st dev	st err	δFull	stdev	st err	δD	st err	δEnd	δcenter	δFull	Quality
Diffusion															
Dif-1	-3.21	1.99	0.35	-3.50	0.59	0.11						-3.21	-3.80	-3.41	2
Dif-3	-3.32	1.90	0.34	-3.53	0.73	0.13						-3.32	-3.74	-3.46	2
Res-1	2.34	2.82	0.58	1.60	0.40	0.07						2.34	0.86	1.85	2
Res-3	1.52	1.85	0.34	1.27	0.59	0.10						1.52	1.01	1.35	2
Cracking															
330-72-1-1	-9.01	1.84	0.33	-3.59	1.23	0.22						-9.01	1.83	-5.39	2
360-72-1-1	-6.94	2.75	0.49	-0.84	0.85	0.15						-6.94	5.26	-2.87	2
360-72-2A	-8.57	1.96	0.35	-0.25	0.32	0.06						-8.57	8.06	-3.03	2
390-72-1-2				2.78	0.29	0.05	0.40	0.16	0.03	64.67	2.05	-4.36	-9.91	-0.40	3
Potiguar															
1	6.82	1.65	0.24	4.88	0.85	0.13						6.82	2.94	5.53	2
01a	4.67	1.62	0.26	5.67	0.51	0.08						4.67	6.66	5.33	2
02b	1.66	1.69	0.69	0.46	0.67	0.12						1.66	-0.74	0.86	2
3	4.84	2.41	0.38	3.72	0.39	0.07						4.84	2.59	4.09	2
3 b	3.19	1.76	0.31	1.41	0.84	0.12						3.19	-0.37	2.00	2
03a	4.58	1.11	0.24	0.41	1.42	0.25						4.58	-3.77	1.80	2
4	4.55	1.92	0.34	4.29	0.51	0.09						4.65	3.94	4.41	2
4	4.56	1.50	0.22	5.53	1.17	0.19						4.56	6.51	5.21	2
04a	6.28	1.89	0.33	4.73	0.63	0.11						6.24	3.23	5.23	2
07a	0.76	2.96	0.52	0.05	0.38	0.29						0.76	-0.67	0.28	2
7m	0.17	2.68	0.42	-0.22	0.61	0.11						0.17	-0.60	-0.09	2
9	3.53	0.82	0.17	1.64	1.17	0.21						3.53	-0.24	2.27	2
Eagle Ford															
ET25	-23.70	5.73	1.17	3.26	0.33	0.06	3.54	0.27	0.05	-66.58	2.01	4.09	2.44	3.54	4
ET22H	-47.72	2.02	0.36	2.87	0.41	0.07	3.25	0.78	0.14	-68.36	1.75	4.00	1.75	3.25	4
IS1H	-24.80	5.75	1.02	3.75	0.31	0.06	4.32	0.23	0.04			5.47	2.03	4.32	4
Antrim															
C2-31-1-1				-1.12	0.22	0.04	-1.34	0.12	0.02	-8.01	1.64	-1.79	-0.46	-1.34	3

Table 3.1: Main data table

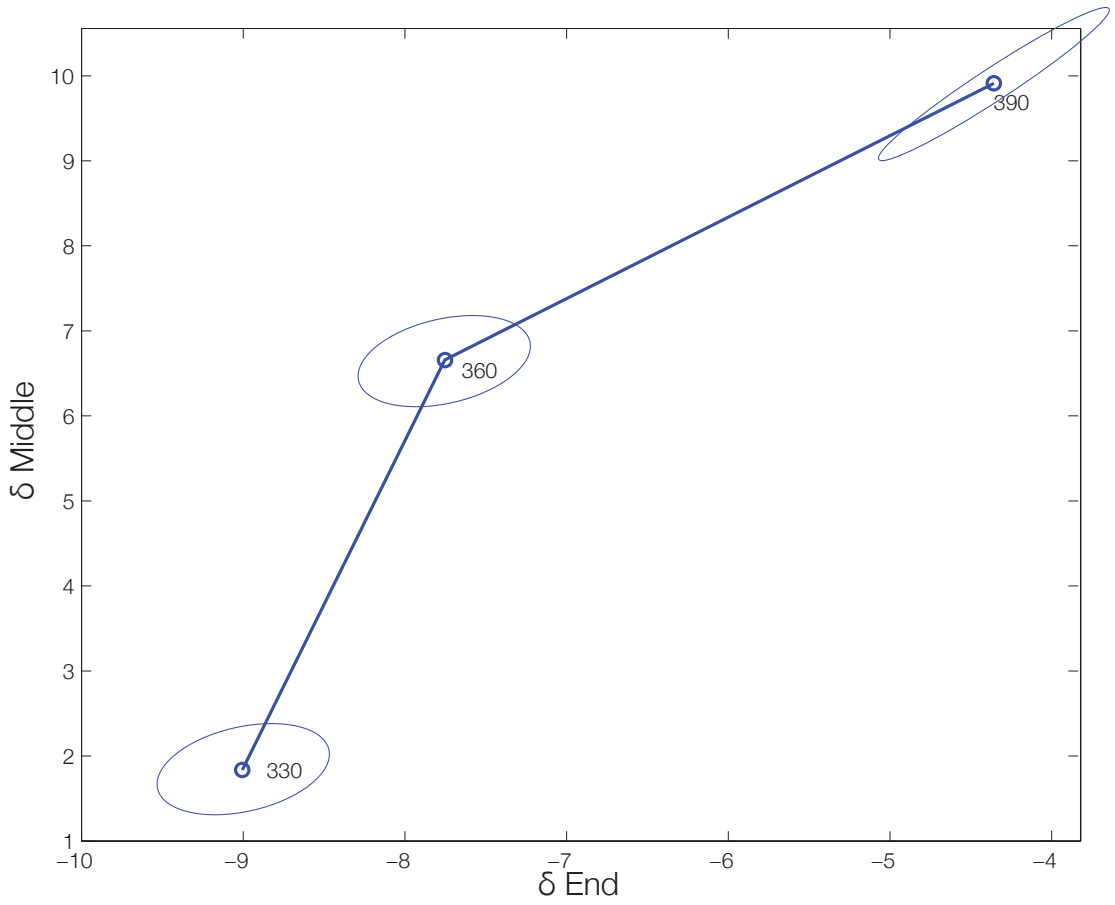

Figure 3.6: This figure shows the result of cracking experiments conducted on natural samples. The temperature of each experiment is shown beside the data point. All experiment times are 72 hours.

purification. We speculate that the longer time and higher reaction temperature produced an unknown species that we failed to remove during sample purification. Therefore, for this sample, we made an additional measurement of the entire propyl ion. This propyl measurement agrees with the externally-known propane molecular δ^{13}C value, and combining it with our measurement of the 2-carbon fragment ion lets us the difference in δ^{13}C of the center and terminal positions. Of course, it is possible that the same factor that compromised the measurement of the 1-carbon fragment ion also compromised the measurement of the 2-carbon fragment ion, but not the 3 carbon ion. However, the mass

spectrum through the mass range of the 2-carbon species was normal for this sample; and, more generally, we find no evidence that the intense 2-carbon fragment ion peaks are influenced by the artifacts that clearly disturb measurements of the weak ion beams of the 1-carbon fragment ions. All samples meet the requirement of being within 20% of the accepted value for the contamination indices.

The results from the cracking experiments are shown in Figure 3.6. Had the samples followed our hypothesis that cracking affects the δ^{13}C of only the carbon adjacent to the bond being broken, and that this carbon ends up as the terminal carbon in propane, then the data would follow a horizontal trend in Figure 3.6, moving from left to right with increasing maturity. Instead, we observe that increasing maturity from 330 to 360°C is associated with a modest increase in δ^{13}C of the terminal position but an even larger increase in the center position; further increase in maturity to 390°C increases both sites further, but more strongly in the terminal than central position. Note that all experiments are cumulative, so likely involve even larger changes in isotopic composition of the instantaneous fractions of newly generated propane.

There are several possible explanations of the trend in Figure 3.6, but we that suggest the hypothesis (motivated principally by independent information regarding the evolution in proportions of kerogen, oil and bitumen in these experiments) that it reflects shifts in the relative contributions of different source substrates of propane at different temperatures. In the lowest temperature experiment, kerogen dominates the non-gaseous products, making it likely that propane is principally derived from kerogen (so called 'primary cracking'). We speculate that propane derived from kerogen is characterized by relatively low δ^{13}C central position carbons; this effect, superimposed on the frac-

Samples	$\delta^{13}C$ CH_4	$\delta^{13}C$ C_2H_6	$\delta^{13}C$ C_3H_8	$\delta^{13}C$ nC_4H_{10}	$\delta^{13}C$ iC_4H_{10}	% CH_4	% C_2H_6	% C_3H_8	% nC_4H_{10}	% iC_4H_{10}
Cracking										
330-72-1-1	-43.55	-38.15	-35.54	-33.65		49.30	27.53	14.22	4.49	1.61
360-72-1-1	-44.62	-34.45	-32.81	-31.44	-31.48	55.06	25.31	12.55	3.59	1.37
360-72-2A	-44.62	-34.45	-32.81	-31.44	-31.48	55.06	25.31	12.55	3.59	1.37
390-72-1-2	-38.72	-29.89	-29.77	-28.92	-29.39	70.08	16.83	8.20	2.11	1.27
Potiguar										
1	-40.79	-31.21	-29.29	-28.49	-27.94					
01a	-40.79	-31.21	-29.29	-28.49	-27.94					
02b	-48.25	-38.01	-34.81	-33.75	-34.64					
3	-47	-34.84	-32.26	-31.75	-33.52					
3 b	-47	-34.84	-32.26	-31.75	-33.52					
03a	-47	-34.84	-32.26	-31.75	-33.52					
4	-45.02	-32.61	-29.84	-29.4	-31.28					
4	-45.02	-32.61	-29.84	-29.4	-31.28					
04a	-45.02	-32.61	-29.84	-29.4	-31.28					
07a	-47.14	-36.79	-34.27	-33.51	-34.53					
7m	-47.14	-36.79	-34.27	-33.51	-34.53					
9	-44.19	-32.86	-30.68	-30.87	-31.65					
Eagle Ford										
ET 25	-45.55	-33.6	-29.3	-28.7	-31.6	77.86	11.8771	4.93	0.98	0.45
ET 22H	-46.08	-33.5	-28.8	-29.1	-31.7	67.40	15.77	9.62	2.063	0.94
IS1H	-47.4	-32.20	-29.32	-30.02	-31.2	77.79	12.6213	5.31	1.28	0.57
Antrim										
C2-31-1-1	-53.3					69.74	6.61	1.97	4.81E-2	0.10

Table 3.2: External Data

tionations effecting the terminal positions, discussed above, should tend to place the early-formed propane in the lower left of Figure 3.6 . The non-gaseous products of the experiments conducted at 360 and 390° C are dominated by oil and bitumen; thus, it seems possible that propane in these experiments contains a larger proportion produced by so-called secondary cracking of oil. We speculate that propane generated from oil has a higher δ^{13}C central-position carbon, but will also tend to evolve from left to right with increasing progress of the cracking reactions that control the terminal position δ^{13}C. According to this hypothesis, increasing maturity will be associated with both a shift from kerogen to oil substrates, increasing the center position, and a 'distillation' of the terminal position, increasing its δ^{13}C. Thus, propanes should move from the lower left to upper right of Figure 3.6 with increasing maturity, perhaps marking the shift from primary to secondary cracking by the sharpest increase in the vertical axis. This scenario may seem to be an overly specific reading of the experimental data in Figure 3.6, but we show below that it is not only consistent with these experimental data, but also provides a useful framework for understanding variations in carbon isotope structure of natural propanes.

Finally, we finish this section with some speculation about the possible effects of thermal degradation of propane–a form of 'secondary cracking.' Propane readily degrades to form smaller hydrocarbons (mostly methane) on heating, particularly in the presence of catalysts. It seems likely that these reactions will be accompanied by kinetic isotope effects, but it is less clear whether such fractionations should be site-specific. Simple disproportionation of propane, if it involved cleaving the C–C bond between terminal and center positions, would presumably enrich the δ^{13}C of both sites in the residue, and

Sample	29/28	43/42	45/44	44/43	58/57
Cracking					
330-72-1-1	out of gas	3.56	3.04E-2	0.96	
360-72-1-1	1.60	3.53	3.09E-2	1.04	
360-72-2A	1.63	4.33	3.22E-2	1.05	4.70E-2
390-72-1-2	1.63	4.34	3.17E-2	1.14	
Eagle Ford					
ET 25	1.53	4.80	3.24E-2	1.04	1.47E-2
ET 22H	1.52	4.72	3.22E-2	0.95	2.63E-2
IIS1H	1.54	4.82	3.24E-2	1.11	
Antrim Suite					
C2-31-1-1	1.58	5.36	3.25E-2	1.07	

Table 3.3: Contamination Indices

we expect that this effect would be even, to first-order. If, instead, propane forms a complex with some other compound or condensed substrate before it 'cracks,' we might expect to see an inverse isotope effect (residual propane becomes lower in δ^{13}C, not higher) due to the tendency of heavy isotopes to stabilize chemical bonds. At present, we have no experimental data or observations of natural samples that speak directly to this issue.

Geologic propane from the Potiguar Basin

In this section, we describe measurements of the site-specific carbon isotope composition of propane from the Potiguar Basin in Brazil (east central, coastal Brazil). This sample suite comes from a conventional natural gas basin that produces gas varying significantly in maturity. The basin was created starting in the Early Cretaceous when the Atlantic Ocean began to rift apart, and is made up of a series of half-graben structures. Since it has been adjacent to a forming or present ocean, there is a mix of lacustrine and marine rocks, which are the protoliths for the natural gas basins in the area (Santos Neto and Hayes,

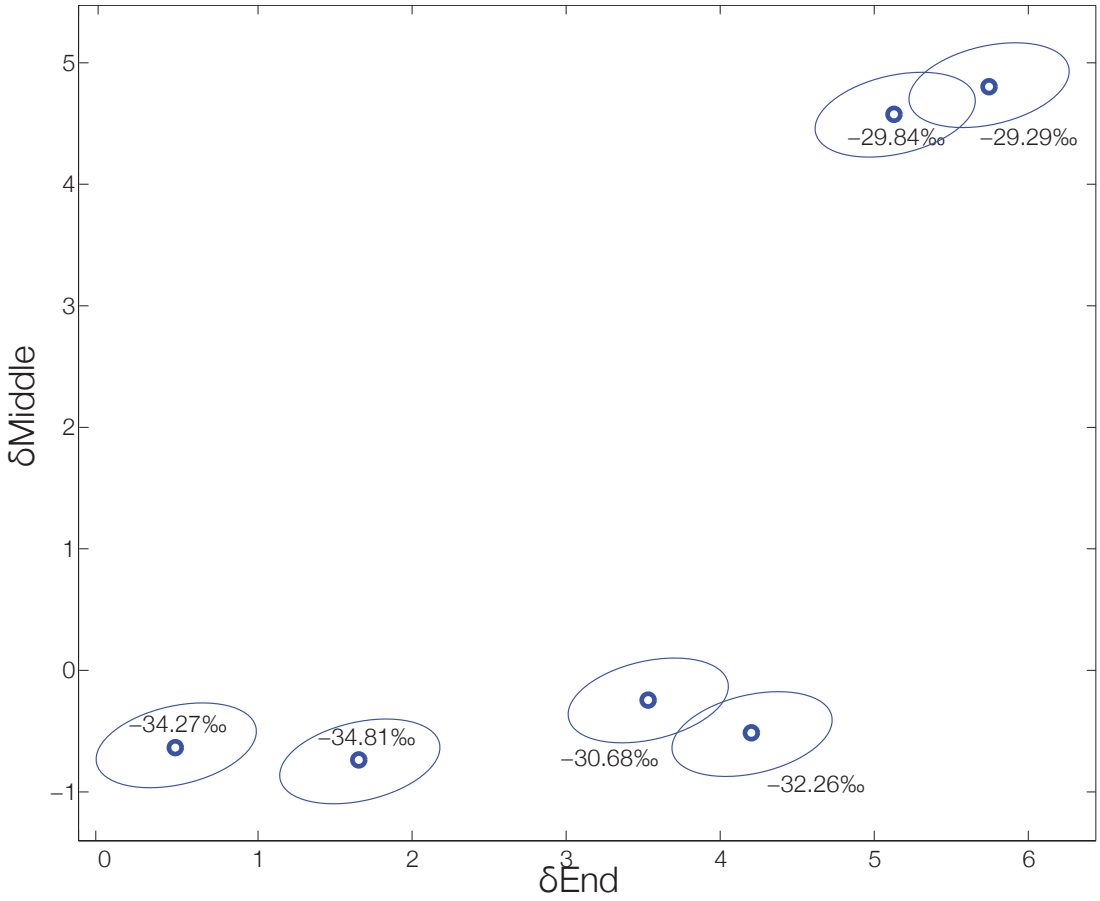

Figure 3.7: Figure showing the internal isotope distribution on a suite of wet gases from the Potiguar Basin. The label on each data point is the externally-measured bulk δ^{13}C. Distribution of data shows that there is an affect both on the center and terminal position as maturity changes.

1999; Ferreira et al., 2012). The Potiguar basin is believed to produce petroleum from both lacustrine and marine source rocks, although the samples we examined are believed to come from only the lacustrine units. Variations in δ^{13}C of propane in Potiguar basin gases are broadly in the range typical of thermogenic gases, and would be conventionally interpreted to indicate increasing thermal maturity with increasing δ^{13}C (Chung, Gormly, and Squires, 1988). There are three main sources of oil within the Potiguar basin. The first is a marine evaporate source which has a pristane to phytane ratio less than one, a peak in n-alkane abundance for C_{16} to C_{18}, and a high sterane concentration. The

lacustrine oil producing member, which is where our samples come from has a high pristane to phytane ratio, more abundant odd length n-alkanes, more abundant large n-alkanes, and abundant hopanes. The third member is mixed between the two, and has intermedeate values for all markers (Santos Neto and Hayes, 1999).

The natural samples were separated into pure alkane components (methane, ethane and propane), and the methane was analyzed for clumped isotope thermometry (Stolper et al., 2014) and ethane for carbon-carbon clumping (Clog et al., 2013), whereas this study examines the site-specific carbon isotopes in propane following the methods outlined above and described in more detail in (Piasecki, 2015a). We evaluated the accuracy of these measurements by comparing the bulk δ^{13}C calculated from our measurements of the single and two-carbon fragment ions to an independently measured bulk δ^{13}C, determined by gas chromatography separation followed by continuous flow online combustion and IRMS. These conventional measurements were made at Petrobras' CENPES research labs. A cross-plot of these two estimates of bulk molecular δ^{13}C are consistent with a 1:1 slope but a non-zero intercept. We suspect this is due to an inter-laboratory difference in standardization. Nevertheless, the correlation between these two independent measurements suggests that our results are accurate (or, at least, that relative differences between samples are accurate).

Potiguar basin propanes exhibit site-specific carbon isotope compositions similar to or heavier than (i.e., higher in δ^{13}C) our reference standard. While we know little about this intralab working standard, it is likely that it comes from a relatively propane-rich, and thus immature, thermogenic source. If so, then we should expect higher δ^{13}C values of the more mature end of the range of Potiguar suite, particularly for the terminal C

position. The most noticeable feature of the trend defined by the Potiguar suite is that, starting at the lowest δ^{13}C sample, first the δ^{13}C of the terminal position increases without change in the central position, and then the center position rises markedly with modest additional increase in the central position. The initial part of this trend is closely similar to our expectation based on the extrapolation of Chung et al.'s interpretation of the bulk δ^{13}C values of natural gas components (Figure 3.4). That is, these first four samples are consistent with the bulk δ^{13}C of propane being controlled by a fractionation that acts only on the terminal carbon site, where increasing maturity involves an evolution from initially highly fractionated, low δ^{13}C terminal carbon toward a terminal carbon composition more like the source organic matter. The increase in the δ^{13}C of the center carbon position is unexpected when viewed in the context of our model extrapolated from Chung et al., but resembles (both in direction and magnitude) the results of cracking experiments on Woodford shale (Figure 3.6).

Considering the evolution in proportions of petroleum products in those experiments, we think that a plausible interpretation of the Potiguar basin data is that it captures the transition from primary cracking of kerogen to secondary cracking of oil or bitumen. This interpretation is at least generally consistent with previous interpretation of the clumped isotope thermometry of Potiguar basin methanes, which suggested mixing between low δ^{13}C, wet gases of moderate maturity and higher δ^{13}C dryer gases of higher maturity (Stolper et al., 2014). This coincidence re-enforces our interpretation of the Woodford shale cracking experiments, and taken together, these two data sets suggest that site-specific carbon isotope compositions of natural propanes provide a significant new proxy for the categenetic evolution of kerogens into more labile petroleum products.

However, the evidence we present is in some respects circumstantial, and we can think of two other factors that might compromise or at least complicate this interpretation: Some component of the carbon isotope variations in Potiguar basin gases could reflect mixing between gases from different sources (lacustrine vs. marine) rather than gases of different maturities. This is not expected based on current interpretations of the geology and petroleum deposits of the basin, but we consider it possible. And, it is possible that the carbon isotope evolution of the center position in both cracking experiments and relatively mature Potiguar basin gases could be influenced by a secondary isotope effect associated with cracking reactions (or even a primary isotope effect if the reactions making propane cleave a bond between the substrate and what will end up being the central carbon atom). We currently know too little about the atomistic chemical kinetics of categenetic propane formation to rule this out.

Natural propane from the Eagle Ford Shale

We also examined samples of natural propane from the Eagle Ford formation in Texas. The Eagle Ford formation is a Late Cretaceous marine shale. It is one of the most actively developing gas reservoirs currently in the US. This organic rich shale from a marine transgressive event, is a type II marine oil prone kerogen, from an anoxic environment, with high sulfur content, and has a total organic content of 1.84 weight percent. It has a sufficient thermal maturity from early, peak, and into late oil window across a range of areas in the deposit (Edman and Pitman, 2011; Ferrill et al., 2014) These are shale gases that extend to relatively low propane contents and high inferred gas maturities;

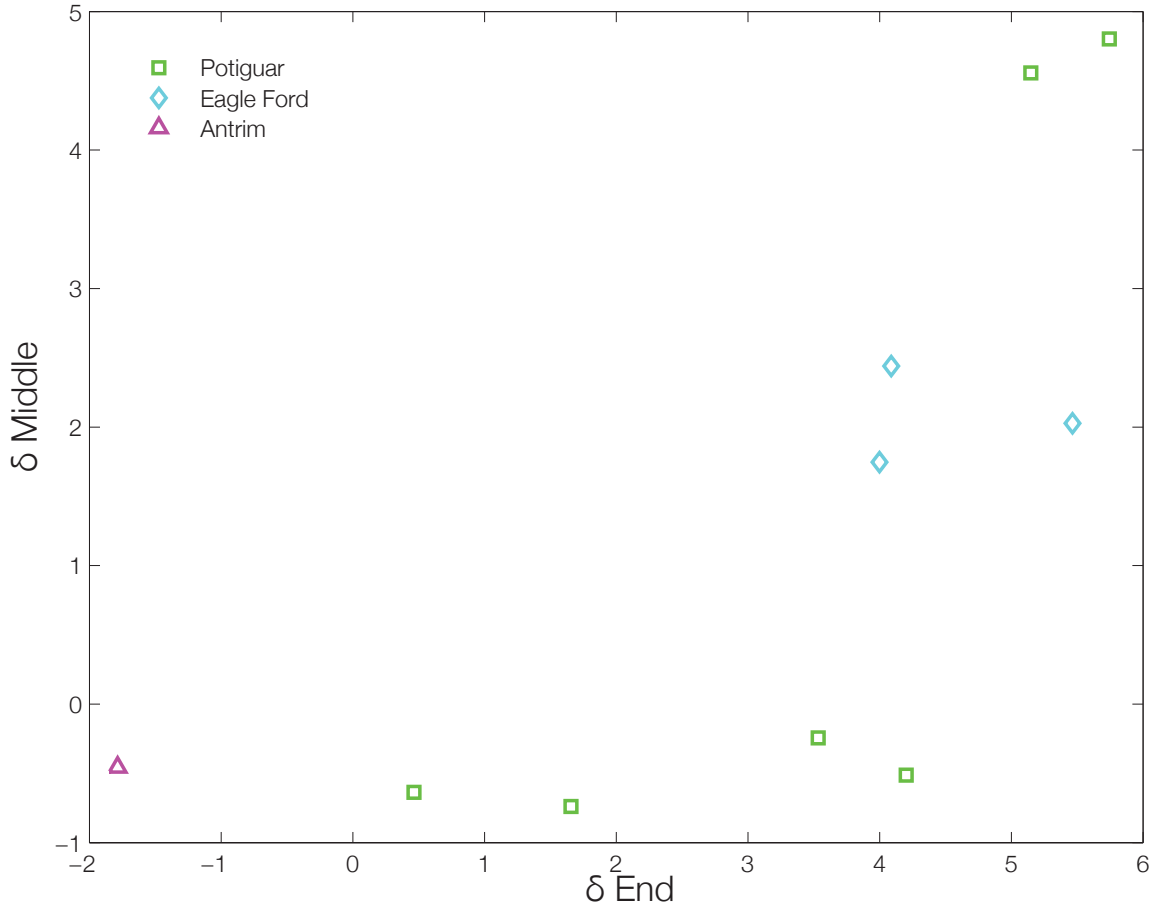

Figure 3.8: Shows data for all of the samples measured, excluding lab diffusion experiments. This includes the Eagle Ford and Antrim samples, which were previously not shown in figures.

and, they come from an 'unconventional' deposit where the gas is inferred to have been stored in its original source rock. This is relevant because the mechanism for cleavage and exchange could be different than a traditional natural gas basin due to the different and presumably more abundant catalytic surfaces on which reactions can occur, and the longer duration spent at high temperature.

The samples for the Eagle Ford formation were prepared as described in the Methods section, above and in Piasecki (2015a). These gases are relatively rich in CO_2, which had to be removed using ascarite. Despite our efforts to purify these gases, all but

three of the samples failed one or both of our data quality checks (i.e., the bulk $\delta^{13}C_{CITP1}$ we determined differed by more than 0.5‰ from that measured independently, and/or the mass spectrum of the sample differed by more than 20 % in relative peak heights from that for concurrently analyzed standard propane). Further evidence for the likely influence of a contaminant comes from our attempts to measure the 1-carbon fragment ion, which resulted in implausibly low apparent $\delta^{13}C$ values. We present the failed measurements of these gases in the appendix, and just focus here on data for the three samples that passed our data quality checks–Emma Tartt 22H and 25, and Irvin Mineral South 1H. Unfortunately, these three gases encompass only a narrow range of relatively low maturity in this suite (perhaps not surprisingly, as the more mature gases are poorer in propane and richer in CO_2).

The results for these three samples define a closely grouped set of compositions that lie within the range spanned by the Potiguar basin suite. If we attempt to interpret their average composition in a way that is consistent with both our Woodford Shale cracking experiments and interpretations of the Potiguar Basin gases, we might conclude that these Eagle Ford shale gases contain the products of a mixture of propane produced by kerogen cracking and gas produced by cracking oil or bitumen (i.e., the more extreme compositions in the Potiguar suite that we attribute to these processes circumscribe our results for the Eagle Ford; thus, the latter gases could be mixtures of components that resemble the extremes of the former). This may be a plausible interpretation, as unconventional shale gases are believed to integrate products across a range of maturities.

A natural propane from the Antrim Shale

We examined several samples of propane from the Antrim Shale, located in the Michigan Basin in the Northern US. This is a black Devonian shale, and the main natural gas producing members are the Norwood and Lachine, which have 0.5-24 weight percent total organic carbon. Propane recovered from the Antrim Shale is believed to be residual to microbial oxidation. It is a type one source rock, or the organic material is platonic algae deposited in restricted seas. It has a thermal maturity on the edges of the basin from 0.4 - 0.6 % Ro value that increases to 1 % in the center of the basin (Martini et al., 2003). At the margins of the basin, ground water has infiltrated the fractured shale gas and promoted microbial oxidation of the higher order alkanes (including ethane and propane). The primary evidence for this process is the increase in bulk δ^{13}C of ethane and propane with decreasing concentration of those species (Martini et al., 2003).

We found Antrim shale gases to be highly problematic for our purposes because most are poor in propane and many are rich in CO_2. As a result, only one sample yielded enough propane for analysis and passed our criteria for data quality. We do not have independent measurements of bulk δ^{13}C for propanes, but prior work on this suite makes it clear what range of values is plausible, letting us reject out of hand some measurements of impure samples with clearly compromised δ^{13}C values for methyl fragment ions. The one measurement we present combines analyses of the 2 and 3 carbon species, and conforms to our selection criteria for the relative heights of peaks that are indicative of contamination. This sample is a relatively wet gas (relative to other members of the Antrim suite), and has a site-specific carbon isotope composition for propane ($\delta^{13}C^{CITP1}_{end}$= -1.8 and

$\delta^{13}C^{CITP1}_{center}$ = -0.4) that resembles the lowest maturity end of the range that we expect for kerogen cracking (Figure 3.6). This finding is consistent with prior suspicions that the thermogenic component of Antrim shale gases has low thermal maturity, and is consistent with the recent finding by Stolper et al. (2015) that the component of thermogenic methane in these gases formed at relatively low temperature (∼115°C, or early in the primary kerogen cracking window). It is likely that this result provides little insight into the isotopic effects of biological propane oxidation, as it was measured on a relatively propane-rich sample having a relatively low bulk $\delta^{13}C$ value ($\delta^{13}C_{PDB}$ = -34 ‰).

3.4 Discussion and conclusions

Confirmation of the technique

The site-specific carbon isotope measurement in propane is complicated, and frequently has a variety of problems that can compromise the data. There are two ways in which data from this study support the validity of our measurements, despite the complications in purification and measurement. The first comes from the diffusion experiments. The data had the expected bulk fractionation between the diffused and the residue. The two pieces also mass-balanced back to close to the initial starting composition. In addition, the experiments spanned a range of $\delta^{13}C$ values but show no evidence of site-specific fractionation, as predicted. Only under fortuitous circumstances would this happen if one or both of our fragment ion measurements were inaccurate.

The second new demonstration of accuracy comes from our finding that many natu-

ral samples can return bulk δ^{13}C values, calculated based on our measurements of two fragment ion species, that agree with independent constraints. Samples containing impurities are exceptions to this statement; nevertheless, it is clear that it is possible to use our techniques to recover measurements of isotopic structure that mass-balance to independently known bulk values.

The causes of site-specific C isotope variations in natural propane

Previous studies have created a framework for understanding the evolution of carbon isotopes in natural gas systems (Chung and Sackett, 1979; Chung, Gormly, and Squires, 1988; Zou et al., 2007; Schimmelmann, Lewan, and Wintsch, 1999; Du et al., 2003; Hill, Tang, and Kaplan, 2003; Lorant et al., 2001; Ma, Wu, and Tang, 2008; Ni et al., 2011; Tang et al., 2005; Tang et al., 2000), and we have tried to build on this to create a simple predictive model of the site-specific properties of propane, and then test those predictions. In particular, we believe that the simplest extrapolation of previous stable isotope models of kinetic isotope effects associated with cleavage or 'cracking' of organic compounds to form propane lead to the expectation that this process simply transfers a carbon from the substrate to the central position of propane, with some small or negligible fractionation, but strongly fractionates the carbon isotope composition of the terminal position (and furthermore, that distillation effects act to effectively remove this terminal position fractionation with increasing maturity).

The results of our measurements, specifically fFigures 3.6, 3.7, and 3.8, show that

thermogenic propane, both in experiments and nature, does not follow our hypothesis based on the Chung et al. model.

The experiments involving hydropyrolysis of Woodford shale offer the most constrained system examined in this study, and, as explained above, suggest that the shift from kerogen-dominated to oil-dominated substrates corresponds to a large ($\sim$ 5‰) increase in the C isotope composition of the central carbon position of propane, perhaps combined with the general increase in δ^{13}C that we predict for the terminal position carbon.

Building on this suggestion based on the cracking experiments, the natural gases from the Potiguar Basin, Antrim Shale and Eagle Ford Shale suites can be interpreted to reflect a similar shift from kerogen to oil (or perhaps bitumen) cracking with increasing maturity. In particular, we suggest that the set of five gases that all share a common, low δ^{13}C value for the center carbon position (one from Antrim and four from Potiguar basin) were generated by primary cracking of kerogen, with increasing extents of reaction driving product propane to the right in Figure 3.8 (increasing δ^{13}C of the terminal position) due to distillation effects. We suggest that the higher δ^{13}C values for the center carbon position seen in the remaining five samples (the highest δ^{13}C Potiguar samples and the Eagle Ford samples) reflect variable amounts of contribution of propane generated by secondary cracking; i.e., that this 'jog' in the overall trend for natural samples marks the point in the maturity scale where propane from secondary cracking becomes a significant fraction of all propane. The Eagle Ford suite lies in between the end-members defined by the Potiguar Basin suite. This could be taken as evidence that the Eagle Ford propane is a mixture of the products of kerogen and oil cracking. This would make sense since the

Eagle Ford is a shale gas sample. It has not migrated from its source rock at all during its geologic history. Therefore, gas generated over a range of maturities may still be there (perhaps minus a fraction that migrated out of the rock). It therefore makes sense that the results would integrate over all of the basin's history as it passes from kerogen into oil cracking, and has the average isotopic value of the cumulative gas somewhere in between these two types of propane.

Referring back to the experimental data set, one could reach a self consistent interpretation of all our observations if the experiment conducted at 330°C just reached kerogen-only cracking, such that even a modest further increase in temperature to 360°C saw the onset of secondary cracking. This interpretation obviously reads more into the results than is required by these experiments alone; nevertheless, it has the advantage of being a testable hypothesis that stitches together all of our findings. A clear target for future work might be to experimentally explore the evolution of propanes over a range of maturities with very small variations in temperature between experiments (say, 5-10°C).

One complication neglected by our interpretations is variations in the δ^{13}C of source kerogens; i.e., propane produced from two sources having substrates with similar isotopic structures, and reaching a similar maturity, could still differ in δ^{13}C if those two sources differ in δ^{13}C. In the simplest case one can imagine, this will result in equal changes in δ^{13}C of both positions in propane. But, given the importance that we place on differences in substrate isotopic structure in dictating the carbon isotope structure of derived propane, we should expect that differences in δ^{13}C between two different sources (e.g., lacustrine vs. marine shales vs. coals) might also be associated with differences in site-specific carbon isotope structures of kerogens or other components of those sources. Substantially more

experimental work on the products of cracking experiments performed on diverse source materials will be required to get a firm grasp on this issue.

A process that we have not discussed in any detail (because we lack experimental constraints or clear examples from natural samples) is secondary cracking of propane into smaller species like ethane and methane. Typically, when this happens, dryness (or [C1]/[C1+...C5]) increases and the δ^{13}C value of the propane increases, in some cases becoming even higher than the organic matter in the parent rock. This leads to a concave downward trend in a Chung diagram (or 'natural gas plot') (Zou et al., 2007). The effect on site-specific fractionations is not known, and cannot be easily guessed.

Another possible mechanism that could influence either or both the terminal and central positions is secondary isotope effects. We use this term to describe instances in which atoms not directly adjacent to a bond influence the bond strength, in turn leading to a change in the isotopic fractionation factor associated with cleaving or exchanging species with that bond (Wang et al., 2009a; Wang et al., 2009b). Molecules containing ^{13}C in a center position can be thermodynamically favored (Piasecki, 2015b), and thus potentially stabilized (i.e., react at slower rates), and therefore contribute less to the production of propane by cracking. Similarly, propane with a center-position ^{13}C may be preferentially retained through secondary cracking.

3.5 Data Appendix

Sample	δEnd	st dev	st err	δEthyl	st dev	st err	δFull	stdev	st err	δD	st err	δEnd	δcenter	δFull	Quality
Mixing															
Aa	163.34	2.27	0.30	100.15	0.27	4.41E-2						163.34	36.96	121.21	2
Ab	530.41	4.11	0.54	287.62	15.58	2.84						530.41	44.83	368.55	2
B3	119.05	10.013	1.25	61.03	0.67	8.97E-2						119.05	3.02	80.37	2
B1	172.80	3.95	0.69	87.67	0.49	8.81E-2						172.80	2.53	116.04	2
C4	73.18	3.57	0.63	35.75	3.25	0.57						73.18	-1.68	48.23	2
C1	88.82	3.44	0.54	47.43	0.36	6.36E-2						88.82	6.03	61.23	2
D4	38.58	3.53	0.47	19.00	0.96	0.12						38.58	-0.57	25.53	2
Eagle Ford															
VF4H	-86.95	2.30	0.40	11.88	0.37	6.70E-2	8.142	0.45	8.09E-2	-34.22	8.26	0.65	23.11	8.142	4
LR22H	-139.87	3.61	0.63	8.68	0.24	4.27E-2	9.35	0.247	4.36E-2			10.71	6.65	9.35	4
LR1H	-58.81	3.14	0.55	11.07	0.28	5.12E-2	9.70	0.29	5.16E-2	-100.18	2.50	6.95	15.19	9.70	4
LR21H	-72.27	2.40	0.42	10.52	1.38	0.24	2.93	0.38	6.73E-2	162.17	3.77	-12.23	33.28	2.93	4
IMS3H	-74.17	1.63	0.28	0.97	0.69	0.123	3.53	0.22	3.97E-2			8.64	-6.69	3.53	4
IHS1	-65.92	4.41	0.90	3.77	0.25	4.59E-2	6.83	0.21	3.73E-2	-133.97	1.13	12.95	-5.41	6.83	4
Antrim															
C2-31	-21.1	3.51	0.62	-2.42	0.69	0.12						-27.32	16.26	-8.65	4
C4-18	-31.42	5.82	1.18	5.05	0.55	0.11						-22.41	41.54	-7.10	4
C4-18	-32.17	3.11	0.55	8.29	0.52	0.18						-16.63	48.76	-5.19	4
B4-28-1	-13.24	2.14	0.37	3.26	2.31	0.40						-11.34	19.77	-2.24	4

Table 3.4: Extra Data

Sample	δ^{13}C CH_4	δ^{13}C C_2H_6	δ^{13}C C_3H_8	δ^{13}C nC_4H_{10}	δ^{13}C iC_4H_{10}	% CH_4	% C_2H_6	% C_3H_8	% nC_4H_{10}	% iC_4H_{10}
Eagle Ford										
VF4H	-40.21	-23.3	-20.12	-20.35	-22.01	82.98	9.1913	2.06	0.56	0.71
LR22H	-39.80	-24.2	-22.52	-23.02	-25.96	80.70	10.64	3.83	1.27	0.98
LR1H	-40.70	-24.6	-22.7	-23.27	-25.8	80.27	11.16	4.04	1.30	1.01
LR21H	-40.70	-24.6	-22.7	-23.27	-25.8	80.27	11.16	4.04	1.30	1.01
IMS3H	-47.5	-32.1	-29.41	-30.67	-31.3	78.08	12.59	5.10 6	1.24	0.56
IHS1	-47.4	-32.20	-29.32	-30.02	-31.2	77.79	12.62	5.31	1.28	0.57
Antrim										
C2-31	-53.3					69.75	6.62	1.97	0.05	0.1
C4-18	-52.3					78.15	1.89	0.64	1.18E-2	8.07E-2
C4-18	-52.3					78.15	1.89	0.64	1.18E-2	8.07E-2
B4-28-1	-52.9					67.65	6.22	1.33	3.52E-2	9.60E-2

Table 3.5: Extra external data

Sample	29/28	43/42	45/44	44/43	58/57
Eagle Ford					
VF4H	1.43	4.01	3.22E-2	0.78	2.65E-2
LR22H	1.33	4.43	3.27E-2	0.88	4.87E-2
LR1H	0.99	4.44	3.25E-2	0.88	3.14E-2
LR21H	1.37	4.09	3.22E-2	0.76	2.12E-2
IMS3H	1.34	4.71	3.22E-2	0.99	5.88E-2
IHS1	1.41	4.95	3.25E-2	1.16	
Antrim					
B4-28-1	1.54	3.87	3.14E-2	0.92	

Table 3.6: Extra contamination indices

References

Abelson, P H and T C Hoering (1961). "Carbon Isotope Fractionation in the Formation of Amino Acids by Photosynthetic Organisms." English. In: *Proceedings of the National Academy of Sciences of the United States of America* 47.5, p. 623. URL: http://www.ncbi.nlm.nih.gov/pmc/articles/PMC221413/.

Betson, Tatiana R, Angela Augusti, and Jürgen Schleucher (2006). "Quantification of Deuterium Isotopomers of Tree-Ring Cellulose Using Nuclear Magnetic Resonance." English. In: *Analytical Chemistry* 78.24, pp. 8406–8411. DOI: 10.1021/ac061050a. URL: http://pubs.acs.org/doi/abs/10.1021/ac061050a.

Bigeleisen, Jacob and Maria Goeppert Mayer (1947). "Calculation of Equilibrium Constants for Isotopic Exchange Reactions." English. In: *The Journal of Chemical Physics* 15.5, p. 261. DOI: 10.1063/1.1746492. URL: http://scitation.aip.org/content/aip/journal/jcp/15/5/10.1063/1.1746492.

Caer, V et al. (1991). "Determination of site-specific carbon isotope ratios at natural abundance by carbon-13 nuclear magnetic resonance spectroscopy." English. In: *Analytical Chemistry* 63.20, pp. 2306–2313. DOI: 10.1021/ac00020a021. URL: http://pubs.acs.org/doi/abs/10.1021/ac00020a021.

Chung, H M, J R Gormly, and R M Squires (1988). "Origin of gaseous hydrocarbons in subsurface environments: theoretical considerations of carbon isotope distribution." English. In: *Chemical Geology* 71.1-3, pp. 97–104. DOI: 10.1016/0009-2541(88)90108-8. URL: http://linkinghub.elsevier.com/retrieve/pii/0009254188901088.

Chung, H M and W M Sackett (1979). "Use of stable carbon isotope compositions of pyrolytically derived methane as maturity indices for carbonaceous materials." English. In: *Geochimica et Cosmochimica Acta* 43.12, pp. 1979–1988. DOI: 10.1016/0016-7037(79)90010-3. URL: http://linkinghub.elsevier.com/retrieve/pii/0016703779900103.

Clog, M et al. (2013). "Doubly 13C-substituted ethane." English. In: *Mineralogical Magazine* 77.5, pp. 805–933. URL: http://openurl.ingenta.com/content/xref?genre=article&issn=0026-461X&volume=77&issue=5&spage=805.

DeNiro, M J and S Epstein (1977). "Mechanism of carbon isotope fractionation associated with lipid synthesis." English. In: *Science* 197.4300, pp. 261–263. DOI: 10.1126/science.327543. URL: http://www.sciencemag.org/cgi/doi/10.1126/science.327543.

Du, J et al. (2003). "Stable carbon isotope compositions of gaseous hydrocarbons produced from high pressure and high temperature pyrolysis of lignite." English. In:

Organic Geochemistry 34.1, pp. 97–104. DOI: 10.1016/S0146-6380(02)00158-4. URL: http://linkinghub.elsevier.com/retrieve/pii/S0146638002001584.

Edman, Janell D. and Janet K. Pitman (2011). "Geochemistry of Eagl Ford Source Rocks and Oils from the First Shot Field Area, Texas." In: *AAPG Search and Discovery Article*.

Eiler, J et al. (2012). "A high-resolution gas-source isotope ratio mass spectrometer." In: *International Journal of Mass Spectrometry*, pp. 1–12. DOI: 10.1016/j.ijms.2012.10.014. URL: http://dx.doi.org/10.1016/j.ijms.2012.10.014.

Eiler, J et al. (2014). "Isotopic Anatomies of Organic Compounds." In: *Goldschmidt Conference*.

Ferreira, Alexandre A et al. (2012). "2H/1H ratio of hopanes, tricyclic and tetracyclic terpanes in oils and source rocks from the Potiguar Basin, Brazil." In: *Organic Geochemistry* 51.C, pp. 13–16. DOI: 10.1016/j.orggeochem.2012.07.007. URL: http://dx.doi.org/10.1016/j.orggeochem.2012.07.007.

Ferrill, David A. et al. (2014). "Control of mechanical stratigraphy on bed-restricted jointing and normal faulting: Eagle Ford Formation, south-central Texas." In: *AAPG bulletin* 98.11, pp. 2477–2506.

Gilbert, Alexis, Keita Yamada, and Naohiro Yoshida (2013). "Exploration of intramolecular ^{13}C isotope distribution in long chain n-alkanes (C_{11}-C_{31}) using isotopic ^{13}C NMR." In: *Organic Geochemistry* 62.C, pp. 56–61. DOI: 10.1016/j.orggeochem.2013.07.004. URL: http://dx.doi.org/10.1016/j.orggeochem.2013.07.004.

Gilbert, Alexis et al. (2012). "Biochemical and physiological determinants of intramolecular isotope patterns in sucrose from C3, C4 and CAM plants accessed by isotopic 13C NMR spectrometry: a viewpoint." English. In: *Natural Product Reports* 29.4, pp. 476–486. DOI: 10.1039/c2np00089j. URL: http://xlink.rsc.org/?DOI=c2np00089j.

Guy, R D, M L Fogel, and J A Berry (1993). "Photosynthetic Fractionation of the Stable Isotopes of Oxygen and Carbon." English. In: *Plant physiology* 101.1, pp. 37–47. DOI: 10.1104/pp.101.1.37. URL: http://www.plantphysiol.org/content/101/1/37.abstract.

Hill, Ronald J, Yongchun Tang, and Isaac R Kaplan (2003). "Insights into oil cracking based on laboratory experiments." English. In: *Organic Geochemistry* 34.12, pp. 1651–1672. DOI: 10.1016/S0146-6380(03)00173-6. URL: http://linkinghub.elsevier.com/retrieve/pii/S0146638003001736.

Hinrichs, K U et al. (2006). "Biological formation of ethane and propane in the deep marine subsurface." English. In: *Proceedings of the National Academy of Sciences* 103.40, pp. 14684–14689. DOI: 10.1073/pnas.0606535103. URL: http://www.pnas.org/content/103/40/14684.full.

Lorant, François et al. (2001). "Ab Initio Investigation of Ethane Dissociation Using Generalized Transition State Theory." English. In: *The Journal of Physical Chemistry A* 105.33, pp. 7896–7904. DOI: 10.1021/jp004094a. URL: http://pubs.acs.org/doi/abs/10.1021/jp004094a.

Ma, Qisheng, Sheng Wu, and Yongchun Tang (2008). "Formation and abundance of doubly-substituted methane isotopologues (." In: *Geochimica et Cosmochimica Acta* 72.22, pp. 5446–5456. DOI: 10.1016/j.gca.2008.08.014. URL: http://dx.doi.org/10.1016/j.gca.2008.08.014.

Macko, S A et al. (1987). "Isotopic fractionation of nitrogen and carbon in the synthesis of amino acids by microorganisms." English. In: *Chemical Geology: Isotope Geoscience Section* 65.1, pp. 79–92. DOI: 10.1016/0168-9622(87)90064-9. URL: http://linkinghub.elsevier.com/retrieve/pii/0168962287900649.

Martini, Anna M et al. (2003). "Microbial production and modification of gases in sedimentary basins: A geochemical case study from a Devonian shale gas play, Michigan basin." English. In: *AAPG bulletin* 87.8, pp. 1355–1375. DOI: 10.1306/031903200184. URL: http://search.datapages.com/data/doi/10.1306/031903200184.

McCollom, T M and J S Seewald (2006). "Carbon isotope composition of organic compounds produced by abiotic synthesis under hydrothermal conditions." In: *Earth and Planetary Science Letters*. DOI: 10.1016/j.epsl.2006.01.027. URL: http://www.sciencedirect.com/science/article/pii/S0012821X06000641.

Monson, K D and J M Hayes (1980). "Biosynthetic control of the natural abundance of carbon 13 at specific positions within fatty acids in Escherichia coli. Evidence regarding the coupling of fatty acid and phospholipid synthesis." English. In: *Journal of Biological Chemistry* 255.23, pp. 11435–11441. URL: http://www.jbc.org/content/255/23/11435.abstract.

— (1982). "Carbon isotopic fractionation in the biosynthesis of bacterial fatty acids. Ozonolysis of unsaturated fatty acids as a means of determining the intramolecular distribution ..." English. In: *Geochimica et Cosmochimica Acta* 46.2, pp. 139–149. DOI: 10.1016/0016-7037(82)90241-1. URL: http://linkinghub.elsevier.com/retrieve/pii/0016703782902411.

Ni, Yunyan et al. (2011). "Fundamental studies on kinetic isotope effect (KIE)of hydrogen isotope fractionation in natural gas systems." In: *Geochimica et Cosmochimica Acta* 75.10, pp. 2696–2707. DOI: 10.1016/j.gca.2011.02.016. URL: http://dx.doi.org/10.1016/j.gca.2011.02.016.

Piasecki, A and J Eiler (2012). "Direct Mass Spectrometric Analysis of Position Specific δ^{13}C in Organics." In:

Piasecki, Alison (2015a). "Analysis of the site-specific carbon isotope composition of propane by gas source isotope ratio mass spectrometry." In:

— (2015b). "Equilibrium fractionations of small alkanes using density functional theory." In:

Rustad, James R (2009). "Ab initio calculation of the carbon isotope signatures of amino acids." English. In: *Organic Geochemistry* 40.6, pp. 720–723. DOI: 10.1016/j.orggeochem.2009.03.003. URL: http://linkinghub.elsevier.com/retrieve/pii/S0146638009000643.

Santos Neto, E V dos and J M Hayes (1999). "Use of hydrogen and carbon stable isotopes characterizing oils from the Potiguar Basin (onshore), Northeastern Brazil." In: *AAPG bulletin*. URL: http://archives.datapages.com/data/doi/10.1306/00AA9BE2-1730-11D7-8645000102C1865D.

Schimmelmann, A, M D Lewan, and R P Wintsch (1999). "D/H isotope ratios of kerogen, bitumen, oil, and water in hydrous pyrolysis of source rocks containing kerogen types I, II, IIS, and III." English. In: *Geochimica et Cosmochimica Acta* 63.22, pp. 3751–3766. DOI: 10.1016/S0016-7037(99)00221-5. URL: http://linkinghub.elsevier.com/retrieve/pii/S0016703799002215.

Schimmelmann, A and A L Sessions (2006). "Hydrogen isotopic (D/H) composition of organic matter during diagenesis and thermal maturation." English. In: *Annu Rev Earth Planet ...* 34.1, pp. 501–533. DOI: 10.1146/annurev.earth.34.031405.125011. URL: http://www.annualreviews.org/doi/abs/10.1146/annurev.earth.34.031405.125011.

Stolper, D A et al. (2014). "Formation temperatures of thermogenic and biogenic methane." English. In: *Science* 344.6191, pp. 1500–1503. DOI: 10.1126/science.1254509. URL: http://www.sciencemag.org/cgi/doi/10.1126/science.1254509.

Stolper, D A et al. (2015). "Distinguishing and understanding thermogenic and biogenic sources of methane using multiply substituted isotopologues." In: *Geochimica et Cosmochimica Acta*, pp. 1–61. DOI: 10.1016/j.gca.2015.04.015. URL: http://dx.doi.org/10.1016/j.gca.2015.04.015.

Tang, Yongchun et al. (2000). "Mathematical modeling of stable carbon isotope ratios in natural gases." In: *Geochimica et Cosmochimica Acta*. DOI: 10.1016/S0016-7037(00)00377-X. URL: http://www.sciencedirect.com/science/article/pii/S001670370000377X.

Tang, Yongchun et al. (2005). "A kinetic model for thermally induced hydrogen and carbon isotope fractionation of individual n-alkanes in crude oil." English. In: *Geochimica et Cosmochimica Acta* 69.18, pp. 4505–4520. DOI: 10.1016/j.gca.2004.12.026. URL: http://linkinghub.elsevier.com/retrieve/pii/S0016703705000578.

Toyoda, Sakae and Naohiro Yoshida (1999). "Determination of Nitrogen Isotopomers of Nitrous Oxide on a Modified Isotope Ratio Mass Spectrometer." English. In: *Analytical Chemistry* 71.20, pp. 4711–4718. DOI: 10.1021/ac9904563. URL: http://pubs.acs.org/doi/abs/10.1021/ac9904563.

Urey, Harold C (1947). "The thermodynamic properties of isotopic substances." English. In: *Journal of the Chemical Society (Resumed)* 0, pp. 562–581. DOI: 10.1039/jr9470000562. URL: http://xlink.rsc.org/?DOI=jr9470000562.

Wang, Ying et al. (2009a). "Equilibrium 2H/ 1H fractionations in organic molecules: I. Experimental calibration of ab initio calculations." English. In: *Geochimica et Cosmochimica Acta* 73.2, pp. 7060–7075. DOI: 10.1016/j.gca.2009.08.019.

— (2009b). "Equilibrium 2H/ 1H fractionations in organic molecules. II: Linear alkanes, alkenes, ketones, carboxylic acids, esters, alcohols and ethers." English. In: *Geochimica et Cosmochimica Acta* 73.2, pp. 7076–7086. DOI: 10.1016/j.gca.2009.08.018.

Wang, Zhengrong, Edwin A Schauble, and J Eiler (2004). "Equilibrium thermodynamics of multiply substituted isotopologues of molecular gases." English. In: *Geochimica et Cosmochimica Acta* 68.23, pp. 4779–4797. DOI: 10.1016/j.gca.2004.05.039. URL: http://linkinghub.elsevier.com/retrieve/pii/S001670370400451X.

Zou, Yan-Rong et al. (2007). "Variations of natural gas carbon isotope-type curves and their interpretation – A case study." English. In: *Organic Geochemistry* 38.8, pp. 1398–1415. DOI: 10.1016/j.orggeochem.2007.03.002. URL: http://linkinghub.elsevier.com/retrieve/pii/S0146638007000691.

Chapter 4

Investigating the clumped isotope blocking temperature of aragonites using experiments and natural metamorphic samples

Abstract

Clumped isotopes have become a powerful tool for measuring the formation or equilibration temperatures of carbonate-bearing materials and simple molecular gases (CO_2, O_2 and CH_4). The method is used on a variety of carbonate phases, most of which have been studied previously to determine their blocking temperature with respect to solid-state internal redistribution of isotopes (i.e., thermally-activated re-setting of the clumped isotope equilibrium) over geologically relevant temperatures. Here we present the results of experimental heating of aragonite in the laboratory and studies of natural aragonite-bearing metamorphic rocks to estimate a blocking temperature for aragonite of between 50-100°C. Most surprisingly, we find evidence that the polymorphic transformation of aragonite to calcite results in a rapid increase in Δ_{47}, to values well in excess of equilibrium at the temperature of conversion, and similar to that in reactant aragonite

prior to any heating. There is no precedent for this finding in prior studies of carbonate clumped isotope kinetics. We hypothesize that it may reflect the mechanism of oxygen transfer between adjacent carbonate ion units during the aragonite-calcite transformation. We examine the clumped isotope compositions of aragonites from a natural sample suite of metamorphic aragonite veins from the San Juan Islands. These samples exhibit a range of apparent temperatures that are correlated with δ^{13}C, varying from values approaching the inferred blocking temperature in high-δ^{13}C aragonite down to near-surface temperatures in low-δ^{13}C aragonite. We interpret this as a reflection of variable addition of carbon from methane oxidation over a range of temperatures, with increasing inputs of methane derived carbon with decreasing temperature.

4.1 Introduction

Stable isotopes have been used for many decades to constrain water-rock reactions and infer approximate temperatures of mineral and rock alteration. Recently, clumped isotope thermometry has added an additional constraint on temperature of such processes without needing an external constrain on the δ^{18}O of the fluid that new-formed minerals are in equilibrium with. This thermometer is based on homogeneous isotope exchange reactions such as:

$$\mathrm{Ca^{13}C^{16}O_3} + \mathrm{Ca^{12}C^{16}O_2^{18}O} \longleftrightarrow \mathrm{Ca^{13}C^{16}O_2^{18}O} + \mathrm{Ca^{12}C^{16}O_3} \tag{4.1}$$

Such reactions are temperature-dependent and require only carbonate species to be measured to completely constrain the equation. This method has been used to determine

paleo-temperatures of soil carbonates (Snell et al., 2014), paleo-elevations (Huntington, Wernicke, and Eiler, 2010), and to reconstruct ocean temperatures using marine fossils (Tripati et al., 2010), to name just a few applications. The equilibrium properties and approximate blocking temperatures with respect to isotopic re-ordering are relatively well-constrained for calcite, carbonate-apatite and dolomite (Passey and Henkes, 2012; Henkes et al., 2014; Stolper and Eiler, 2015; Lloyd and Eiler, 2014). However, aragonite remains little explored, and we are aware of only a single (to-date unpublished) study of the kinetics of aragonite clumped-isotope re-ordering (Staudigel, Swart, and Waite, 2014).

It is important to study aragonite because it is one of the major carbonate phases, and it has very different geochemical properties from calcite, apatite, or dolomite. In modern oceans, and many ancient ones, aragonite is the primary carbonate phase that precipitates out of seawater. Calcite precipitation from sea water is kinetically inhibited in the presence of magnesium, so aragonite, which can contain magnesium in low amounts, precipitates first (Zeebe and Wolf-Gladrow, 2001). There are also many mollusks, corals, and other creatures that precipitate aragonite.

Aragonite is stable only at high pressures over the temperature range of the surface and shallow crust ($\geq$ 5 kbar 100°C, or $\geq$ 11 kbar at 400°C), and readily converts to or is replaced by stable calcite if it is subject to recrystallization or water-rock reaction at low pressures. As a result, if aragonite is still present in a sediment or sedimentary rock, it is generally interpreted to be primary, and when studied as a paleoclimate archive, is often assumed to be unaltered in its chemical composition (although recent work questions this assumption; (e.g., (Zhang et al., 2014)). In addition, aragonite is also a high-pressure,

low-temperature metamorphic phase present in many blueschist environments as veins or altered limestone. It is challenging to estimate the pressure and temperatures of aragonite growth in such rocks because rocks often fail to reach heterogeneous equilibrium over length scales of hand samples or thin sections at the low temperatures of blueschist facies environments.

A goal of this study is to improve understanding of the conditions under which aragonite resets its clumped isotope composition through solid state, intracrystalline isotopic redistribution. This information may help interpret clumped isotope measurements of aragonite in paleoclimate studies, and might lead to the use of clumped isotope equilibria in aragonite as a low-grade metamorphic geothermometer or geospeedometer. We approach this problem through a combination of laboratory experiments in which we observe the time-dependent change in clumped isotope compositions of aragonites during heating at low pressure, and by analyzing a suite of rapidly exhumed metamorphic rocks. We use these data to develop Arrhenius parameters that can be extrapolated to estimate rates of clumped isotope reactions; we also report an unexpectedly strong effect of the aragonite-calcite transition on clumped isotope compositions, and present a hypothesis that explains this effect as a consequence of the atomistic mechanisms of the transition.

4.2 Methods

Geologic background of natural samples

The suite of natural metamorphic rocks examined in this study comes from the San Juan Islands in Washington State, and was obtained from Professor Mark Brandon at Yale.

The San Juan Islands were created through a complex system of late Cretaceous nappe style faults that juxtaposed a series of five distinct terranes. The terranes include an upper Triassic arc volcanic sequence, a Paleozoic arc sequence, a Permian to lower Jurassic ocean island sequence, a Permo-Triassic high pressure metamorphic unit, and a mid-to-upper Jurassic ophiolite and arc volcanic sequence. There are also massive clastic deposits associated with the exhumation and erosion of these units (Brandon, Cowan, and Vance, 1988; Saleeby, 1983).

During late Cretaceous thrusting, there was a significant metamorphic overprinting at relatively high-pressure, low-temperature conditions (approximately prehnite pumpellyite facies). Lawsonite- and aragonite-bearing assemblages formed during this late Cretaceous event. Maximum pressure estimates are estimated to be approximately 6 kbar, constrained in part by the presence of aragonite (Brandon, Cowan, and Vance, 1988). Thrusting and subsequent exhumation occurred between 100 and 84 Ma, requiring vertical transport rates of 2 km/myr. The rapid uplift contributes to the preservation of aragonite, which can easily convert to calcite during slow decompression (Sotin and Madon, 1988; Wolf et al., 1996; Simmons and Bell, 1963).

The aragonite in San Juan Islands is specifically associated both with veins and with metamorphic alteration of limestone. The marble is almost all still aragonite, with very

little having retrograded back to calcite, most likely due to the large crystal size causing low permeability, and a lack of pervasive fluid flow through the body (Plummer and Busenberg, 1982).

Even though the limestone has been metamorphosed, there are frequently well-preserved fossils of foraminfera and other carbonate-shell-precipitating organisms, indicating that metamorphism was not associated with a significant amount of shear in many of the marble units. Many of the aragonite locations lack blueschist facies minerals and other high-pressure indicators (i.e., in addition to aragonite itself). Assemblages in these rocks are consistent with prehnite-pumpellyite facies conditions, suggesting low temperatures; if geothermal gradients conform to expectations, this indicates lower pressure than is sometimes expected for aragonite stability within metamorphic environments. The phase stability of aragonite within the system suggests a geotherm of approximately 10°C/km (Vance, 1968; Boettcher and Wyllie, 1968; Jamieson, 1953). In short, the estimated pressures are outside of the typical aragonite stability field, but the presence of aragonite in the low-grade prehnite pumpellyite facies in the San Juan Islands is well-documented.

The samples that were measured in this study come from an outcrop on Lopez Island. All samples come from aragonite veins (i.e., we have not yet analyzed any marbles), hosted in a Mesozoic pillow basalt related to the Fidalgo Ophiolite, which overlies a mudstone on the southern portion of the island. There are several veining events paracontemporaneous with deformation, as indicated by cross cutting, folding, and boudinage of aragonite veins. There is a wide range of transformation to calcite from aragonite ranging from none to complete transformation. Preliminary carbon isotope analyses conducted by M. Brandon in preparation for this study revealed exceptionally low $\delta^{13}C_{PDB}$

values in some of the veins, down to -50‰, suggesting that the aragonite could have grown from fluids containing a carbon source derived directly or indirectly, from biogenic methane, possibly biologically mediated through anerobic methane oxidation (Paull et al., 1992).

Experimental setup

For the experiments, an aragonite standard was used from Tazouta, Sefrou Province, Fes-Boulemane Region, Morocco. The sample precipitated from groundwater within the shallow subsurface. It is a fist-sized aggregate of faceted inter-grown crystals approximately 0.5 - 1.0 cm in diameter. This sample was chosen due to its size, apparent homogeneity (i.e., from visual inspection), and low-temperature origins. A low-temperature origin is helpful for our heating experiments because it maximizes the amplitude of the change in Δ_{47} between the initial composition and the composition the sample will have once equilibrated at high temperatures in the laboratory. It yields an apparent temperature of mineral growth, based on clumped isotope analysis, of 31°C (Δ_{47} of 0.670±0.030‰, 1sd of replicate analyses, in the absolute reference frame). This result is consistent with near-equilibrium growth in a shallow subsurface environment. Replicate analyses are less producible than typical precision on carbonate standards (on average, $\pm 0.010 - 0.015$‰ in Δ_{47}), we suspect due to growth over a range in temperature, and/or kinetic isotope effects associated with evaporation (a common problem for speleothems and some soil carbonates). In any event, this heterogeneity is 10x smaller than the amplitudes of signals that we anticipate producing through heating experiments, and so is a modest

source of experimental uncertainty.

In preparation for heating experiments, the sample was coarsely crushed with a hammer into small (100 mg) shards, several of which were then fit into $\frac{1}{4}$" pyrex tubing. Whole crystal shards are used instead of powder or sand sized fragments in order to minimize the effect of adsorbed water on the surface. If the samples were powdered, there would be more surface area, and therefore a greater chance of water to be adsorbed onto the surface. Since water readily exchanges with CO_2, we wished to minimize its presence (Clog, Stolper, and Eiler, 2015). The tubes were sealed with CO_2 in the headspace to prevent decrepitation upon heating; the CO_2 was first cleaned with a dry-ice-ethanol slush to minimize the water. Samples were put in a furnace and heated for the prescribed time and temperature for the given experiment, and temperatures were monitored twice daily to ensure accuracy. There were at least two separate samples for each time and temperature step.

After the duration of the experiment, the tubes were attached to a glass vacuum line by way of a tube-cracker, broken, and the vapor in the headspace was cryogenically recovered and purified for isotopic analysis (except for some cases when it was lost or there was not enough gas). The tube was then removed from the vacuum line, the carbonate mineral shards were recovered and powdered to a fine sand grain size with an agate mortar and pestle (without sieving). Aliquots of approximately 10 mg were weighed out for stable isotope analysis, and approximately 30 mg of sample was saved for X-ray diffraction (XRD) analysis.

The XRD analysis was done in Professor Nate Lewis' group in the Chemistry Division of the California Institute of Technology. It utilized a Bruker D2 Phaser tabletop XRD

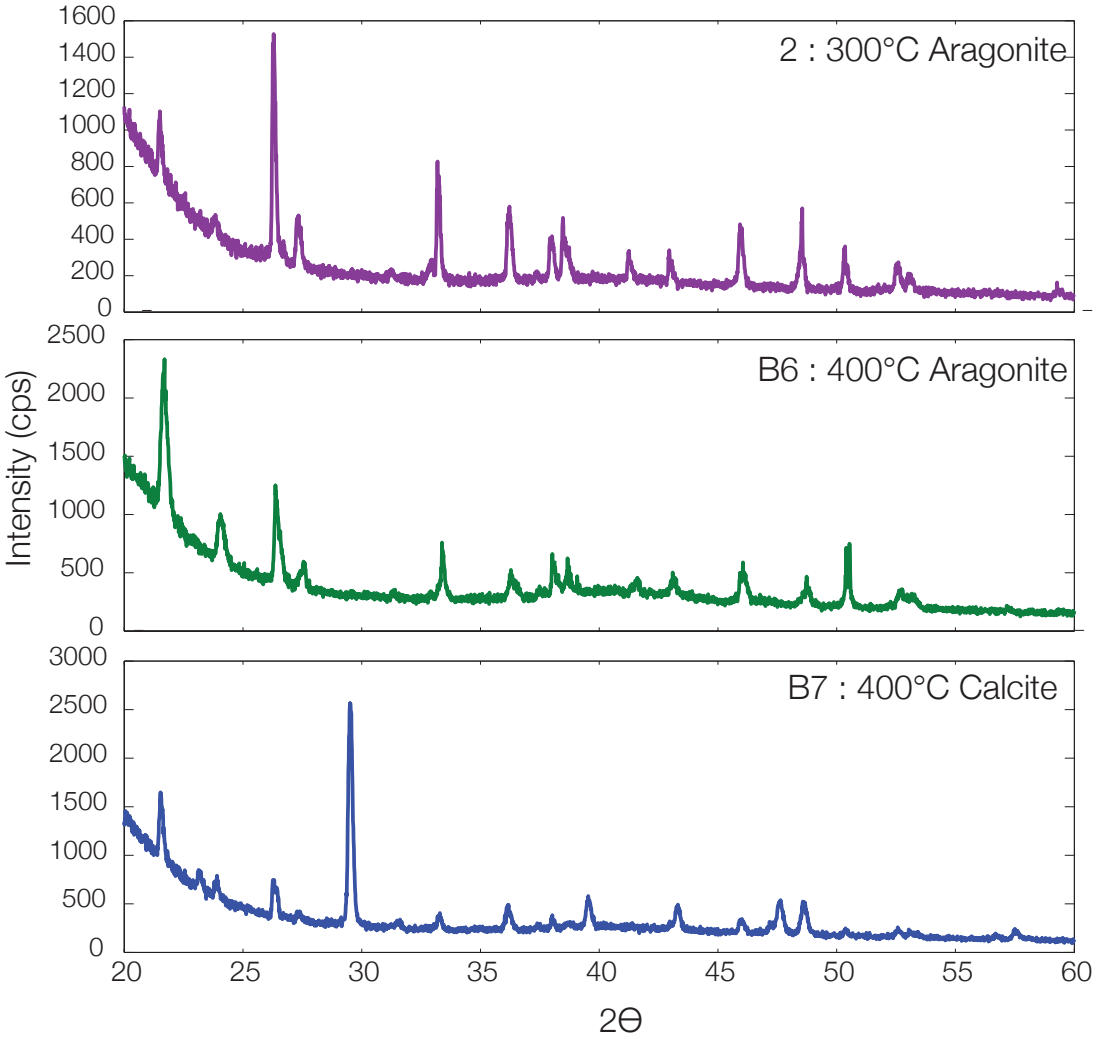

Figure 4.1: Figure shows representative XRD spectra from different samples that are aragonite or calcite made with a Cu K α beam. Experimental conditions are shown for each of the representative scans.

machine. X-ray diffraction spectra were deconvolved to recover calcite/aragonite ratios following the previous technique (Dickinson and McGrath, 2001). This method compares relative peak heights for two characteristic peaks ($2\Theta = 40$ for calcite, and $2\Theta = 46$ for aragonite) to calculate the relative abundance of each phase. Representative crystal spectra are shown in Figure 4.1. Most experimental samples were analyzed by XRD, though several of the last experiments performed in this study have yet to be measured

in this way.

Clumped isotope analytical techniques

The methods of carbonate clumped isotope measurement are discussed in detail in several recent papers, but a brief summary is provided (Schauble, Ghosh, and Eiler, 2006; Ghosh et al., 2006; Dennis et al., 2011; Passey and Henkes, 2012; Huntington et al., 2009). Fine powders of carbonate samples weighing around 10 mg are loaded into silver capsules that are then placed in an automatic sample device, and the headspace of the sample device is evacuated. The samples are dropped into 90°C phosphoric acid, and the evolved CO_2 gas is then cleaned of water and other impurities using a dry-ice-ethanol slush and a gas chromatography column packed with Poropak Q50 held at -20°C. The sample is then introduced into the bellows of a Thermo-Fischer Mat-253 gas source mass spectrometer. It is measured by comparing mass ratios to a standard of independently-known composition. Measured values of 45/44, 46/44 and 47/44 ratios are used to calculate δ^{13}C, δ^{18}O, and Δ_{47} — a proxy for temperature that has been calibrated with a number of natural standards. The exact measurement that is made is

$$\Delta_{47} = \left(\frac{R^{47}_{SA}}{R^{47}_{ST}} - 1 \right) \times 1000 \tag{4.2}$$

where SA is the sample and ST is the stochastic. All gas analyses are standardized for Δ_{47} value by comparison with heated gases having a range of bulk isotopic compositions, following the methods of Huntington et al. (2009) (the so-called 'Caltech reference frame'). All data were also cast into the absolute reference frame of Dennis et al. (2011),

by additional comparison to gases of equilibrated at 25°C and having a range of bulk stable isotope compositions. Previously studied interlaboratory carbonate standards, Carrarra Marble and TV-03, were analyzed concurrently with unknown samples to monitor accuracy and precision. Most unknown samples were analyzed three times, unless sample amount was limited. Table 4.1 indicates the number of replicates, as well as their standard deviation and external standard error of their mean. The table shows these values as well as exp T which is the temperautre of heating, Time which is the length of heating, and % Arag which is the measured araongite percentage by XRD.

4.3 Results

Experimental results

We find that when aragonite is heated at low pressure at temperatures of 200-400 °C, Δ_{47} values decrease, on average, as expected, but the temporal variation of Δ_{47} deviates strongly from first order kinetics. As shown in Figure 4.2, the initial period of aragonite heating is associated with relatively rapid, high-amplitude decreases in Δ_{47} value (i.e., increase in apparent temperature). This initial decrease occurs in less than an hour at 400°C, and over the course of approximately 10 hours at 300°C (these latter experiments decrease in Δ_{47} slowly enough that their rate of decrease is relatively well-documented). The two experiments conducted at 200°C and times of approximately 1 day yielded discrepant results: one may indicate a slight decrease in Δ_{47}, but is not statistically resolved from the starting composition; the second is actually higher than the nominal

Name	$\delta^{13}C_{PDB}$	δ^{13}Cstdev	$\delta^{18}OGas_{SMOW}$	$\delta^{18}OMin_{PDB}$	δ^{18}OStdev	$\delta47$	$\delta47$Stdev	$\Delta47$
A	7.285	0.005	31.232	-7.786	0.010	16.678	0.038	-0.053
B	6.968	0.007	30.816	-8.185	0.014	15.973	0.039	-0.032
1	7.707	0.004	31.603	-7.428	0.012	17.501	0.034	-0.013
8	6.800	0.010	30.593	-8.400	0.018	15.582	0.053	-0.035
7	7.461	0.005	32.222	-6.834	0.010	17.882	0.035	-0.015
15	7.410	0.004	31.381	-7.642	0.008	16.987	0.044	-0.016
C3	7.374	0.002	31.007	-8.002	0.005	16.692	0.025	0.096
C1	6.859	0.003	30.836	-8.166	0.004	16.023	0.025	0.099
4	7.233	0.006	31.084	-7.928	0.011	16.477	0.042	-0.054
L	7.327	0.004	31.321	-7.700	0.010	16.816	0.035	-0.046
2	7.392	0.005	31.799	-7.240	0.010	17.366	0.053	-0.037
10	7.813	0.004	31.875	-7.167	0.010	17.950	0.034	0.058
D6	7.001	0.003	30.970	-8.037	0.006	16.272	0.031	0.075
G	7.096	0.004	31.458	-7.568	0.009	16.587	0.040	-0.184
B4	6.135	0.005	31.991	-7.055	0.010	16.142	0.033	-0.226
E	7.386	0.003	31.426	-7.599	0.006	16.961	0.027	-0.062
B2	7.292	0.005	31.224	-7.793	0.011	16.583	0.040	-0.144
B11	7.724	0.007	31.479	-7.547	0.015	17.219	0.038	-0.185
Name	$\Delta47$Stdev	$\Delta47$Sterr	$\delta48$	$\delta48$Stdev	$\Delta48$	$\Delta48$Stdev	HGslope	HGint
A	0.034	0.012	16.721	0.450	4.454	0.581	0.013	-0.784
B	0.030	0.011	14.621	0.634	3.189	0.603	0.013	-0.789
1	0.027	0.009	18.526	0.372	5.511	0.363	0.013	-0.776
8	0.046	0.016	14.646	0.734	3.649	0.694	0.013	-0.789
7	0.027	0.010	20.227	0.619	5.986	0.596	0.013	-0.776
15	0.039	0.014	17.943	0.578	5.370	0.559	0.013	-0.776
C3	0.027	0.010	21.549	0.443	9.664	0.436	0.016	-0.711
C1	0.024	0.009	20.684	0.448	9.146	0.439	0.016	-0.711
4	0.033	0.012	16.041	0.639	4.069	0.615	0.013	-0.775
L	0.031	0.011	18.162		5.704	0.632	0.013	-0.780
2	0.041	0.015	19.065	0.639	5.666	0.619	0.014	-0.753
10	0.031	0.011	18.211	0.617	4.672	0.593	0.014	-0.753
D6	0.028	0.010	21.909	0.344	10.093	0.334	0.016	-0.711
G	0.033	0.012	18.179		5.457	0.783	0.013	-0.780
B4	0.030	0.011	18.201	0.475	4.435	0.453	0.013	-0.783
E	0.024	0.008	17.819		5.162	0.775	0.013	-0.780
B2	0.032	0.011	16.453	0.594	4.205	0.569	0.013	-0.781
B11	0.029	0.010	16.790	0.497	4.039	0.475	0.013	-0.789
Name	Δ_{47}ARF	TEMP	eqm Δ_{47}	progress	exp T	Time(h)	%Arag	
A	0.660	37.297	0.413	0.040	176	18		
B	0.743	12.195	0.393	-0.264	200	1	92	
1	0.656	35.121	0.393	0.051	200	1		
8	0.745	11.728	0.393	-0.270	200	18	100	
7	0.649	37.289	0.393	0.076	200	18		
15	0.661	33.683	0.393	0.033	200	29	100	
C3	0.709	20.257	0.393	-0.142	200	90		
C1	0.723	16.821	0.393	-0.193	200	144		
4	0.673	31.049	0.340	-0.011	304	1	100	
L	0.635	41.728	0.340	0.106	300	2		
2	0.619	47.223	0.340	0.155	304	13	100	
10	0.720	17.686	0.340	-0.150	304	41		
D6	0.693	24.444	0.340	-0.070	300	216		
G	0.473	121.461	0.310	0.547	405	1	100	
B4	0.503	103.997	0.310	0.464	400	2	1	
E	0.608	51.089	0.310	0.172	405	17		
B2	0.586	60.010	0.310	0.234	401	24.6	0	
B11	0.549	75.958	0.310	0.336	400	48	6	

Table 4.1: Experimental data table

average value of the starting material. These are completely separate experiments (i.e. separate crystals and tubes) that were run at the same time as the other similar data

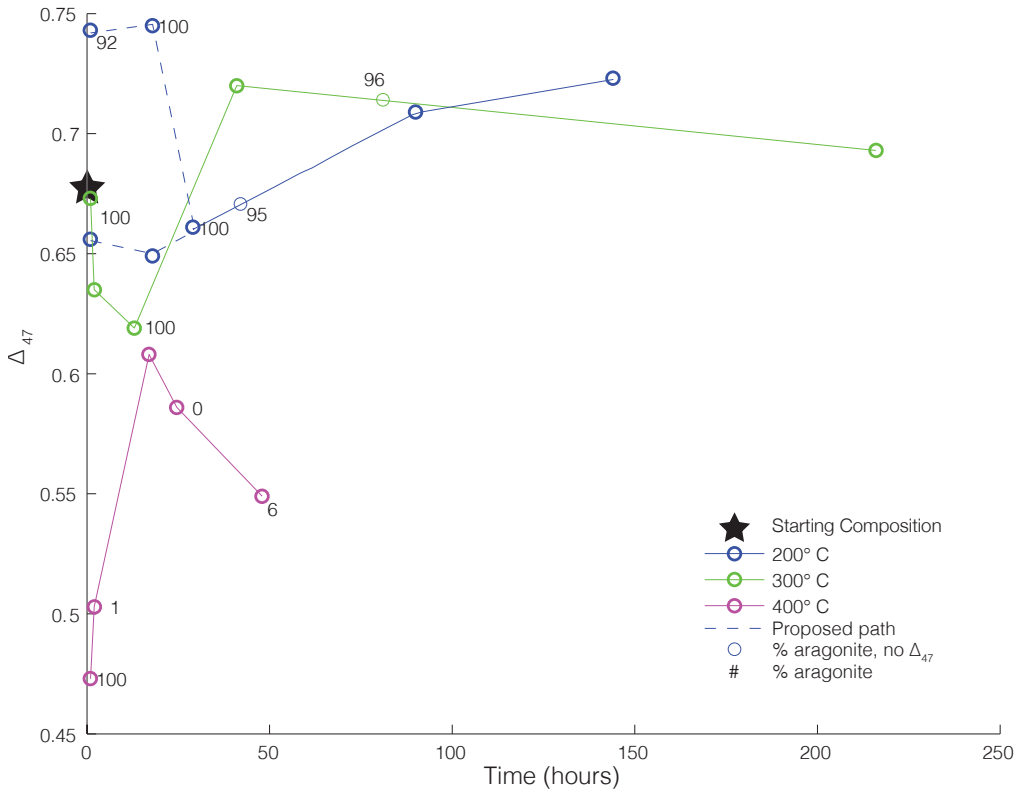

Figure 4.2: Figure shows results from the aragonite heating experiments. Different colors represent different experimental temperatures. Data point labels are the % aragonite of the samples after experiments. The faint data points have been measured for the % aragonite, but not yet for Δ_{47}; their position on the vertical axis is based on interpolation between bracketing time steps. All Δ_{47} values are reported in the absolute reference frame of Dennis et al. (2011).

points. It is possible that these reflect inhomogeneities in Δ_{47} of the starting material (whose variance, at ±0.03 ‰, 1sd, is 2-3 times analytical precision). Note that many of the data points in Figure 4.2 are averages of multiple replicates, but in these cases are derived from the same crystal 'shard' that has been powdered and then split.

Note that all of the experiments that are at or before the initial 'trough' in Δ_{47} values were 100 % aragonite when recovered. Following this initial decrease in Δ_{47} at each temperature (most clearly expressed for the 300 and 400 °C time series), further heating leads to increases in the Δ_{47} value. At 400 °C, this rise in Δ_{47} occurs rapidly (within 10

hours), and early in that period aragonite is completely converted to calcite. Following this rise, Δ_{47} values again fall with continued heating, though at a rate significantly slower than the initial decrease in Δ_{47} of aragonite. At 300 °C, a similar pattern is observed, but the rate of increase in Δ_{47} may be somewhat slower, and the conversion from aragonite to calcite is just barely beginning as this peculiar rise in Δ_{47} is completed. Again, as at 400 °C, Δ_{47} decreases again after this peak, and also as at 400 °C, the rate of this second decline is more gentle than the initial drop in Δ_{47}. The results at 200 °C are ambiguous both because of discrepancies between the replicate studies of the early parts of the time series, and because the overall amplitude of possible subsequent increases and decreases is subtle. We do not attempt to interpret these 200 °C data in detail, simply noting that they could be consistent with low extents of the same changes seen at 300 and 400 °C, obscured by both analytical precision and natural variability in the starting materials.

This peculiar fall-rise-fall pattern of variations in Δ_{47} during heating is unprecedented in our experience of several prior studies of the kinetics of clumped isotope changes during moderate heating of calcite, carbonate-apatite and dolomite, and we are not aware of any such result in prior published studies. The only comparable increase in Δ_{47} that we have observed in a high-temperature experiment was associated with violent decrepitation of calcite heated for 1 minute at 1000 °C (Youry Aglyamov and Max Lloyd, pers. com.). In this case, increases in Δ_{47} are associated with dramatic (20 ‰) increases in δ^{13}C, presumably due to kinetic isotope effects associated with decrepitation. No such changes in bulk δ^{13} or δ^{18}O were observed at any stage of our experiments, so we believe these two results are likely to have different causes.

We hypothesize that the experiments presented in this study captured the combined

influences of solid state, diffusion controlled re-ordering of isotopic 'clumps,' as seen previously for other minerals, combined with the distinctive chemical kinetics of the crystal transformation from aragonite to calcite. In particular, we propose that the 300 and 400 °C time series reflect initial thermally-activated, diffusion-limited 'randomizing' of clumps in aragonite (the early decrease in Δ_{47}), followed by a peculiar 're-clumping' that is coincident with transformation of aragonite to calcite (though not exactly correlated to the reaction progress of this transformation), followed by a second period of more 'normal' decrease in Δ_{47} associated with diffusion-limited re-ordering of clumps in the calcite structure.

The key question is what process could control the rise in Δ_{47} seen near the time of aragonite to calcite transformation. It is possible one could ascribe this effect to a kinetic isotope effect having some arbitrary set of rate constants that conspire to raise Δ_{47}. However, it is challenging to see how this will work in a system that is closed to gain or loss of other species. We note that the Δ_{47} value in these 300 and 400 °C experiments never rises above that of the starting material. This may be a coincidence, or may reflect the fact that the aragonite to calcite transformation is partially recovering the initial clumped isotope abundance of the starting material rather than superimposing a new kinetic isotope effect. In the discussion section, below, we propose a hypothesis that is inspired by these observations, and by a recently-published model of calcite reordering kinetics (Stolper and Eiler, 2015).

A second question is whether we can estimate the blocking temperature with respect to diffusion-limited re-ordering in aragonite, just based on the rates of decrease in Δ_{47} observed in the first hours of the experiments at 300 and 400 °C. We are obviously

limited in what we can conclude because of the complex behavior later in these time series. Nevertheless, it is clear that the rate if decrease in Δ_{47} at these temperatures is greater than the subsequent decrease after conversion to calcite, and is significantly faster than the decreases observed in previous calcite heating experiments. This suggests that aragonite has a significantly lower blocking temperature than calcite. In the discussion section, below, we conduct a more quantitative analysis of these data, concluding that the aragonite clumped isotope blocking temperature is on the order of 100°C.

Natural samples

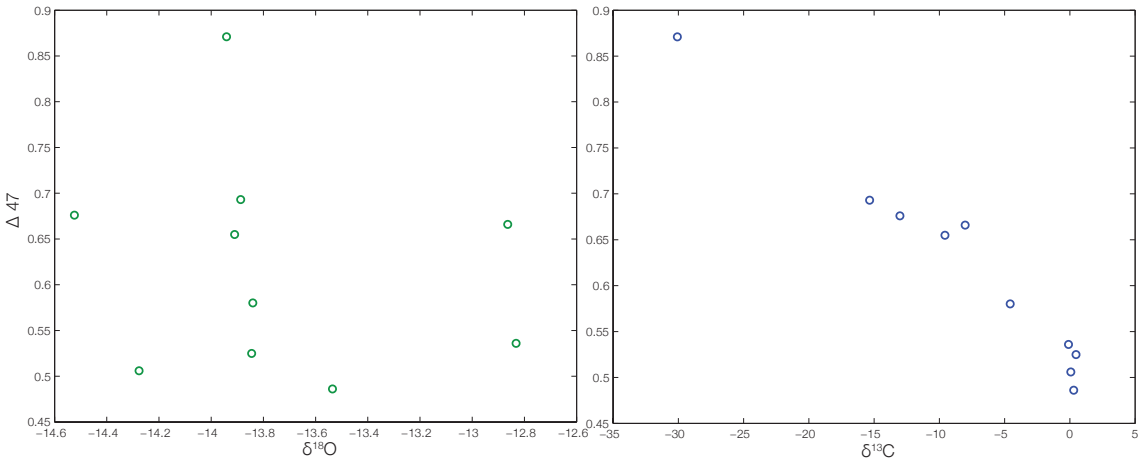

Figure 4.3: This figure shows the range of δ^{13}C, δ^{18}O, and Δ_{47} of the natural Lopez samples. The δ^{18}O varies over a very small range, and is effectively constant over all of the samples, while there is a very significant and large range in the δ^{13}C of the samples. Note the tight correlation and monotonic trend of Δ_{47} vs. δ^{13}C.

Our analyses of this sample suite document a wide range in Δ_{47} and δ^{13}C, and correlation between these two variables, a narrow range in δ^{18}O, and no obvious relationships between stable isotope composition and either ratio of aragonite to calcite or degree of deformation. The lowest δ^{13}C values (approximately -30‰) resemble the very ^{13}C-depleted

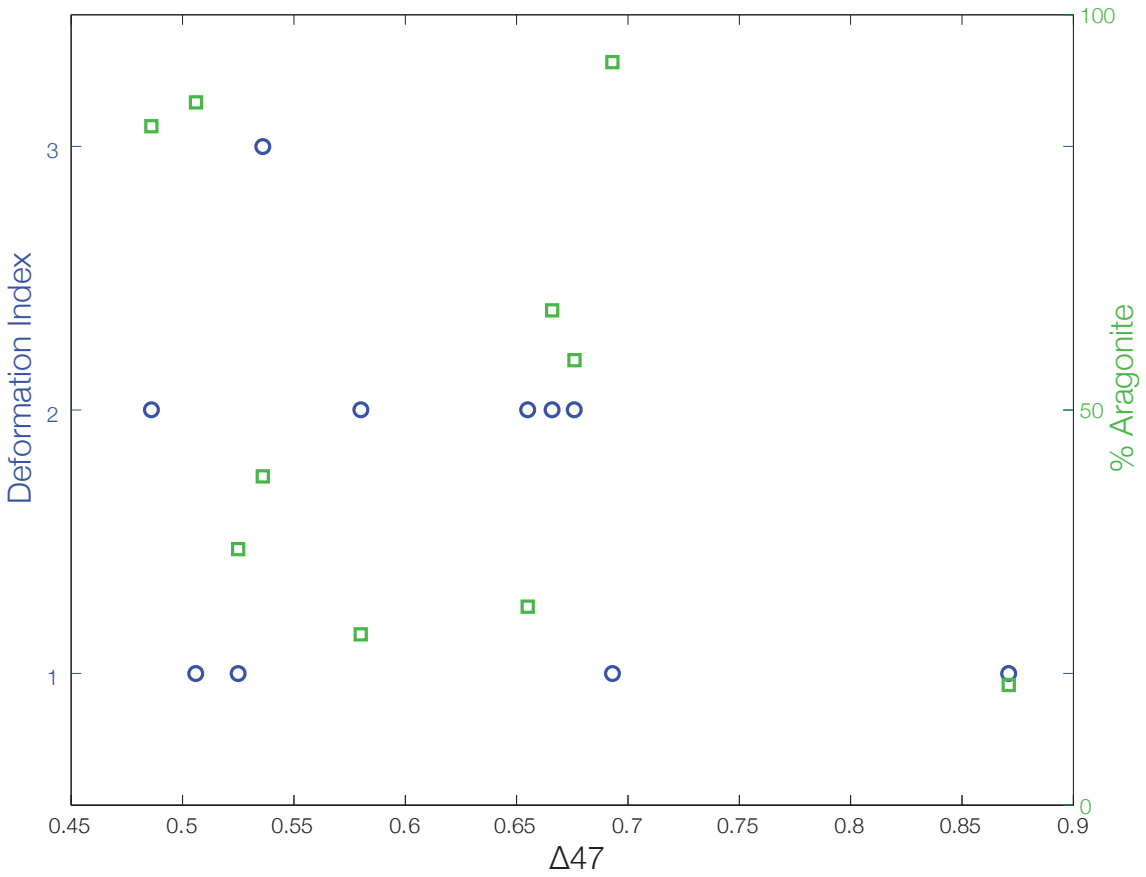

Figure 4.4: This figure shows the relationship between Δ_{47} and estimates of the amount of deformation and the percent aragonite for the samples from Lopez Island. Neither of these latter two variables is significantly correlated with each other or the Δ_{47} value of the sample (clearly no relationship as coherent as that between Δ_{47} and δ^{13}C). These data suggest the apparent temperatures of carbonate are not controlled by deformation or the extent of aragonite to calcite transition (note these two properties are not well correlated with each other).

compositions previously observed in aragonites that are suggested to be associated with microbial carbon cycling (Paull et al., 1992). In such systems, biogenic methane is oxidized, and the resulting dissolved inorganic carbon is precipitated as aragonite, preserving the very low carbon values. Since the oxygen is coming from environmental water and not from microbial activity, it does not have a distinctive isotope value. The lowest $\delta^{13}C_{PDB}$ value measured in all of the samples from the general area of our study (i.e., counting samples analyzed by M. Brandon but not included in this work) extends down

to -50‰.

Sample	rep.	$\delta^{13}C_{PDB}$	δ^{13}Cstdev	$\delta^{18}OGas_{SMOW}$	$\delta^{18}OMin_{PDB}$	δ^{18}OStdev	d47
MB-2b	1	-8.014	0.003	25.953	-12.864	0.007	-3.815
MB-3	2	-13.021	0.003	24.228	-14.525	0.007	-10.580
MB-4	3	-9.574	0.003	24.866	-13.910	0.005	-6.508
MB-5	3	-30.067	0.003	24.834	-13.941	0.007	-26.750
MB-6	3	-15.350	0.003	24.890	-13.887	0.006	-12.212
MB-9	3	-4.563	0.003	24.939	-13.840	0.005	-1.519
MB-12	2	0.464	0.002	24.946	-13.833	0.004	3.447
MB-14	3	0.296	0.004	25.256	-13.535	0.007	3.545
MB-15	2	0.069	0.003	24.491	-14.272	0.004	2.554
MB-16	3	-0.107	0.003	25.987	-12.832	0.007	3.965

Sample	d47Stdev	D47	D47Stdev	D47Sterr	d48	d48Stdev	D48
MB-2b	0.037	-0.484	0.040	0.014	2.976	0.187	1.232
MB-3	0.028	-0.710	0.028	0.010	-2.629	0.353	-0.987
MB-4	0.025	-0.594	0.027	0.010	-0.550	0.370	-0.165
MB-5	0.026	-1.023	0.027	0.010	-0.514	0.341	0.024
MB-6	0.026	-0.745	0.029	0.010	-0.458	0.294	-0.095
MB-9	0.037	-0.517	0.037	0.013	-0.447	0.289	-0.226
MB-12	0.026	-0.414	0.025	0.009	-0.283	0.218	-0.099
MB-14	0.027	-0.463	0.024	0.009	0.855	0.242	0.436
MB-15	0.030	-0.471	0.031	0.011	-1.881	0.378	-0.808
MB-16	0.022	-0.382	0.021	0.007	2.973	0.264	1.129

Sample	D48Stdev	HGslope	HGint	Δ_{47}	TEMP	% arag	Def
MB-2b	0.181	0.036	-0.774	0.666	32.086	0.626	2
MB-3	0.351	0.036	-0.774	0.676	29.169	0.563	2
MB-4	0.364	0.036	-0.774	0.655	35.331	0.251	2
MB-5	0.339	0.036	-0.774	0.871	-12.461	0.152	1
MB-6	0.292	0.036	-0.774	0.693	24.382	0.94	1
MB-9	0.286	0.036	-0.774	0.580	62.122	0.216	2
MB-12	0.217	0.036	-0.774	0.525	87.833	0.324	1
MB-14	0.239	0.036	-0.774	0.486	111.494	0.859	2
MB-15	0.377	0.036	-0.774	0.506	98.555	0.889	1
MB-16	0.262	0.036	-0.774	0.536	82.438	0.416	3

Table 4.2: Natural samples data

We suggest two possible explanations for the correlation between Δ_{47} and δ^{13}C in our suite: (1) the measured Δ_{47} values may accurately preserve the temperatures of carbonate growth, in which case this system precipitated carbonate over a range of temperatures from somewhat in excess of 100 °C down to near earth-surface conditions, and the proportion of carbon in the system derived from oxidation of biogenic methane increased with decreasing temperature. In this case, the trend in Figure 4.3 documents the gradual cooling of the system and concomitant rise in importance of biogenic methane in the system's carbon budget. Or, (2) a generation of higher temperature, higher δ^{13}C

carbonates first existed in these rocks (forming at or above 100 °C), and these carbonates were partially replaced at low temperature with a second generation of carbonate having low δ^{13}C value. The trend in Figure 4.3 is a mixing trend between early-formed and late-formed carbonate. Field work in the area has yielded no evidence for two generations of carbonate (i.e., low temperature replacement of pre-existing veins; M. Brandon, pers. com). This should lead us to favor the first hypothesis. Nevertheless, we suggest it would be useful to conduct further petrographic and geochemical observations aimed at the second of these ideas.

The relatively homogeneity of δ^{18}O values of the San Juan Island carbonate veins that we examined may reflect the fact that fluids from which these carbonates grew were buffered in their δ^{18}O by the rocks through which they flowed (or perhaps just reactive components of some of those rocks, such as the carbonate-rich marbles in the section). Given that carbonate growth temperatures (as reflected by Δ_{47} values) apparently varied while δ^{18}O of carbonate did not, this explanation would imply that the buffering was effective continuously over the varying temperature history, such that newly formed carbonate always has a δ^{18}O value controlled by the bulk δ^{18}O of surrounding rocks (or components of those rocks).

The apparent temperatures of carbonate growth in the San Juan Island carbonate veins varies from 111°C down to 24 °C. The data are organized into two crude groups: a hotter apparent temperature of 100 °C, corresponding to a Δ_{47} around 0.50‰, and a range of lower apparent temperatures (60-30 °C, with one exceptional outlier discussed below), corresponding to Δ_{47} values greater than 0.6 ‰ (Figure 4.3). The hotter apparent temperatures are within error of one another, whereas the cooler apparent tem-

peratures are resolved from one another (given our nominal analytical precision) and so seem to represent a true variability in growth temperature. This distribution suggests at least two environments (and perhaps processes) of carbonate formation: a relatively hot event associated with deep basin processes and/or metamorphism, occurring at 100 °C, or perhaps at higher temperatures if this group is controlled by the aragonite blocking temperature, and a second event or process happening at cooler temperatures. The correlation between Δ_{47} and δ^{13}C suggests that it is only this second carbonate growth process that samples carbon from biogenic methane (or other low δ^{13}C source).

Our isotopic measurements can be compared with petrographic estimates of the extent of deformation and with measurements of the % of carbonate present as aragonite in each sample (all these measurements were made by the same collaborators at Yale who did the field work to collect the samples). The fraction of carbonate present as aragonite varies widely among our samples, but does not correlate with the measured Δ_{47} value (figure 4.4). This result was unexpected, as we anticipated that the conversion of aragonite to calcite would have controlled or at least disturbed the clumped isotope temperatures in this suite (i.e., assuming all carbonate began as aragonite grown at one temperature and was later transformed to calcite at some other temperature). All samples were analyzed as bulk carbonate, so besides comparing the aragonite % to the isotopic measurements, it is impossible to completely confirm that all calcite is derived from primary aragonite. We assume that this is the case due to the lack of correlation between aragonite % and other values. Our findings suggest instead that whatever process controls the proportions of aragonite to calcite in the samples does not control the apparent temperature recorded by the samples. Similarly, the deformation index (ranging between 1–mildly

deformed–and 3–severely deformed) appears unrelated to the Δ_{47} value. This also violates our expectation that deformation at some post-metamorphic temperature might have controlled or influenced aragonite transformation to calcite. (It is also worth noting that the fraction of carbonate present as aragonite is uncorrelated with the deformation index.) The only compelling correlation we observe is between the apparent temperature of carbonate growth and δ^{13}C of carbonate. This could represent a simultaneous cooling of the system and increasing role of biogenic methane oxidation in the local carbon budget. However, in this case, it is difficult to understand why aragonite is present and what controls its relative abundance — the lower δ^{13}C samples preserve apparent temperatures so low that they must correspond to low pressures where aragonite is unstable, yet several are aragonite-rich. One might argue that these samples have had their Δ_{47} values elevated by the same process that we observed experimentally, associated with aragonite to calcite transformation, but in this case we should have seen a relationship between Δ_{47} and proportion of aragonite. The only remaining conclusion that seems consistent with all these observations is that aragonite in this suite is a metastable precipitate that grew over a range of generally low temperatures, in relatively low-pressure veins.

4.4 Discussion

Experimental data

As described in the results section, the experimental data can be split up into three different behaviors: aragonite reordering (initial decrease in Δ_{47}), phase transition to

calcite (sharp rise in Δ_{47}), and calcite reordering (later decrease in Δ_{47}). In this section, we discuss possible mechanisms and rate constants associated with each of these steps.

The rate of the process we associate with thermally activated, diffusion-controlled isotopic re-ordering of aragonite (the first step) can be calculated at 300 °C (first three experiments) and 400 °C (comparison of starting composition and first two steps), and a maximum rate estimated at 200 °C (based on the average values of the first two steps). We estimate rates by plotting the reaction progress variable F (calculated following (Passey and Henkes, 2012) versus time, in seconds, and fitting a first-order kinetic model to yields a fundamental reaction rate, The initial starting composition of $\Delta_{47} = 0.670$ is also used as a point in fits for all three temperatures.

Aragonite	k (1/s)
200°C	8.65E-07
300°C	3.32E-06
400°C	2.19E-04
Calcite	
400°C	1.91E-06

Table 4.3: Rates of reordering

Using the rates calculated from Figure 4.5, an Arrhenius relationship is calculated and plotted as shown in Figure 4.6. The maximum rate estimate at 200°C is not useful for estimating the Arrhenius equation (other than that our fitted line should not violate that maximum), so we are effectively fitting a line in Figure 4.6 to the estimated rates at 300 and 400 °C, and simply checking that the resulting line falls under the estimated maximum rate at 200 °C. The fitted activation energy is 1.34 E+5 J/mol, and the pre-exponential factor is 1.72E-7 s^{-1} . The published activiation energy for calcite is around

2.0 E+5 J/mol for Passey, as well as for the second phase of Stolper's long-term equilibration (1.5 E+5 J/mol for his first phase), with a pre –exponential factor of 4.4E-7 s^{-1} for Passey (Passey and Henkes, 2012; Stolper and Eiler, 2015).

	300 and 400 C	All Data
Ea (J/mol)	1.34E+05	7.03E+04
pre-exp. Factor	1.72E-07	0.0332

Table 4.4: Arrhenius parameters

Our constraints on the Arrhenious parameters for clumped isotope reordering in aragonite can be used to estimate the blocking temperature of this thermometer as a function of cooling rate. Following Lloyd and Eiler (2014) and Dodson (1973) with a shape parameter set between a sphere and an ellipse (1.78 following Passey and Henkes (2012)), a cooling model is made. It assumes that the crystal is far away from the peak temperature, the blocking temperature is independent of the current temperature, a constant cooling rate, and that the entire crystal has a homogenous temperature. The results are shown in Figure 4.6. Based on this approach, we find the blocking temperature for clumped isotope thermometry of aragonite over geologically relevant cooling rates is between 50-100°C, as shown in figure 4.7. This finding suggests aragonite has a blocking temperature 50-100 °C lower than that for calcite (Passey and Henkes, 2012), and approximately 200 °C lower than that for dolomite (Lloyd and Eiler, 2014). The inferred blocking temperature is low enough that we should anticipate partial or complete diffusion-controlled resetting of apparent temperatures in rocks that have been shallowly buried to diaganetic conditions — possibly as shallow as 1-2 km. This finding implies that previous measurements of Δ_{47} values of aragonitic fossils may be more influenced by subsequent burial history

than has been previously appreciated.

Our interpretation of our experiments also implies new constraints on the rate for thermally-activated, diffusion-controlled clumped isotope reordering in calcite (calculated here using methods similar to those described above; Table 4.3). The last three points of the 400°C experiment were used, and the starting composition was not used (as previous events in the heating history had already changed the carbonate from this value). Therefore, the reaction progress variable was calculated based on the change from the highest value in Δ_{47} reached after the aragonite to calcite transition (i.e., this peak serves as the starting time and composition in this fit). The reaction rate calculated as such for 400°C reordered calcite is 1.90E-6 s^{-1}, compared to 1.39E-6 s^{-1} as calculated by Passey and Henkes, or 9.25 E-5 s^{-1} as calculated by Stolper and Eiler. Considering the complexity of the experiments we performed, this similarity to prior studies of calcite reordering suggests our interpretation of the sequence of events in our experimental time-series at 400 °C (at least) is correct.

Finally, we consider the mechanism and rate of the peculiar isotopic re-ordering that we associate with the aragonite to calcite transition (i.e., the increase in Δ_{47} that occurs near the time when mineralogical transformation occurs). Our interpretation of this effect draws on the recent suggestion that thermally-activated, diffusion limited re-ordering of clumps in calcite proceeds through an initial step that dissociates a 'clump' to form a 'pair' of singly substituted isotopologues that are immediately adjacent to each other in the crystal lattice (Stolper and Eiler, 2015). The two adjacent single substitutions have two possible fates: they might back-exchange to reform a clumped isotopologue, or solid state diffusion might allow them to migrate apart and be isolated single substitu-

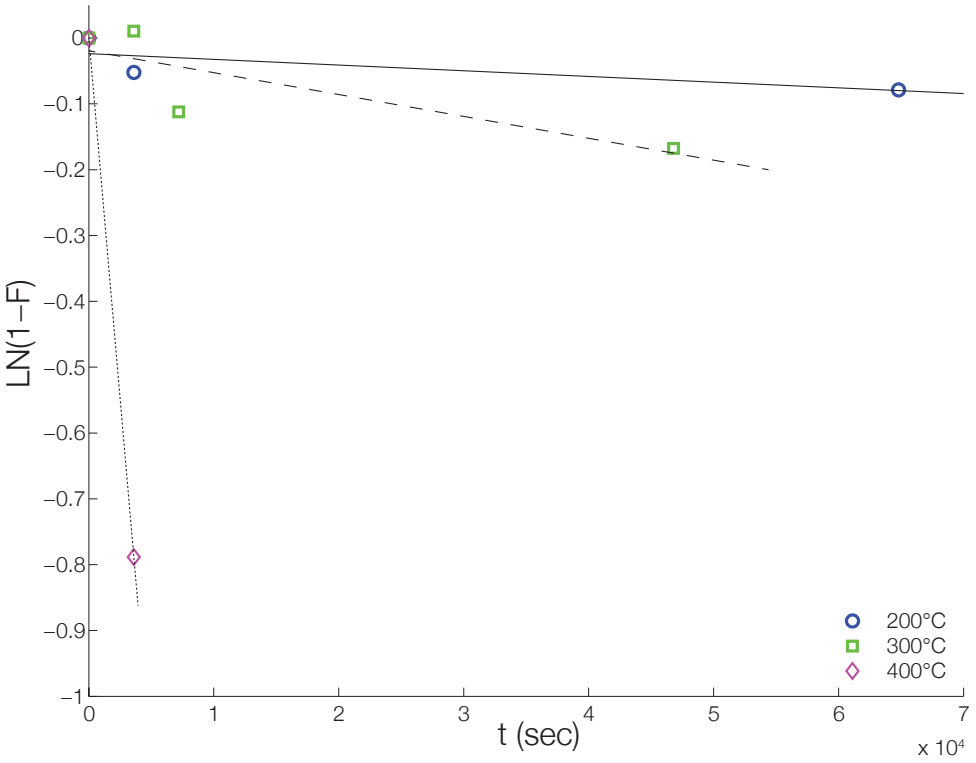

Figure 4.5: Shows the aragonite reordering for the experiments. F is the reaction progress as defined by Passey and Henkes. Slope of lines shows the rate of reaction for the different temperatures.

tions ('singletons' in the nomenclature of the Stolper and Eiler model). This model was originally used to describe the non-first-order behavior of thermally activated clumped isotope resetting in calcite. Here we extend this idea and suggest the phenomenon of converting 'pairs' back into 'clumps' may be responsible for the sharp rise in Δ_{47} during the aragonite to calcite transition. In particular, we hypothesize that the initial drop in Δ_{47} that occurs when aragonite is heated at 300 and 400 °C involves only the pair forming mechanism — longer-range solid-state diffusion of isotopes apart from one another to form 'singletons' has not yet occurred to any significant extent at this point in our heating schedule. When the aragonite to calcite transition occurs, these still-adjacent pairs back react to reform clumps. Importantly, the amplitude of the resulting rise in

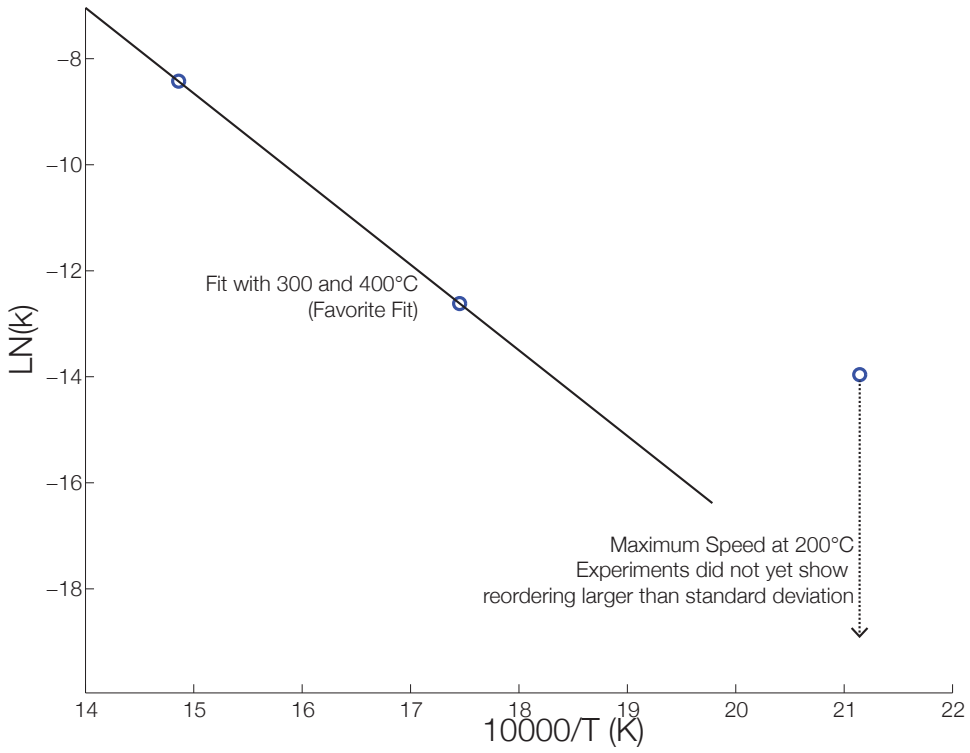

Figure 4.6: Arrhenius plot of aragonite data. The three points are included in the dashed line fit. Since there was no conclusive reordering in the 200°C experiment it is more of an upper bound on the rate at that temperature. Therefore, the preferred fit is using the 300° and 400° C experiment, as shown in the solid line.

Δ_{47} is similar to the initial fall; i.e., the sample recovers most of the previous decrease in Δ_{47}. This can only happen if the aragonite-to-calcite transition involves an oxygen transfer between adjacent carbonate ion units that exactly reverses the oxygen transfer that converted the clump to the pair in the first place. This, in turn, could only occur if there exists a strong preference for oxygen exchange between two specific oxygens in adjacent carbonate ion units, both during aragonite heating and during the aragonite-calcite transition. This could only be possible if there are asymmetries in the bonding environments of the various oxygens in the carbonate ion units in aragonite, such that a low activation-energy 'channel' exists between pairs of them, and that this channel is somehow activated during the polymorphic transformation. This is a rather specific (and

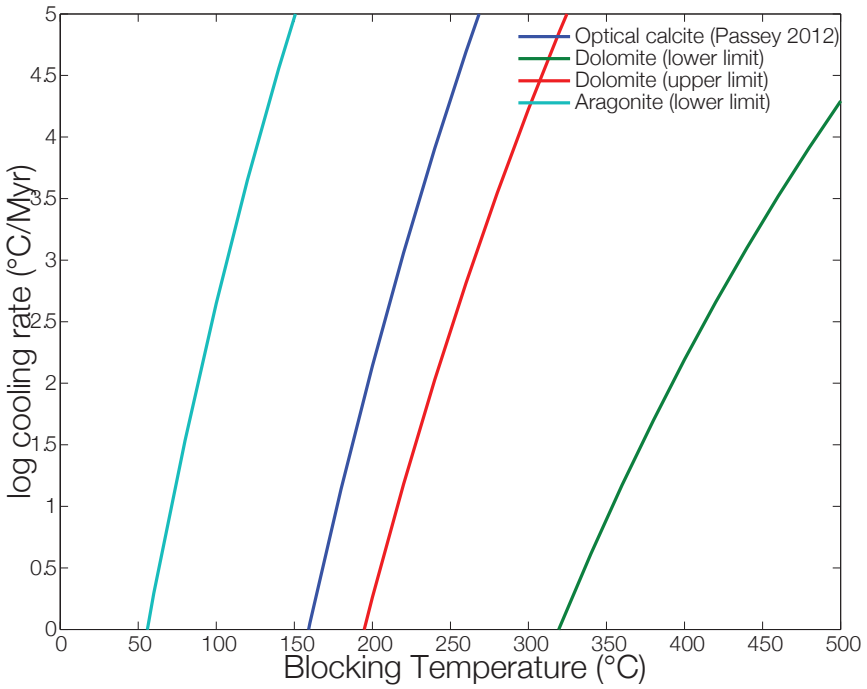

Figure 4.7: This figure shows the blocking temperature of aragonite, calcite, and dolomite as a function of cooling rate.

speculative) hypothesis, though we were not able to think of an alternative that did not violate some feature of our observations. In any case, we consider this an attractive target for future studies using experiments and first principles models. For example, if we are correct, then heating aragonite for long times at high pressure eventually should allow the pairs to diffuse apart into singletons, such that subsequent heating at low pressure will not re-form clumps.

Natural samples

Finally, we consider the implications of our experimental study for the geological interpretation of the natural aragonite-bearing carbonate veins from Lopez Island. There are two main ways that these data can be explained. The first involves a simple two component mixing model. There is one group of samples in the data that represent a

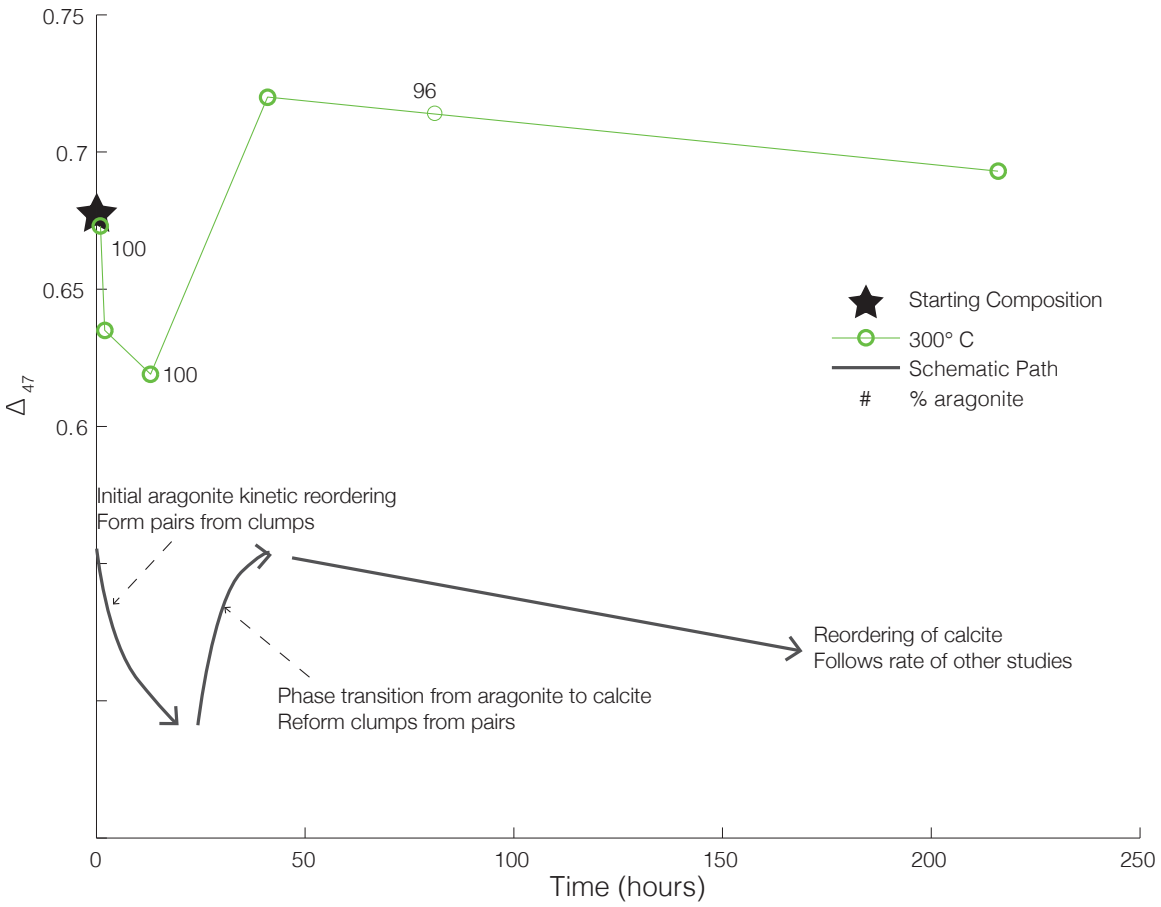

Figure 4.8: Figure showing the three schematic steps to aragonite reordering, as observed by our experiments.

high-temperature end-member. The group is characterized by apparent temperatures around 100°C (within error). This could be the temperatures of growth, or could be blocking temperature during exhumation from some higher tempreature. These samples are also relatively high in $\delta^{13}C_{PDB}$–around 0‰. The other end member in this scenario would be derived from low-temperature precipitation from a pore fluid containing low $\delta^{13}C$ carbon (perhaps the product of oxidation of biogenic methane). The lowest $\delta^{13}C_{PDB}$ value sample measured by M. Brandon is -50‰, although we observed values only down to -30 ‰ and thus consider that to be the end-member value when fitting our data. The lower $\delta^{13}C$ samples have a range of Δ_{47} values, but several cluster around

an apparent temperature of 30°C. There is one exceptionally low δ^{13}C, high Δ_{47} sample that is either an outlier or an extreme end member of this array. Unfortunately, this sample was analyzed in an analytical session that did not include any appropriately-low δ_{47} heated gases, so we are not confident that its Δ_{47} value is well-standardized. This measurement should be repeated. We have no reason to doubt the δ^{13}C measurement of this sample, and thus consider the value of -30 to be a valid (and plausible) end member. However, we are not confident that the measured Δ_{47} value of this sample is the correct value to use in a mixing model fit to the remainder of the data set.

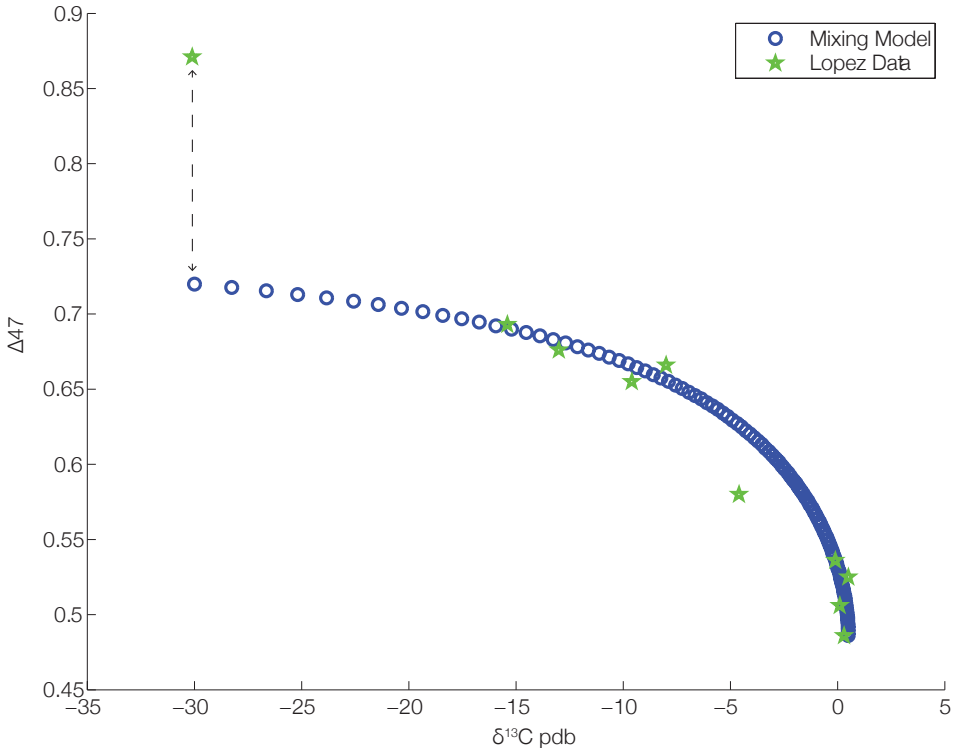

Figure 4.9: Figure showing the results of a mixing model for the Lopez Island samples. The model mixes a high T, 0‰ δ^{13}C species with a low T, -30‰ species. The last data point that falls off the line is not expected to fall on the line due to it being so depleted that the Δ_{47} value was unconstrained.

We propose a mixing model in which a population of high-temperature, high-δ^{13}C crystals are variably replaced by a second generation of low-temperature, low-δ^{13}C car-

bonate, having a Δ_{47} value of 0.73, corresponding to 30°C. In order to fit the curvature of our data trend, we found it was necessary to stipulate that the replacement carbonate is uniformly high in Δ_{47} (equal to the low-temperature end-member), but that the δ^{13}C of the newly-grown carbonate is a mixture between the newly-added low-δ^{13}C end-member and the higher δ^{13}C reservoir of the first-generation carbonate undergoing replacement. That is in this model, the carbon budget of the rock is not entirely buffered by the low-δ^{13}C fluid. The model was evaluated by performing mixing calculations on concentrations of each independent isotopologue, such that non-linearities in d and Δ_{47} units should not influence our results. This model results in a satisfactory fit to the data, and is over-constrained by the data (i.e., our model includes only five fixed parameters–δ^{13}C and Δ_{47} of each end-member, and the relative contributions of the new carbon source and existing rock to the overall carbon isotope budget controlling the δ^{13}C of the newly-grown carbonate). We conclude this model is a successful description of the stable isotope data (including δ^{18}O, which can be readily explained by rock buffering of the water δ^{18}O, as described above).

However, based on field observations, collaborator M. Brandon has proposed that there is no evidence for this two-generation, replacement process, and suggests instead that carbonate grew in multiple phases over a range of temperatures from fluids having variable mixing ratios of carbon from oxidation of biogenic methane. The challenge of this hypothesis is explaining how aragonite forms at all at the low temperatures (and presumably pressures) recorded by the low-δ^{13}C carbonate veins.

4.5 Conclusions

Aragonite re-equilibrates its clumped isotope composition during moderate heating faster than the other carbonate phases that have been previously studied. Based on our findings for aragonite subjected to controlled experiments, the apparent blocking temperature for aragonite, over geologically-relevant cooling rates, is in the range of 50-100°C. The most unexpected and significant finding of this study is that transformation of aragonite to calcite is associated with an increase in the Δ_{47} value, to values well below those in equilibrium with the experimental temperature (and approaching values in the aragonite prior to any heating). We propose that this is caused by reforming clumped species from adjacent pairs of single isotope substitutions, although this requires a very specific set of conditions for the kinetic pathways of initial 'disordering' of the aragonite and 'reordering' on conversion to calcite. After aragonite has transformed to calcite, it reverts to the expected decrease in Δ_{47} with continued heating, at a rate broadly consistent with previously-published studies of calcite.

Our experimental results provide a context for interpreting clumped isotope analyses of mixed aragonite/calcite veins from Lopez island (San Juan Islands, WA). The samples represent at least one metamorphic aragonite generation event that occurred at or above the blocking temperature for aragonite (100 °C). This was followed either by continued formation of aragonite bearing veins at lower temperatures (down to 30 °C) or partial replacement by a lower-temperature carbonate population; in both cases, this lower temperature carbonate is low in δ^{13}C, presumably from sampling carbon sourced from oxidation of biogenic methane.

The relatively low blocking temperature of aragonite implies that future clumped isotope studies focused on paleoclimatic reconstructions will need to be mindful of the maximum temperature reached by a sample. Even though there might not be evidence for secondary recrystallization, the low blocking temperature could result in reordering in samples that still have many primary features present. On the other hand, the relative susceptibility of aragonite to thermally-activated isotopic re-ordering might contribute to studies of the temperature-time histories associated with burial and exhumation, particularly when such data are combined with clumped isotope studies of associated calcite, dolomite and/or carbonate-apatite.

References

Boettcher, A L and P J Wyllie (1968). "The Calcite-Aragonite Transition Measured in the System $CaO - CO_2 - H_2O$." English. In: *The Journal of Geology* 76.3, pp. 314–330. DOI: 10.1086/627331. URL: http://www.journals.uchicago.edu/doi/abs/10.1086/627331.

Brandon, Mark T, Darrel S Cowan, and Joseph A Vance (1988). "The Late Cretaceous San Juan thrust system, San Juan Islands, Washington." English. In: *Geological Society of America Special Papers* 221, pp. 1–83. DOI: 10.1130/SPE221-p1. URL: http://specialpapers.gsapubs.org/lookup/doi/10.1130/SPE221-p1.

Clog, M, Daniel Stolper, and J Eiler (2015). "Kinetics of CO2(g)-H2O(1) isotopic exchange, including mass 47 isotopologues." In: *Chemical Geology* 395.C, pp. 1–10. DOI: 10.1016/j.chemgeo.2014.11.023. URL: http://dx.doi.org/10.1016/j.chemgeo.2014.11.023.

Dennis, Kate J et al. (2011). "Defining an absolute reference frame for 'clumped' isotope studies of CO." In: *Geochimica et Cosmochimica Acta* 75.22, pp. 7117–7131. DOI: 10.1016/j.gca.2011.09.025. URL: http://dx.doi.org/10.1016/j.gca.2011.09.025.

Dickinson, Steven R and K M McGrath (2001). "Quantitative determination of binary and tertiary calcium carbonate mixtures using powder X-ray diffraction." English. In: *The Analyst* 126.7, pp. 1118–1121. DOI: 10.1039/b103004n. URL: http://xlink.rsc.org/?DOI=b103004n.

Dodson, Martin H (1973). "Closure temperature in cooling geochronological and petrological systems." English. In: *Contributions to Mineralogy and Petrology* 40.3, pp. 259–274. DOI: 10.1007/BF00373790. URL: http://link.springer.com/10.1007/BF00373790.

Ghosh, Prosenjit et al. (2006). "13C–18O bonds in carbonate minerals: A new kind of paleothermometer." English. In: *Geochimica et Cosmochimica Acta* 70.6, pp. 1439–1456. DOI: 10.1016/j.gca.2005.11.014. URL: http://ac.els-cdn.com/S0016703705009087/1-s2.0-S0016703705009087-main.pdf?_tid=edf0f89a-60a6-11e4-80dd-00000aacb35e&acdnat=1414723260_e8123bc438ea90b317496e1fb59d274c.

Henkes, Gregory A et al. (2014). "Temperature limits for preservation of primary calcite clumped isotope paleotemperatures." In: *Geochimica et Cosmochimica Acta* 139.C, pp. 362–382. DOI: 10.1016/j.gca.2014.04.040. URL: http://dx.doi.org/10.1016/j.gca.2014.04.040.

Huntington, K W, B P Wernicke, and J Eiler (2010). "Influence of climate change and uplift on Colorado Plateau paleotemperatures from carbonate clumped isotope ther-

mometry." English. In: *Tectonics* 29.3, n/a–n/a. DOI: 10.1029/2009TC002449. URL: http://doi.wiley.com/10.1029/2009TC002449.

Huntington, K W et al. (2009). "Methods and limitations of 'clumped' CO 2isotope (Δ 47) analysis by gas-source isotope ratio mass spectrometry." English. In: *Journal of Mass Spectrometry* 44.9, pp. 1318–1329. DOI: 10.1002/jms.1614. URL: http://doi.wiley.com/10.1002/jms.1614.

Jamieson, John C (1953). "Phase Equilibrium in the System Calcite-Aragonite." English. In: *The Journal of Chemical Physics* 21.8, pp. 1385–7. DOI: 10.1063/1.1699228. URL: http://scitation.aip.org/content/aip/journal/jcp/21/8/10.1063/1.1699228.

Lloyd, Max K and J Eiler (2014). "Laboratory and Natural Constraints on the Temperature Limit for Preservation of Dolomite Clumped Isotope Thermometer." In: *American Geophysical Union Abstract*.

Passey, B and Gregory A Henkes (2012). "Carbonate clumped isotope bond reordering and geospeedometry." In: 351-352.C, pp. 223–236. DOI: 10.1016/j.epsl.2012.07.021. URL: http://dx.doi.org/10.1016/j.epsl.2012.07.021.

Paull, C K et al. (1992). "Indicators of methane-derived carbonates and chemosynthetic organic carbon deposits: examples from the Florida Escarpment." In: *Palaios* 7.4, p. 361. DOI: 10.2307/3514822. URL: http://palaios.sepmonline.org/cgi/doi/10.2307/3514822.

Plummer, L N and E Busenberg (1982). "The solubilities of calcite, aragonite and vaterite in CO 2-H 2 O solutions between 0 and 90 C, and an evaluation of the aqueous model for the system CaCO 3-CO 2-H . . . " English. In: *Geochimica et Cosmochimica Acta* 46.6, pp. 1011–1040. DOI: 10.1016/0016-7037(82)90056-4. URL: http://linkinghub.elsevier.com/retrieve/pii/0016703782900564.

Saleeby, Jason B (1983). "Accretionary tectonics of the North American cordillera." In: *Annual Review of Earth and Planetary Sciences*. URL: http://adsabs.harvard.edu/full/1983AREPS..11...45S.

Schauble, Edwin A, Prosenjit Ghosh, and J Eiler (2006). "Preferential formation of 13C–18O bonds in carbonate minerals, estimated using first-principles lattice dynamics." English. In: *Geochimica et Cosmochimica Acta* 70.10, pp. 2510–2529. DOI: 10.1016/j.gca.2006.02.011. URL: http://linkinghub.elsevier.com/retrieve/pii/S0016703706000913.

Simmons, Gene and Peter Bell (1963). "Calcite-Aragonite Equilibrium." English. In: *Science* 139.3560, pp. 1197–1198. DOI: 10.1126/science.139.3560.1197. URL: http://www.sciencemag.org/cgi/doi/10.1126/science.139.3560.1197.

Snell, Kathryn E et al. (2014). "High elevation of the 'Nevadaplano' during the Late Cretaceous." In: *Earth and Planetary Science Letters* 386.C, pp. 52–63. DOI: 10.1016/j.epsl.2013.10.046. URL: http://dx.doi.org/10.1016/j.epsl.2013.10.046.

Sotin, C and M Madon (1988). "Generalized nonlinear inversion of kinetics data: application to the calcite↔ aragonite transformation." English. In: *Physics of the earth and planetary interiors* 52.1-2, pp. 159–171. DOI: 10.1016/0031-9201(88)90064-7. URL: http://linkinghub.elsevier.com/retrieve/pii/0031920188900647.

Staudigel, Philip, Peter K Swart, and Amanda Waite (2014). "Solid-state bond reordering through thermal aragonite-calcite inversion: Implications for sample handling and preparation." In: *Clumped Isotope Workshop*.

Stolper, D A and J Eiler (2015). "The kinetics of solid-state isotope-exchange reactions for clumped isotopes in inorganic calcites and apatites from natural and experimental samples." In: *American Journal of Science*.

Tripati, Aradhna K et al. (2010). "13Câ"18O isotope signatures and â˜clumped isotopeâ^{TM} thermometry in foraminifera and coccoliths." In: *Geochimica et Cosmochimica Acta* 74.20, pp. 5697–5717. DOI: 10.1016/j.gca.2010.07.006. URL: http://dx.doi.org/10.1016/j.gca.2010.07.006.

Vance, Joseph A (1968). "Metamorphic aragonite in the prehnite-pumpellyite facies, northwest Washington." English. In: *American Journal of Science* 266.4, pp. 299–315. DOI: 10.2475/ajs.266.4.299. URL: http://www.ajsonline.org/cgi/doi/10.2475/ajs.266.4.299.

Wolf, G et al. (1996). "Thermodynamics of CaCO3 phase transitions." English. In: *Journal of thermal analysis* 46.2, pp. 353–359. DOI: 10.1007/BF02135013. URL: http://link.springer.com/10.1007/BF02135013.

Zeebe, Richard E and Dieter Wolf-Gladrow (2001). *CO2 in seawater: equilibrium, kinetics, isotopes*. Elsevier.

Zhang, Haiwei et al. (2014). "Stable isotope composition alteration produced by the aragonite-to-calcite transformation in speleothems and implications for paleoclimate reconstructions." In: *Sedimentary Geology* 309.C, pp. 1–14. DOI: 10.1016/j.sedgeo.2014.05.007. URL: http://dx.doi.org/10.1016/j.sedgeo.2014.05.007.